3-12-2008

Demonstrative Maneuvers for Aircraft Agility Predictions

David M. Hall

Demonstrative Maneuvers for Aircraft Agility Predictions

THESIS

David M. Hall, Captain, USAF

AFIT/GAE/ENY/08-M13

DEPARTMENT OF THE AIR FORCE
AIR UNIVERSITY

AIR FORCE INSTITUTE OF TECHNOLOGY

Wright-Patterson Air Force Base, Ohio

The views expressed in this thesis are those of the author and do not reflect the official policy or position of the the United States Air Force, the Department of Defense, or the United States Government.

AFIT/GAE/ENY/08-M13

Demonstrative Maneuvers for Aircraft Agility Predictions

THESIS

Presented to the Faculty

Department of Aeronautics and Astronautics

Graduate School of Engineering and Management

Air Force Institute of Technology

Air University

Air Education and Training Command

In Partial Fulfillment of the Requirements for the

Degree of Master of Science in Aeronautical Engineering

David M. Hall, B.S.

Captain, USAF

March 2008

AFIT/GAE/ENY/08-M13

Demonstrative Maneuvers for Aircraft Agility Predictions

David M. Hall, B.S.

Captain, USAF

Approved:

//signed//	12 Mar 2008
Lt Col Christopher M. Shearer, PhD (Chairman)	date
//signed//	12 Mar 2008
Dr. Bradley S. Liebst (Member)	date
//signed//	12 Mar 2008
Dr. Donald L. Kunz (Member)	date

Abstract

This study was motivated by a need to develop a reliable method of predicting the agility characteristics of various aircraft. To fully investigate the agility of an aircraft, maneuvers which push the limits of an aircraft's maneuvering capabilities must be simulated. In these cases, classic trajectory optimization techniques either require too many assumptions for a realistic solution or require a good guess of the final solution before the problem is even attempted. This study investigated both the utility of pseudospectral optimization methods for robust trajectory optimization as well as the potential for demonstrating differences in aircraft agility characteristics of several specific maneuvers.

Building off of a pseudospectral optimization software package named DIDO, a robust maneuver definition and trajectory optimization system was developed to simulate various maneuvers specifically designed to demonstrate aircraft maneuvering limits. This system was used to optimize the trajectories of three variations of a baseline F-16 mathematical model developed to simulate important differences in aircraft agility characteristics. Initial results showed significant instabilities in the interface between the mathematical model and the optimization scheme. These instabilities were mitigated through modifications of the system's cost function and the resulting trajectories demonstrated the relative advantages which can be created by subtle differences in aircraft designs.

Future work in this area should include further refinement of the driving cost function and creation of a graphical user interface to simplify the maneuver definition process. The resulting system could be highly useful in other trajectory optimization research as well as non-related areas such as accident investigation and reverse engineering.

Acknowledgements

I would like to take this opportunity to express my sincere appreciation to the numerous people who provided their guidance and support throughout the course of my time here at AFIT. First and foremost, I must thank my advisor, Lt Col Chris Shearer, for the countless hours spent in his office discussing various aspects of this effort and countless ancillary topics. Along similar lines, I would also like to thank Dr. Bradley Liebst, Dr. Donald Kunz, and Maj Paul Blue for their help in polishing this final product and for the always being available for spur-of-the-moment questions. My sincere thanks also goes out to the late Dr. Fred Lutze for the unforgettable introduction to the world of aircraft control that I received in his classroom and for his efforts in laying the foundation upon which my work here at AFIT was built.

Additionally, I would also like to thank my classmates, especially those in the LINUX lab, for consistently taking time away from their own projects to provide invaluable advice, insights, and distractions. This paper would not have been possible without a healthy dose of each.

Of course, I must also thank my entire family, without whom I would not be the person that I am today. I especially wish thank the former officers and aviators in my family for the honor and privilege of extending a family tradition into it's fourth generation. Most importantly, I must thank my wife and daughter for their consistent support and understanding throughout my many long days and nights of academic pursuits. I am indebted to you all.

David M. Hall

Table of Contents

Page

Abstract iv

Acknowledgements v

List of Figures ix

List of Tables xi

List of Symbols xiii

List of Abbreviations xv

I. Introduction 1
- 1.1 Aircraft Performance Comparisons 1
- 1.2 Aircraft Agility 2
- 1.3 Trajectory Optimization 3
- 1.4 Research Objectives 3
- 1.5 Thesis Overview 4

II. Theoretical Development 5
- 2.1 Previous Research and Motivation 5
- 2.2 The Trajectory Optimization Problem 8
  - 2.2.1 Problem Formulation 8
  - 2.2.2 Solution Methods 10
  - 2.2.3 Legendre Pseudospectral Method 12
  - 2.2.4 Revised Problem Formulation 13
  - 2.2.5 Scaling and Balancing 15
- 2.3 Equations of Motion 17
  - 2.3.1 Summary of Assumptions 17
  - 2.3.2 Coordinate systems 18
  - 2.3.3 Aircraft Equations of Motion 20

III. Modeling & Implementation 25
- 3.1 Aircraft Models 25
  - 3.1.1 Physical Layout 25
  - 3.1.2 Physical Parameters 26
  - 3.1.3 Aerodynamic Model 27
  - 3.1.4 Engine Model 28

Page

3.1.5 Model Control Actuator Limits 28
3.1.6 Model State Limits 29
3.2 Optimization Software 30
3.2.1 Problem Definition Structure 30
3.2.2 Method Verification 33
3.3 Simulation Setup 36
3.3.1 Scaling and Balancing 36
3.3.2 Box Constraints 36
3.3.3 Maneuvers 38
3.3.4 Result Verification 47

IV. Simulations & Results 49
4.1 Stability Adjustments 49
4.1.1 Aircraft Model Stability 49
4.1.2 Optimization Routine Stability 49
4.2 Results Format 55
4.3 Demonstration Maneuvers 57
4.3.1 Northing Position Change 57
4.3.2 Unconstrained 3-D Position Change 59
4.3.3 Constrained 3-D Position Change 60
4.4 Agility Maneuvers 60
4.4.1 Bank Angle Capture 60
4.4.2 Unconstrained Heading Capture 62
4.4.3 Constrained Heading Capture 65
4.4.4 Position Free Heading Reversal 65
4.4.5 Position Fixed Heading Reversal 67
4.4.6 Position Free Heading Reversal with Altitude Floor 69
4.4.7 Initial State Capture 69
4.4.8 Initial State Capture with Altitude Floor 72
4.5 Compound Maneuvers 73
4.5.1 4-Point Position Change 73
4.6 Potential as Control Method and Agility Prediction Tool 73
4.7 Overall Analysis 75

V. Conclusions and Recommendations 78
5.1 Conclusions 78
5.2 Recommendations 79

Page

Appendix A. Expanded Simulation Results 81
A.1 Northing Position Change 81
A.2 Unconstrained 3-D Position Change 82
A.3 Constrained 3-D Position Change 83
A.4 Bank Angle Capture 84
A.5 Unconstrained Heading Capture 85
A.6 Constrained Heading Capture 86
A.7 Position Free Heading Reversal 87
A.8 Position Fixed Heading Reversal 88
A.9 Position Fixed Heading Reversal with altitude floor . . . 89
A.10 Initial State Capture 90
A.11 Initial State Capture with altitude floor 91
A.12 4-Point Position Change 92

Bibliography 93

Vita 96

List of Figures

Figure		Page
2.1.	Aircraft Axis Definitions.	18
2.2.	Degree of Freedoms Definitions.	20
3.1.	Aircraft Layout	26
3.2.	Results for the Bryson 727 sample optimization problem.	34
3.3.	Notional Minimum Time Trajectory	47
4.1.	Departure of propagated trajectory from the optimal solution.	50
4.2.	Optimization induced oscillation development over time.	52
4.3.	Stable optimization trajectory development over time.	56
4.4.	Northing position change results.	58
4.5.	Unconstrained 3-D position change results	59
4.6.	Constrained 3-D position change results.	61
4.7.	Constrained bank angle capture results	62
4.8.	Unconstrained Heading Capture Results.	63
4.9.	Variation of the Unconstrained Heading Capture Maneuver.	64
4.10.	Aerodynamic Model Asymmetries.	65
4.11.	Constrained heading capture results	66
4.12.	Position Free Heading Reversal Results.	68
4.13.	Position Fixed Heading Reversal Results.	69
4.14.	Position free heading reversal with altitude floor results.	70
4.15.	Initial state capture results.	71
4.16.	Initial state capture with altitude floor results.	72
4.17.	4-Point position change results.	74
4.18.	Control interchangeability example.	75
4.19.	Maneuver final times for the various aircraft.	77
A.1.	Northing position change state and control histories.	81

Figure Page

A.2. Unconstrained 3-D position change state and control histories. 82

A.3. Constrained 3-D position change state and control histories. . . 83

A.4. Constrained bank angle capture state and control histories. . . 84

A.5. Unconstrained heading capture state and control histories. . . . 85

A.6. Constrained heading capture state and control histories. 86

A.7. Position free heading reversal state and control histories. 87

A.8. Position free heading reversal state and control histories. 88

A.9. Position free heading reversal with altitude floor state and control histories. 89

A.10. Initial state capture state and control histories. 90

A.11. Initial state capture with altitude floor state and control histories. 91

A.12. 4-Point Position Change state and control histories. 92

List of Tables

Table		Page
2.1.	Summary of the assumptions inherent in the mathematical model.	17
2.2.	Aircraft Equations of Motion	22
3.1.	Summary of Baseline Aircraft Model Physical Parameters . . .	26
3.2.	Summary of Aircraft Models Deviation from Baseline Model . .	27
3.3.	Summary of Aerodynamic Lookup Tables.	28
3.4.	Summary of control limits inherent in mathematical model . .	29
3.5.	Summary of state limits inherent in mathematical model. . . .	30
3.6.	Bryson 727 problem solution comparison.	35
3.7.	Scaling and balancing factors used in the optimization scheme.	36
3.8.	Box constraints used in the optimization scheme.	37
3.9.	Initial spatial setup for each maneuver.	38
3.10.	Northing Position Change maneuver definition	39
3.11.	Unconstrained 3-D Position Change maneuver definition	40
3.12.	Constrained 3-D Position Change maneuver definition	41
3.13.	Bank Angle Capture maneuver definition	42
3.14.	Unconstrained Heading Capture maneuver definition	42
3.15.	Constrained Heading Capture maneuver definition	43
3.16.	Position-Free Heading Reversal maneuver definition	44
3.17.	Position-Fixed Heading Reversal maneuver definition	44
3.18.	Initial State Capture maneuver definition	45
3.19.	4-Point Position Change maneuver definition	48
4.1.	Summary of Aircraft Models Deviation from Baseline Model . .	57
4.2.	Northing position change maneuver times.	58
4.3.	Unconstrained 3-D position change times.	60
4.4.	Constrained 3-D position change times.	60

Table Page

4.5. Constrained bank angle capture times. 62

4.6. Unconstrained heading capture times. 63

4.7. Constrained heading capture times. 66

4.8. Position free heading reversal times. 67

4.9. Position fixed heading reversal times. 68

4.10. Position free heading reversal with altitude floor times. 70

4.11. Initial state capture times. 71

4.12. Initial state capture with altitude floor times. 72

4.13. 4-Point position change times. 73

List of Symbols

Symbol		Page
J	Performance Index	9
x	System State Vector	9
u	System Control Vector	9
t	System Time	9
t_f	System Final Time	9
x_f	System State Vector at the Final Time	9
N	Number of nodes (discritization points)	12
V_T	Velocity	21
α	Angle of Attack	21
β	Sideslip Angle	21
ϕ	Euler Roll Angle	21
θ	Euler Pitch Angle	21
ψ	Euler Yaw Angle	21
P_s	Roll Rate (stability axis)	21
Q_s	Pitch Rate (stability axis)	21
R_s	Yaw Rate (stability axis)	21
P_N	Northing Position	21
P_E	Easting Position	21
h	Altitude Position	21
pow	Engine Thrust Dynamics Lag State	21
δ_T	Throttle Command	21
δ_e	Evevator Command	21
δ_a	Aileron Command	21
δ_r	Rudder Command	21
m	Mass of the Aircraft	22

Symbol		Page
L	Lift Force Acting on the Aircraft	23
D	Drag Force Acting on the Aircraft	23
C	Side Force Acting on the Aircraft	23
F_T	Thrust Force Acting on the Aircraft	23
α_T	Thrust Force Angle with respect to the aircraft's centerline	23
J_x	Moment of Inertia about x-axis	23
J_y	Moment of Inertia about y-axis	23
J_z	Moment of Inertia about z-axis	23
J_{xz}	Cross-Product of Inertia	23
J_{xy}	Cross-Product of Inertia	23
J_{yz}	Cross-Product of Inertia	23
l	Torque about the x-axis	23
m	Torque about the y-axis	23
n	Torque about the z-axis	23
U	Velocity component along x-axis (body axis)	23
V	Velocity component along y-axis (body axis)	23
W	Velocity component along z-axis (body axis)	23
T/W	Thrust-to-Weight Ratio	25
W/S	Wing Loading	25
$\bar{c}$	Mean Aerodynamic Chord	26
M	Mach Number	30
σ^2	Variance	53
MA	Moving Average	54

List of Abbreviations

Abbreviation		Page
DOF	Degree of Freedom	8
EOM	Equations of Motion	9
NLP	Nonlinear Programming Problem	11
UAV	Unmanned Air Vehicle	11
PS	Pseudospectral	12
LPM	Legendre Pseudospectral Methods	12
LGL	Legendre-Gauss-Lobatto	12
CG	Aircraft Center of Gravity	18
DCM	Direction Cosine Matrix	18
NED	North-East-Down Coordinate System	19
AFIT	Air Force Institute of Technology	20
MAC	Mean Aerodynamic Chord	26
AOA	Angle-of-Attack	27

Demonstrative Maneuvers for Aircraft Agility Predictions

I. Introduction

1.1 Aircraft Performance Comparisons

For reasons too numerous to fully address, pilots and aircraft designers have been attempting to compare the characteristics of different aircraft since long before aircraft were even viable modes of transportation. The characteristics used for comparing two aircraft vary greatly depending on the intended audience and the specific reason for the comparison study. These characteristics can range from something as simple as the weight of the aircraft to something as abstract as an aircraft's combat effectiveness. In the world of high-performance aerobatic and military aircraft, the comparison of various aircraft usually revolve around an aircraft's performance characteristics.

Initially, the majority of these comparisons were of basic performance measures of merit. These included classic measures such as climb rates, turn rates, speed, acceleration, and range [8]. Though most of these parameters are based on an assumed steady state, they are well understood, are fairly easy to determine, and adequately describe the flight regimes of most aircraft.

These comparison tools break down when attempting to compare the highly transient motion of high performance aircraft, particularly when involved in close range combat. The advent of energy-maneuverability comparisons partially alleviated the measure of merit deficiency, but studies in the early 1990's began to suggest that these still failed to quantify the ability of an aircraft to rapidly and accurately transition from one flight condition to another, often defined as an aircraft's agility [10].

1.2 Aircraft Agility

Whether sitting in a cockpit engaged in air-to-air combat, taking aim at an enemy aircraft with a shoulder launched surface-to-air missile, or attempting to coordinate the impatient traffic at a congested civilian airport, how quickly and precisely a pilot is capable of changing the state of their aircraft is a very important piece of information for everyone involved. The ability to rapidly change an aircraft's state, known as an aircraft's agility, has been the focus of numerous studies and research efforts in the last two decades. Though a great deal of effort has been spent developing a common definition of an aircraft's agility and a set of metrics to quantify that agility, there still exists a need for a method of accurately predicting and comparing the dynamic performance and agility of various aircraft.

Assuming that the aircraft to be compared are available and that money is not a concern, a series of flight tests could be developed to run various aircraft through the same maneuvers to determine which aircraft can achieve a specific maneuver faster than the others. The real problem at this point is that it is perfectly feasible for the best way for one aircraft to achieve a certain maneuver to be drastically different from the best method for another aircraft. A simple example of this phenomenon would be to consider two propeller aircraft which are exactly the same except for the direction which the propeller spins. If the target maneuver is a 360° roll in minimum time, the aircraft with a standard propeller configuration would roll clockwise to benefit from the torque from the engine. A clockwise roll for the non-standard aircraft would actually be fighting the torque from the engine and would result in a larger time required to complete the maneuver. If, on the other hand, the non-standard aircraft were to roll in a counter-clockwise direction it would complete the maneuver in exactly the same amount of time as the standard configuration aircraft.

Unfortunately, funding and time are almost always severely limited and depending on the application, the aircraft in question are most likely unavailable or even still on the drawing board. These reasons, among others, necessitate the use of computer

simulations in predicting aircraft agility characteristics. The most common method for accomplishing this is through the use of trajectory optimization.

1.3 Trajectory Optimization

The basic goal of trajectory optimization is to determine the "best" way for an object to move from Point A to Point B while both minimizing some performance index and adhering to the object's basic equations of motion. The complexity of trajectory optimization arises when one considers that Point A and Point B are not necessarily points in space, but actually states which are each defined by a set of variables and that the performance index is potentially a complex function of those same state variables as well as the system's time and control variables. Furthermore, one could define a set of boundaries which define limits for any or all of the state, control, and time variables. These boundaries may be system limits such as a minimum speed, environmental constraints such as an obstacle, or performance limits such as a maximum amount of time allowed to complete the maneuver.

Though the trajectory optimization problem is well known and is often used in the field of aircraft agility predictions, classic trajectory optimization techniques either require significant assumptions or a good guess of the final solution before the problem can even be attempted. The assumptions required for classic optimization methods rule out the ability to optimize a full aircraft mathematical model and the guess restrictions place severe limitations of the ability to detect drastic maneuver differences between aircraft. Recent advancements in the field of pseudospectral optimization methods now allow for the optimization of full 6-Degree-of-Freedom models with minimal assumption and guess requirements.

1.4 Research Objectives

The focus of this effort was aimed at developing a method of controlling an aircraft independent flight simulator for use as a tool for comparing the flight characteristics of various aircraft. Previous attempts at providing external controls had

resulted in only simulating fairly benign maneuvers. This study investigated both the utility of pseudospectral optimization methods for robust trajectory optimization as well as the potential for demonstrating differences in aircraft agility characteristics of several specific maneuvers. The goal of this research is to develop a trajectory optimization system which will allow a user to investigate and compare the agility characteristics of various aircraft by simulating a wide range of maneuvers. Once optimal trajectories have been determined, these results can be used as the control inputs to a flight simulator model for visualization and more detailed analysis purposes.

1.5 Thesis Overview

In Chapter 2, further discussion on the topic of aircraft agility is provided along with a theoretical development of the trajectory optimization problem and the basic aircraft equations of motion. Chapter 3 details the specific aircraft mathematical model and trajectory optimization methods used in this research as well as an overview of the specific maneuvers which were simulated. The results and subsequent analysis of the optimization runs are presented in Chapter 4. Finally, Chapter 5 contains the conclusions and recommendations for future work which resulted from this research.

II. Theoretical Development

2.1 Previous Research and Motivation

When attempting to compare the performance capabilities of different aircraft, the parameters used generally fall into two categories: point or integral [8]. Point parameters are those which are valid at a specific point in time and do not take into account what occurs at any other point in time, whereas integral parameters take into account changes in the aircraft's state over time. Examples of point parameters include most of the classic aircraft performance terms including stall speed, maximum turn rate, maximum speed, and minimum drag speed. Of the classic performance terms, the notable exceptions to the point parameter generalization are the range and endurance terms. To determine an aircraft's maximum range and endurance, one must integrate the aircraft's state over time.

Each of these classic performance parameters have one basic assumption in common: steady state flight conditions. Since flight profiles for the vast majority of aircraft are generally dominated with large portions of steady state flight, it clearly makes sense to base the fundamental comparison parameters on that assumption. On the other hand, as combat aircraft technologies have advanced and aircraft capabilities have increased, the need to quantify an aircraft's performance characteristics in non-steady flight regimes has also increased. Efforts to characterize an aircraft's "agility" resulted from this need to quantify non-steady flight characteristics.

Aircraft "agility"is both a widely used and widely debated term due to the simple fact that researchers have failed to agree on one universally accepted definition. Proposed definitions for "agility" have ranged from one extreme of sticking to a dictionary definition of agility [10] to simply observing how successful an aircraft is in combat [27] at the other extreme. The one unifying factor among all of the various definitions is that they all encompass some conglomeration of dynamics, maneuverability, performance, and flying qualities [10]. For the purposes of this research, agility is defined as *the ability of an aircraft to rapidly and accurately transition from one state*

to another. This definition is an amalgamation of several proposed definitions [8, 17], and will be used throughout the rest of this paper.

Research in the area of aircraft agility has mostly focused on two distinct areas: developing a set of agility metrics and developing methods of determining those metrics. While the various proposed agility metrics are not the focus of this effort, they should be mentioned in the context that, just like the various definitions for agility, the proposed metrics are just as numerous and wide ranging [17]. Many of the proposed metrics are based on how quickly an aircraft can accomplish a specific maneuver, with maneuvers ranging from 90° bank angle captures to maximum accelerations turns followed by regaining lost energy. Other metrics are combinations of energy states and aircraft physical properties such as wing area and load factors, while others stills are based on relative pointing positions between two adversary aircraft in a dogfight. The main point to take away from the wide variety of proposed metrics is that, until all interested parties decide on a standardized set of metrics, any method of determining those metrics must be able to cover the gamut of metrics or potentially become useless if its specific metrics are not chosen.

As is the case when attempting to determine most aircraft characteristics, there are basically two proposed methods for determining agility metrics: modeling & simulation; and flight testing. While a great deal of effort has gone into developing techniques for determining agility metrics through flight test, the cost and complexity of obtaining repeatable flight test data for one aircraft, let alone numerous aircraft, prohibits the estimation of aircraft agility, especially if an aircraft in question is not readily available or not yet even fully designed. As is usually the case, a simple cost/benefit analysis points towards modeling & simulation as the best option for rapidly determining the agility characteristics of a wide variety of aircraft.

As many of the proposed agility metrics deal with how quickly an aircraft can perform a specified maneuver, many of the simulation methods focus on determining optimal maneuvers and limits to an aircraft's maneuvering capabilities. To this end,

trajectory optimization techniques have been used by numerous researchers working towards methods for determining aircraft agility. In one such endeavor, Bocvarov [5] investigated time-optimal reorientation maneuvers and the benefit which thrust vectoring control could provide to those maneuvers. The main concern with this research, as with much of the previous research, is that the assumptions which were made in an effort to make the problem more feasible, invalidate that method for a wide variety of situations. In this instance, among other simplifying assumptions, Bocvarov neglected translational motion of the aircraft and only looked at rotational motion. This assumption was based on previous research which suggested that, during rapid maneuvers, an aircraft's center of gravity was relatively stationary in comparison with the changes that the aircraft's attitude underwent.

In another effort, the authors address the issue that although assumptions of a point mass model facilitate getting a solution for the trajectory optimization problem, those same assumptions invalidate the solution results [9]. Since the attitude dynamics of a point-mass model do not adhere to Newtonian Mechanics, it is a poor choice for a trajectory optimization routine because, unlike a real aircraft, the model is capable of instantaneously changing it's attitude, which makes a study of agility a trivial endeavor. Instead, the authors modify a point-mass model to take into account the fact that the forces acting on the vehicle and thus the attitude cannot be changed instantaneously. The results are promising, but again the results are not very representative of an actual aircraft, and if necessary could not be used to actually control a non-linear simulation.

In a followup effort to his earlier work, Bocvarov [4] presents the results of optimizing two heading reversal maneuvers with a model based on the F/A-18 High Angle-of-Attack Research Vehicle. The results from these two maneuvers, which will be addressed again later, depict the stark difference between the results of two fairly similar maneuvers when seeking an optimum trajectory. In the first maneuver, where the aircraft is simply attempting to reverse it's heading, the results show the aircraft should roll inverted then pull through until heading the opposite direction.

The second maneuver similarly requires the aircraft to reverse it's heading, but also stipulates that the aircraft must end the maneuver at it's initial position and velocity. The results from this run show the aircraft performing a climb and descent along an arc which returns to it's original position. Once more, the results from these methods are quite revealing, but this group also assumed a near point-mass model and the control history results are nearly meaningless if one wants to control a full 6-Degree of Freedom(DOF) model through the same maneuvers.

Each of these efforts have shown that, given a certain number of simplifying assumptions, one can gain a decent understanding of an aircraft's inherent agility through trajectory optimization schemes. With the addition of recent advancements in the field of trajectory optimization, results suitable for controlling a full 6-DOF model should be possible without needing a large portion of those simplifying assumptions.

2.2 The Trajectory Optimization Problem

2.2.1 Problem Formulation. The trajectory optimization problem, also known as an optimal control problem, falls under the broader umbrella of Dynamic Optimization and, following the Hull's notation format [12], is characterized by the following statement: Determine the control history $u(t)$ that minimizes the performance index

$$J = \phi(t_f, x_f) + \int_{t_0}^{t_f} L(t, x, u)dt, \tag{2.1}$$

subject to the system dynamics

$$\dot{x} = f(t, x, u), \tag{2.2}$$

the specified initial conditions

$$t(0) = t_0, x(0) = x_0, \tag{2.3}$$

the specified final conditions

$$\psi(t_f, x_f) = 0, \tag{2.4}$$

the path control constraints

$$C(t, x, u) \leq 0, \tag{2.5}$$

and the path state constraints

$$S(t, x) \leq 0. \tag{2.6}$$

The performance index, J in Equation 2.1, also known as the system's Cost Function, is a scalar function of the system's state vector, x, control vector, u, time, t, final time, t_f, and state vector at that final time, x_f. Since this research focuses on minimizing the time required to complete a specified maneuver, the performance index can be simplified to

$$J = t_f. \tag{2.7}$$

Another common parameter to include in the performance index would be the fuel expended over the course of the maneuver. This would create a minimum fuel optimization setup.

The system dynamics in Equation 2.2, also known as the system's equations of motion (EOM), are those equations which govern how the aircraft behaves in flight. As depicted, these equations are also functions of time, the current state, and the control inputs.

The initial and final conditions in Equations 2.3 and 2.4 respectively define the state variables and time at both the initiation and termination of the maneuver. Unlike the dynamic constraints, where all variables must be defined, the initial and final condition functions do not require that all of the variables be defined, just enough to fully define the desired maneuver. Normally, one would fully define the initial states and time and only define those final states and time that are necessary to define the target state. For example, a minimum time to climb problem, where you were not

concerned with any of the final state variables except the altitude would only require a definition of the altitude variable for the final conditions constraints.

The control and state inequality path constraints included in equations 2.5 and 2.6 define the operating boundaries of the system. In the case of the control history, these constraints represent the physical control control deflection limits. For example, without these path constraints, the optimization system may try to push a throttle setting, which will be defined later as $0 \leq \delta_T \leq 1$, beyond its limits and achieve some unfeasible result. The state path constraints include both physical limitations, such as defining sea level as a minimum altitude, and additional factors which are included to define the exact problem that the user is trying to simulate. By coupling the ability to change the desired initial and final conditions with the ability to add or remove path constraints on any of the state variables, the user is provided a robust tool which can simulate a wide variety of maneuvers.

Each of these parameters is combined into an adjoint cost function through the use of Lagrange Multipliers which are also known as the adjoint or costate variables [3]. The major impact of this is that, by changing any of the the basic constraints in the problem, the cost function which is actually being optimized also changes. As a result, the solution to an optimal control problem is highly dependent of the problem formulation and the method of adjoining the constraints.

2.2.2 Solution Methods. Given this basic problem, there are many methods for attempting to solve the trajectory optimization problem. Many of these methods are covered by Betts in an enlightening survey paper [2]. In this paper, Betts categorizes the majority of solution methods into two categories: indirect and direct methods. Indirect methods, as described by Betts, require the determination of explicit solutions of the equations defined by the problem's EOM, the necessary and transversality conditions, and the maximum principle. In effect, these methods don't solve the actual optimal control problem, but instead create a dualization, or transformation, of that problem by way of the Hamiltonian and then solve that new

problem [22]. In order to accomplish this, one is usually required to solve a non-linear multipoint boundary-value problem. If this description weren't daunting enough, the utility of indirect methods is fairly limited due to the fact that one must not only have analytical expressions of the EOM, but also possess a good guess as to the final answer. Even with these caveats, indirect methods have a very small region of convergence [2]. For these, and other, reasons, indirect methods are rarely used for anything other than fairly simple problems.

With direct methods, on the other hand, a solution is found by manipulating parametric representations of the state and/or control variables to directly affect the objective function. These methods, also known as nonlinear programming problems (NLP), are generally the preferred choice, as they do not require the labor intensive dualization of the problem and the analytic derivation of the necessary conditions associated with that task [22]. Additionally, direct methods generally have larger convergence regions, which in turn creates less stringent restrictions on the initial guess. Of each of these methods, the most common are various forms of what are known as shooting methods. Shooting methods basically take initial guesses of the optimal control histories and integrate the EOM to determine the performance index associated with those guesses. As expected, these methods still require fairly good initial guesses before a solution is even feasible and even then can result in massive numbers of iterations. Unfortunately, these methods generally cannot handle what one author terms "industry-strength" problems. These problems, as is often the case for higher end aircraft flight simulations, are usually characterized by complexities such as non-differentiable table-lookups [22].

Over the last several years, a great deal of work has gone into development of advanced trajectory optimization techniques. This push has resulted from increasing needs in two major areas: satellite orbit transfers and Unmanned Air Vehicle (UAV) control. Work in the area of UAV control has ranged from efforts looking at aircraft engagements of air defense systems [15,16], to guidance in windy environments [14,28], to real-time trajectory optimization [18]. However, in each of these cases, in order

to find solutions using traditional trajectory optimization methods, the problems are simplified to the point that the results, though often very enlightening, can not be translated into useful products for either real aircraft applications or even high end 6-DOF simulations. Many of these issues can now be addressed due to recent advances in the field of Pseudospectral (PS) methods.

2.2.3 Legendre Pseudospectral Method. Depending on which terms are discritized, direct solution methods can be divided into several categories, the most common of which are *control parameterization* and *state and control parameterization* [13]. The previously mentioned shooting methods are examples of *control parameterization* solution methods in that the control history is approximated and the differential equations are propagated forward through numerical integration schemes. As would be expected, the size of the NLP significantly increases when the states are included in the parameterization, but *state and control parameterization* methods are able to avoid several of the pitfalls of the common direct shooting methods.

Pseudospectral methods, also known as orthogonal collocation methods, are a subclass of state and control parameterization methods which approximate the states and controls with a finite set of interpolating polynomials [13]. These polynomials, evaluated at N discritization points (*nodes*), are then differentiated and constrained to equal the differential equations of the original problem thereby approximating the state derivatives.

The PS solution software package used for this research is based on recent developments in the area of Legendre Pseudospectral Methods (LPM), a further subset of basic PS methods. Legendre Pseudospectral Methods are characterized by their approximation of the system's states by a basis of N Lagrange interpolating polynomials, $\mathcal{L}_i(i = 1, \ldots, N)$, and by N nodes, the placement of which are defined by Legendre-Gauss-Lobatto (LGL) points [13]. Using this new format, the state vector

is approximated as

$$x(\tau) \approx X(\tau) = \sum_{i=1}^{N} \mathcal{L}_i(\tau) X(\tau_i), \tag{2.8}$$

and the state derivatives at the k^{th} node are subsequently approximated as

$$\dot{x}(\tau_k) \approx \dot{X}(\tau_k) = \sum_{i=1}^{N} \dot{\mathcal{L}}_i(\tau_k) X(\tau_i), \quad (k = 1, \ldots, K). \tag{2.9}$$

The control vector is similarly approximated as

$$u(\tau) \approx U(\tau) = \sum_{i=1}^{N} \mathcal{L}_i(\tau) U(\tau_i). \tag{2.10}$$

The resulting problem is then solved via a nonlinear programming method based on sequential quadratic programming [13].

Since the dualization of a problem via indirect methods and the discritization of the same problem via direct methods are not necessarily commutative operations, the major benefit of the LPM is that it is one of only two methods which have been shown to preserve the order of the original problem [22]. The implication of this statement, which is a very watered down form of the *Covector Mapping Principle*, is that the solution to an LPM problem also satisfies the problem's necessary conditions, thereby making the solution method both direct and indirect at the same time [22].

2.2.4 Revised Problem Formulation. In order for a PS method to work, the system's dynamics and other equations which were originally used to define the problem must be translated into algebraic constraint equations which can then be applied at each of the nodes along the approximated trajectory. For this reason, it is desirable to rewrite the problem formulation in terms of constraint equations. As described by Ross [20], the problem statement is now the following: Determine the state and control pair, $\{x, u\}$, and possibly event times, τ_0 and τ_f, that minimize the

performance index

$$J = E(x_0, x_f, \tau_0, \tau_f) + \int_{\tau_0}^{\tau_f} F(\tau, x, u) d\tau, \tag{2.11}$$

subject to the dynamic constraints

$$\dot{x} = f(\tau, x, u), \tag{2.12}$$

the event constraints

$$e^L \leq e(x_0, x_e, x_f, \tau_0, \tau_e, \tau_f) \leq e^U, \tag{2.13}$$

the state and control path constraints

$$h^L \leq h(x, u, \tau) \leq h^U, \tag{2.14}$$

and the state and control variable box constraints

$$x^L \leq x(\tau) \leq x^U, \tag{2.15}$$

$$u^L \leq u(\tau) \leq u^U, \tag{2.16}$$

The cost function, J, in equation 2.11 is known as a Bolza function and is comprised of an event cost function, E, called the Mayer Cost, and a running or integral cost, F, called the Lagrange Cost. Note that this problem formulation has benefited from a variable substitution in that time has been effectively removed from the system and can now be included as another variable that can be solved for. This is a crucial step in enabling the minimum time problem which is the main focus of this research.

The dynamic constraints are equivalent to the previously defined dynamic equations with the addition of a τ substitution. The event constraints, e, are used to define the boundary and internal node constraints are defined. A basic problem will have

two event constraint equations, one for the initial conditions, e_0, and one for the terminating conditions, e_f, as described previously. Note that the superscript L and U are used to signify the lower and upper constraint boundaries. It is also convenient to introduce the idea of a knot at this point. Any node along the trajectory which will have specific event constraints applied to it will be referred to as a knot. While the initial and final nodes are obviously knots at time τ_0 and τ_f respectively, a knot can also be defined at any internal event time, $\tau_0 \leq \tau_e \leq \tau_f$ as well. This method of specifying internal knots, incidently known as the *knotting method* [23], is extremely useful in defining points which a trajectory must pass through or points where dynamics change, such as a multi-stage rocket losing a stage.

The path constraints, as previously defined by Equations 2.5 and 2.6, are now divided into two constraint categories. This division is performed to increase numerical efficiency as well as readability. Those path constraints which are imposed over the entire trajectory, state and control physical limits for example, are now termed Box Constraints as in Equations 2.15 and 2.16. Neither path nor box constraints are required to fully define a problem, but box constraints allow a user to confine the solution space to realistic values, provide arbitrary numerical limits to ease computation times, and avoid known singularities in the mathematical model. For example, instead of defining the Northing Position, P_N, limits as $-\infty \leq P_N \leq \infty$, which is perfectly reasonable, one would define the limits with values which are much smaller than infinity, but larger than any value which the system is expected to see. In this way, the constraints do not actually inhibit a solution, but do drastically decrease the solution space over which the optimization routine must search. This method of formulating the problem through a series of constraints will be readdressed in Chapter 3 when the problem for this specific research project is defined.

2.2.5 Scaling and Balancing. A crucial step in any numerical method is to properly scale and balance a problem. Without properly scaling and balancing a problem it is entirely possible that an otherwise well defined problem can behave

very poorly within a numerical method routine. The basic idea behind this step is to convert the units of a problem from a physically meaningful unit system to a system which behaves in a desirable fashion during an optimization routine [11]. There are two basic rules for transforming the unit system of an optimization problem.

First, each of the parameters to be optimized must be of similar magnitude [11]. This is where the scaling step comes into play. When the constraint and cost equations of an optimization problem are combined into an adjoint cost function, the optimization scheme is essentially looking at scalar representation of the combination of each of those terms. If the parameters are of significantly differing orders of magnitude the behaviors of one parameter might mask those of another, possibly more important, parameter. For a simple example of this issue, consider a satellite in an orbit around the Earth which is concerned with observing some property of the Sun. Two parameters which could easily be included in this problem are the distance between the satellite and the Sun and the attitude angles of the satellite. In this case, one term is on the order of 1×10^8 km and the other might be on the order of 20°. The most common solution to this problem is to scale each respective parameter by a representative value in a linear fashion as defined by

$$\hat{x} = Dx \tag{2.17}$$

where $\hat{x}$ is scaled version of the state vector, x, and D is the associated scaling matrix.

After the problem's units have been properly scaled there still exists a problem that the values may still have a widely varying range. Using the same satellite example from before, the scaled distance from the satellite to the Sun might vary by 15,000 km, which would be 1.000015 in the scaled unit system, but an attitude angle could still vary from 0° to 360°, which would be 0 to 18 in a dimensionless systems scaled by 20°. The relative values still pose a problem for the optimization routine. The solution to this problem is to balance the unit system by shifting the units such that each parameter has a similar range [11]. A common method for performing this operation

is to use the minimum, a, and maximum, b, values which a parameter, x_i, is expected to see during the course of the trajectory and balance the basic unit according to

$$\hat{x}_i = \frac{2x_i}{b_i - a_i} - \frac{a_i + b_i}{b_i - a_i}, \tag{2.18}$$

which can also be written as

$$\hat{x} = Dx + c. \tag{2.19}$$

Through the use of Equation 2.19, each of the parameters in the optimization routine now exist in the same range as defined by $-1 \leq \hat{x}_i \leq 1$.

2.3 Equations of Motion

2.3.1 Summary of Assumptions. Mathematical models of real systems are, at best, approximations of the actual systems. In almost all situations, it is impractical, and often impossible, to fully capture every aspect of a physical system in a mathematical representation. As discussed in Section 2.1, the requirement for making significant simplifying assumptions before a problem can be attempted is a prevalent issue in aircraft agility research. Though this effort avoids major assumptions, such as the assumption of a point mass, there are several minor assumptions which were made in the construction of the mathematical model. The assumptions inherent to the mathematical model used in this research are listed in Table 2.1. The assumptions

Table 2.1: Summary of the assumptions inherent in the mathematical model.

1. The aircraft is assumed to be a rigid body.
2. The aircraft is assumed to be symmetric about the x-z plane.
3. The aircraft does not expend fuel and therefore has a constant mass.
4. Control actuator dynamics are neglected.
5. No external wind or environment effects are included.
6. The Earth is assumed to be flat and non-rotating.
7. Gravity is assumed to be constant throughout the entire reference frame.

in Table 2.1 include common assumptions about the physical properties of the aircraft

as well as the properties of the physical environment. This collection of assumptions, though fairly numerous, does not alter the problem significantly.

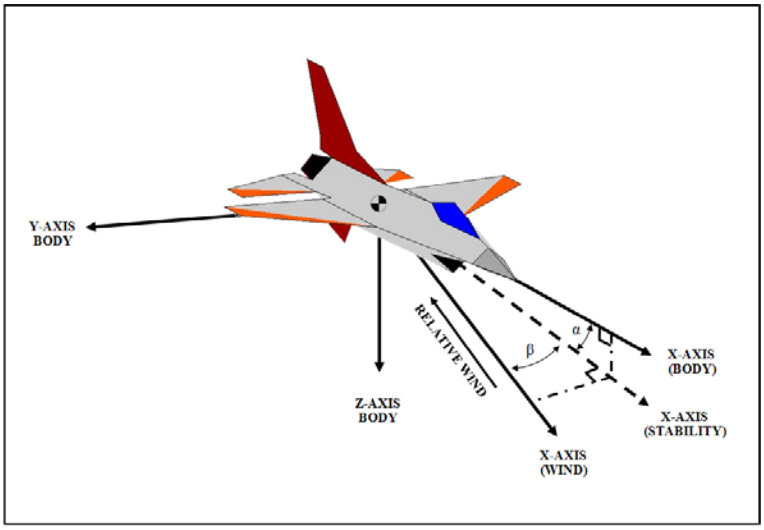

Figure 2.1: Aircraft Axis Definitions.

2.3.2 Coordinate systems. The development of the aircraft equations of motion, as used in this research, required three basic coordinate systems. The first of these is the basic aircraft body-axis system. This system, as seen in Figure 2.1, is defined as having it's origin at the aircraft's center of gravity (CG) with the x-axis out the nose of the aircraft, the y-axis out the right wing, and the z-axis out the bottom of the aircraft as defined in a standard right-handed system.

The second coordinate system used is the stability-axis system. The stability-axis system, as also seen in Figure 2.1, is a rotation of the body-axis system about the y-axis, by an angle of α, where α is the angle between the x-axis in the body-axis system and the relative wind. The direction cosine matrix (DCM) associated with this rotation is defined as follows:

$$C_b^s = \begin{bmatrix} \cos(\alpha) & 0 & \sin(\alpha) \\ 0 & 1 & 0 \\ -\sin(\alpha) & 0 & \cos(\alpha) \end{bmatrix} \tag{2.20}$$

where the subscripts b and s are respectively used to denote the body-axis and stability-axis systems. It should be noted that the main reason for writing the equations of motion in the stability-axis coordinate system, as will be done later, is that it offers some fairly significant advantages when attempting to linearize the system. Though linearization is not used in this research, the aircraft model used was previously developed for those purposes and for reasons of consistency, the equations of motion were kept in the stability-axis coordinate system.

Finally, an inertial reference system was required for the purpose of tracking the relative position of the aircraft throughout a maneuver since neither the body-axis system nor the stability-axis system is suitable for this purpose. The standard North-East-Down (NED) navigation coordinate system was used for this purpose. This is an earth fixed coordinate system with the origin at an arbitrary point on the surface of the Earth ($(0, 0, 0)$ in the case of this research) with the x-axis aligned with the North direction, the y-axis aligned with the East direction, and the z-axis pointed into the Earth as defined in a standard right-handed system. In this case, the system is also defined as the inertial reference system. The relationship between the navigation system and the body system is defined by the Euler angles in a standard yaw-pitch-roll sequence, as seen in the following DCM:

$$C_n^b = \begin{bmatrix} c\theta\ c\psi & c\theta\ s\psi & -s\theta \\ (-c\phi\ s\psi + s\phi\ s\theta\ c\psi) & (c\phi\ c\psi + s\phi\ s\theta\ s\psi) & s\phi\ c\theta \\ (s\phi\ s\psi + c\phi\ s\theta\ c\psi) & (-s\phi\ c\psi + c\phi\ s\theta\ s\psi) & c\phi\ c\theta \end{bmatrix} \tag{2.21}$$

where the subscript n is used to denote the navigation system. Also note that for space saving purposes in Equation 2.21 the trigonometric functions *sine* and *cosine* are abbreviated as s and c respectively.

As would be expected from the definition of the body-axis system, Figure 2.2 depicts the positive directions for each of the six degrees of freedom modeled in the equations of motion. The three translational degrees of freedom are denoted as posi-

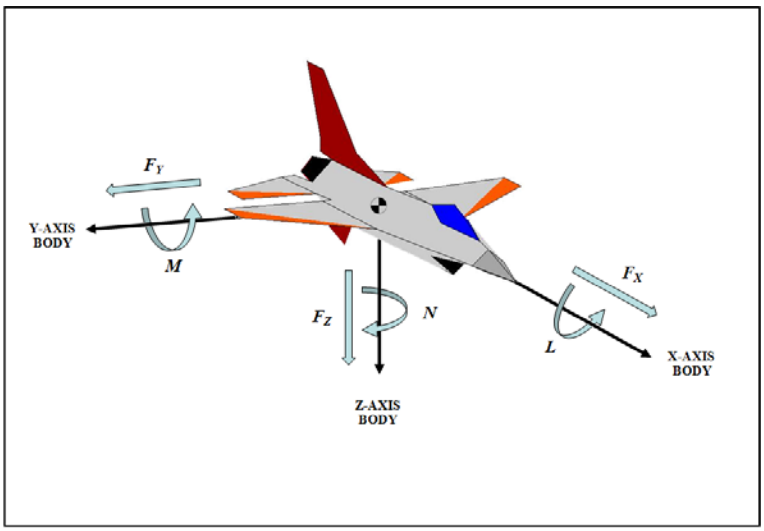

Figure 2.2: Degree of Freedoms Definitions.

tive in the directions of the positive axes and the three rotational degrees of freedom are defined as positive according to right handed rotations about the respective axes.

2.3.3 Aircraft Equations of Motion. The aircraft model used for this effort is based on the F-16 model presented by Stevens and Lewis [26]. The code that was used to simulate this model is contained in a set of MATLAB files created by previous AFIT students as replacements for the FORTRAN files provided by Stevens and Lewis. The original FORTRAN files as well as the derived MATLAB files have been used for numerous years and have been extensively tested to ensure correct results. The only modifications made to the model for this effort are all found in the physical properties of the aircraft that will be described in Chapter 4. The baseline dynamics and equations of motion remained the same.

The aircraft model is defined by the state vector

$$x = \left\{ \begin{array}{c} V_T \\ \alpha \\ \beta \\ \phi \\ \theta \\ \psi \\ P_s \\ Q_s \\ R_s \\ P_N \\ P_E \\ h \\ pow \end{array} \right\} = \left\{ \begin{array}{c} \text{Velocity} \\ \text{Angle of Attack} \\ \text{Sideslip Angle} \\ \text{Euler Roll Angle} \\ \text{Euler Pitch Angle} \\ \text{Euler Yaw Angle} \\ \text{Roll Rate} \\ \text{Pitch Rate} \\ \text{Yaw Rate} \\ \text{Northing Position} \\ \text{Easting Position} \\ \text{Vertical Position} \\ \text{Engine Thrust Dynamics Lag State} \end{array} \right\}. \tag{2.22}$$

Similarly, the control vector is defined as:

$$u = \left\{ \begin{array}{c} \delta_T \\ \delta_e \\ \delta_a \\ \delta_r \end{array} \right\} = \left\{ \begin{array}{c} \text{Throttle Control} \\ \text{Elevator Control} \\ \text{Aileron Control} \\ \text{Rudder Command} \end{array} \right\} \tag{2.23}$$

It should be noted here that the aircraft's altitude, h, is defined as the negative of the vertical position in the NED system and that the aircraft's pitch rate (Q_s) in the stability system is exactly equal to the pitch rate (Q_b) in the body-axis system since the transformation is about the y-axis and therefore does not affect the pitch rate. It is only denoted as Q_s here for purposes of consistency. In terms of the controls, positive control deflections are defined as those which cause negative rotations about their respective axes as previously defined. Using this convention, the equations of motion in the stability axis are found in Table 2.2.

Table 2.2: Aircraft Equations of Motion [26].

FORCE EQUATIONS

$$\dot{V_T} = \frac{F_T \cos(\alpha + \alpha_T)\cos(\beta) - D + \mathrm{m}g_1}{\mathrm{m}} \tag{2.24}$$

$$\dot{\alpha} = \frac{-F_T \sin(\alpha + \alpha_T) - L + \mathrm{m}g_3 + \mathrm{m}V_T(Q\cos(\beta) - P_s \sin(\beta))}{\mathrm{m}V_T \cos(\beta)} \tag{2.25}$$

$$\dot{\beta} = \frac{-F_T \cos(\alpha + \alpha_T)\sin\beta - C + \mathrm{m}g_2 - \mathrm{m}V_T R_s}{\mathrm{m}V_T} \tag{2.26}$$

KINEMATIC EQUATIONS

$$\dot{\phi} = P + \tan(\theta)(Q\sin(\phi) + R\cos(\phi)) \tag{2.27}$$

$$\dot{\theta} = Q\cos(\phi) - R\sin(\phi) \tag{2.28}$$

$$\dot{\psi} = \frac{Q\sin(\phi) + R\cos(\phi)}{\cos(\theta)} \tag{2.29}$$

MOMENT EQUATIONS

$$\dot{P} = \frac{J_{xz}[J_x - J_y + J_z]PQ - [J_z(J_z - J_y) + J_{xz}^2]QR + J_z l + J_x n}{J_x J_z - J_{xz}^2} \tag{2.30}$$

$$\dot{Q} = \frac{(J_z - J_x)PR - J_{xz}(P^2 - R^2) + m}{J_y} \tag{2.31}$$

$$\dot{R} = \frac{[(J_x - J_y)J_x + J_{xz}^2]PQ - J_{xz}[J_x - J_y + J_z]QR + J_{xz} l + J_x n}{J_x J_z - J_{xz}^2} \tag{2.32}$$

NAVIGATION EQUATIONS

$$\dot{P_N} = Uc\theta\ c\psi + V(-c\theta\ s\psi + s\phi\ s\theta\ c\psi) + W(s\phi\ s\psi + c\phi\ s\theta\ c\psi) \tag{2.33}$$

$$\dot{P_E} = Uc\theta\ s\psi + V(c\theta\ c\psi + s\phi\ s\theta\ s\psi) + W(-s\phi\ c\psi + c\phi\ s\theta\ s\psi) \tag{2.34}$$

$$\dot{h} = Us\theta - Vs\phi\ c\theta - Wc\phi\ c\theta \tag{2.35}$$

There are several variables and notations included in Table 2.2 for space and ease of reading purposes which must be defined for the reader. In the Force Equations, Equations 2.24-2.26, L, D, and C respectively define the Lift, Drag, and Side forces acting on the aircraft. In this same equation, the Thrust Force and Thrust Angle are represented by F_T and α_T respectively. Additionally, P_s is the roll rate in the stability axis and R_s is similarly the yaw rate in the stability axis. Finally, the wind axis gravity terms are defined as:

$$\begin{aligned} g_1 &= g(-c\alpha c\beta s\theta + s\beta s\phi c\theta + s\alpha c\beta c\phi c\theta) \\ g_2 &= g(c\alpha s\beta s\theta + c\beta s\phi c\theta - s\alpha s\beta c\phi c\theta) \\ g_3 &= g(s\alpha s\theta + c\alpha c\phi c\theta) \end{aligned} \tag{2.36}$$

The moment equations, Equations 2.30-2.32, contain the moment of inertia (J_x,J_y, J_z) and cross-product of inertia (J_{xz}, J_{xy}, J_{yz}) terms. Note that here it is assumed that the x-z plane is a plane of symmetry for the aircraft, which causes each of the cross-products of inertia terms, except J_{xz}, to be equal to zero. The moment equations also include the torque terms l, m, and n. It is through these torque terms, as depicted in Equations 2.37-2.39,

$$l = f(\beta, P, R, \delta_a, \delta_r), \tag{2.37}$$

$$m = f(V_T, \alpha, \dot{\alpha}, Q, \delta_T, \delta_e, T_\alpha), \tag{2.38}$$

$$n = f(\beta, P, R, \delta_a, \delta_r, T_\beta), \tag{2.39}$$

that the elevator, aileron, and rudder are able to exert their control over the aircraft [26]. Note that T_α and T_β in Equations 2.38 and 2.39 are the thrust offset angles, both of which are assumed to be zero for this research. Additionally, the Navigation Equations, Equations 2.33-2.35, contain the velocity components U, V, and W in the body-axis system. These components of velocity are related to V_T, α, and β through

Equations 2.40-2.42.

$$V_T = \sqrt{U^2 + V^2 + W^2} \tag{2.40}$$

$$\alpha = \tan^{-1}\left(\frac{W}{U}\right) \tag{2.41}$$

$$\beta = \sin^{-1}\left(\frac{V}{V_T}\right) \tag{2.42}$$

The addition of the engine thrust dynamics lag state, pow, is an artifact of the specific aircraft model used in this research. As will be discussed later, this state will be represented as a first-order lag as in Equation 2.43,

$$\dot{pow} = \frac{1}{T}(pow_c - pow), \tag{2.43}$$

where T is the lag constant and pow_c is the commanded power setting which is a function of the commanded throttle setting, δ_T.

III. Modeling & Implementation

3.1 Aircraft Models

Three aircraft models were used for this endeavor, all of which are based on the NASA-Langley F-16 wind tunnel test data presented by Stevens and Lewis [26] and the mathematical model derived from that data. In order to demonstrate the difference in time-optimal trajectories for various aircraft, three derivatives of the basic F-16 model were utilized. The three models used include a baseline F-16 model, a model with increased thrust, and a model with increased wing area. These changes were chosen as a way of modifying the two most important aircraft performance parameters: thrust-to-weight ratio (T/W) and wing loading (W/S).

With all else being equal, an aircraft with higher T/W will be able to reach higher velocities, climb faster, accelerate quicker and sustain higher turn rates [19]. On the other hand, an aircraft with a lower W/S will be capable of lower stall speeds and tighter instantaneous turns [19]. Together, the three models should simulate a baseline fighter aircraft, a second fighter which is more prone to vertical maneuvers and a third aircraft which is more prone to horizontal maneuvers.

3.1.1 Physical Layout. The F-16, as depicted in Figure 3.1, is a classic single engine multi-role tactical aircraft design. The design features a single vertical tail and a wing and stabilizer configuration which creates a neutrally stable platform. Control of the aircraft is obtained through the use of the ailerons, elevators, and rudder. Note that the actual F-16 elevators are differentially controllable, which allows them to roll the aircraft, especially during transonic speeds. The mathematical model does not include the ability to differentially articulate the elevators which means that the elevators cannot be used for roll control. The aircraft has a single afterburning turbofan engine along the centerline which is assumed to act along the x-axis in the body system. The configuration in Figure 3.1 is the nominal configuration of the baseline aircraft model. The two model variants developed in during this research effort are notional only and are therefore not physically depicted here.

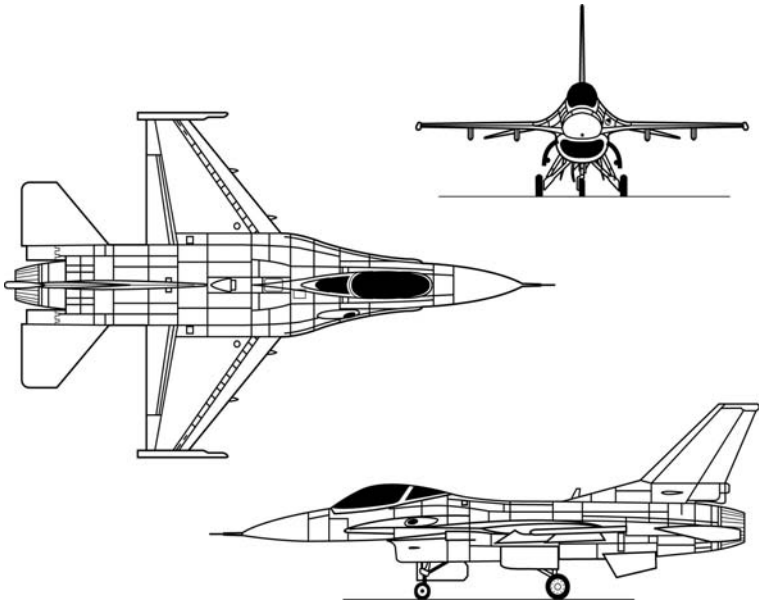

Figure 3.1: Aircraft Layout [1].

3.1.2 Physical Parameters. The relevant physical parameters for the baseline aircraft model are summarized in Table 3.1. These values are obtained from the mathematical model description provided by Stevens and Lewis in Reference [26] and are all assumed to remain constant throughout each simulation. The only value in Table 3.1 which deviates from the Stevens and Lewis model is the value of the CG location. The original CG location value was actually 0.35 $\bar{c}$, but, as will be discussed in Chapter 4, it was necessary to move the CG location to 0.25 $\bar{c}$ for stability reasons.

Table 3.1: Summary of Baseline Aircraft Model Physical Parameters

Parameter	**Value**	
Weight (W)	20,500	lbs
J_x	9,496	$slug \cdot ft^2$
J_y	55,814	$slug \cdot ft^2$
J_z	63,100	$slug \cdot ft^2$
J_{xz}	982	$slug \cdot ft^2$
CG Location	25	$\%\ MAC$
Span (b)	30	ft
Area (S)	300	ft^2
MAC ($\bar{c}$)	11.32	ft

As previously mentioned, the thrust-to-weight ratio and wing loading of the two notional models were varied by increasing the available thrust or increasing the wing area of the model. Table 3.2 summarizes the changes to the baseline model which were used to create the two notional models. Note that Max Thrust is defined as the static thrust available at sea level. These deviations are equivalent to a 25% increase in available thrust for Model # 2 and a 25% increase in wing area for Model # 3.

Table 3.2: Summary of Aircraft Models Deviation from Baseline Model

Parameter	**Model # 1**	**Model # 2**	**Model # 3**	
Weight (W)	20,500	20,500	20,500	lbs
Max Thrust (T)	20,000	25,000	20,000	lbs
Wing Area (S)	300	300	375	ft^2
Wing Loading (W/S)	68.33	68.33	54.67	lbs/ft^2
Thrust-to-Weight Ratio (T/W)	0.9756	1.2195	0.9756	–

3.1.3 Aerodynamic Model. The aerodynamic model consists of a series of table lookup routines which are used to calculate the aerodynamic force and moment buildup. These calculations are all completed in the body-axis frame and then transferred to the stability-axis system and navigation system as required. A summary of the aerodynamic lookup tables is found in Table 3.3. The sign convention for each of the coefficients adhere to the conventions outline in Figure 2.2. A separate routine is also provided to model the standard atmosphere.

The data in these lookup tables was modified from the original NASA-Langley data by Stevens and Lewis to include the effects of the F-16's leading-edge flap. The data for the leading-edge flap, the actual deployment of which is scheduled based on Angle-of-Attack (AOA) and Mach Number, was originally contained in several other lookup tables. By merging the data tables, Stevens and Lewis were able to significantly reduce the number of table lookups required while still maintaining the leading-edge flap effects minus the associated actuator dynamics [26].

Table 3.3: Summary of Aerodynamic Lookup Tables.

Coefficient	**Component**	**Function of**
Damping Derivatives	Basic	α
X-axis Force (C_x)	Basic	α, δ_e
Y-axis Force (C_y)	Basic	β, δ_a, δ_r
Z-axis Force (C_z)	Basic	α, δ_a, δ_e
Rolling Moment (C_l)	Basic	α, β
- Aileron Component	δ_a	α, β
- Rudder Component	δ_r	α, β
Pitching Moment (C_m)	Basic	α, δ_e
Yawing Moment (C_n)	Basic	α, β
- Aileron Component	δ_a	α, β
- Rudder Component	δ_r	α, β

3.1.4 Engine Model. The engine model is based on a model developed by NASA-Langley in parallel with their wind tunnel measurement efforts. Again, this data is provided by Stevens and Lewis [26]. The engine model is comprised of two MATLAB routines. The first routine is a model of the engine power response to the power setting commanded and is modeled as a basic first-order lag with a variable time constant which is a function of the actual engine power setting (pow) and the commanded power setting (pow_c). The second routine is a table lookup of the thrust values as a function of the power setting (pow), the aircraft's altitude (h), and the current Mach Number (M). The lookup tables include data for idle power, military power, and maximum power, where the change from military power setting to maximum power settings occur when $pow \geq 0.77$ [26]. Also of note is that the engine is modeled as having a constant angular momentum of 160 $slug \cdot ft^2/s$.

3.1.5 Model Control Actuator Limits. Within the mathematical model, the control surface actuators are modeled with both deflection and rate limits. Additionally, they are modeled with a basic first-order lag. A summary of the limits on the control system is provided in Table 3.4.

Table 3.4: Summary of control limits inherent in mathematical model [26].

Control	Deflection Limit	Rate Limit	Time Constant
Elevator	$\pm 25.0^\circ$	$60^\circ/s$	0.0495 $s\ lag$
Aileron	$\pm 21.5^\circ$	$80^\circ/s$	0.0495 $s\ lag$
Rudder	$\pm 30.0^\circ$	$120^\circ/s$	0.0495 $s\ lag$

3.1.6 Model State Limits. As will be shown later, the solution space for the trajectory optimization problem is defined by the physical limits on state and control variables. Before the optimization routine will work correctly, there are two key sets of limits which must be addressed: those which are defined by the physics of the problem, and those which are inherent in the mathematical model. Limits which are defined by the physics of the problem are fairly intuitive. For example, except for a few rare situations, none of which were considered here, the altitude of an aircraft is limited by $h \geq 0$.

On the other hand, limits inherent in the mathematical model, though arguably more important to the optimization routine, are not nearly as obvious without a good working knowledge of the model being used. These limits correspond to the limits of the model itself and are the result of various assumptions which were made in the construction of the mathematical model. In the case of the F-16 model used in this effort, the majority of these limits are the result of incomplete data sets within table lookups. For example, without an intimate knowledge of the aircraft model, one would not know that the altitude is actually restricted to $0\ ft \leq h \leq 50,000\ ft$ by the simple fact that these are the limits of the available altitude data from the original wind tunnel testing.

Table 3.5 contains a summary of the limits on the state variables which are inherent in the F-16 mathematical model. One item of note within this table is the upper limit on AOA. The data lookup tables support angles as high as 45°, but the upper limit was lowered to 25° to avoid stall and the deep stall issues inherent in the F-16 model [26]. Allowing the optimization routine to search in this region would

simply waste time and possibly confuse the algorithm. The remaining limits are based on the limits of the data lookup tables for various components within the model.

Table 3.5: Summary of state limits inherent in mathematical model.

Parameter	**Minimum**	**Maximum**	**Units**
Mach Number (M)	0	1	–
Altitude (h)	0	50,000	ft
Angle of Attack (α)	-10	45	$degrees$
Sideslip Angle (β)	-30	30	$degrees$

3.2 Optimization Software

Solutions for the complex trajectory optimization problems in this research were possible through the use of a new and novel dynamic optimization software package, which was created by researchers at the Naval Post-Graduate School and published by Elissar, LLC. This package, which is provided as a set of MATLAB p-code, exploits the advantages of Pseudospectral Methods to create a user friendly and versatile optimization package.

The DIDO software package, named after Queen Dido of Carthage who was the first person to solve a dynamic optimization problem [21], is a robust dynamic optimization package which is specifically tailored to the optimal control problem. Through the use of this package, a user is able to define an optimal control problem in a very intuitive fashion.

3.2.1 Problem Definition Structure. Within the DIDO framework, trajectory optimization problems are defined by sets of equality and inequality constraints. These constraints fully define the system dynamics, the valid solution space, and the performance index for the optimization problem. This setup is accomplished through the use of five specific files, which are basically the only input to the optimization routine.

3.2.1.1 Problem Setup File. The first, and most important, of the DIDO input files is the Problem Setup File. This file is used to define the numerical values of the scaling factors and constraints for each of the state and control variables. In this capacity, the values in this file completely define a specific maneuver and this file is therefore the only file which needs to be changed to simulate a different maneuver. To this end, the setup file contains the initial and target state values as well as any state values which are prescribed along the trajectory path as described in Equation 2.13.

Additionally, the setup file contains the limit values for the path and box constraints from Equations 2.14-2.16. Unlike the other constraint equations, which are explicitly defined in the additional input files, the box constraint equations are assumed to be in the form of Equations 2.15 and 2.16 and DIDO enforces these constraints internally.

It should be noted that this structure is a slight deviation from the format suggested in the DIDO User's Manual [21], in which the numerical constraint information is all included in the problem's Main file. This change was made due to the simple fact that, with a model comprised of 13 states and 4 controls, the amount of information needed to define the problem warranted its own file for readability purposes.

3.2.1.2 Dynamic Constraints File. The second DIDO input file, the dynamic constraints file, contains the problem's differential equations and is very similar in structure to the input function for the various initial value problem solvers, such as *ode23*, within MATLAB. The dynamics file receives the values of the state and control variables at a specific point along a notional trajectory and then calculates the differential values of the state variables and returns those values to DIDO. DIDO then compares this information to what it predicted the differentials to be based on the derivatives of the interpolating polynomials and then updates that prediction accordingly.

In this capacity, the dynamic constraints file is required to contain all of the functions and equations necessary to determining the derivatives of the state variables. For this research, this means that the dynamic constraints file is the equivalent of the F file presented in Stevens and Lewis [26] and contains the entire mathematical model of the aircraft motion dynamics and all of the requisite table lookup calls.

One consideration for this file is that the dynamics file must contain, or be able to retrieve, the system's scaling factors. This is necessary for situations where the dynamic equations are written in the unscaled unit system since the input states provided by DIDO are already scaled. Similarly, the state derivatives returned to DIDO must also be returned to the scaled unit system.

3.2.1.3 Event Constraints File. The Events file contains the event constraint functions laid out in Equation 2.13 as functions of the state variables along the trajectory. Note that the Events file does not contain the actual target values for the desired state points as previously laid out in the Problem Setup file, just the equations needed to determine how closely the trajectory meets those requirements.

In the case of maneuvers which are defined by an initial state and a final target state, the Events file contains a function for each of the state variables which are prescribed at the initial state and another set of functions for each of the state variables that are used to define the target state. Any additional points which the trajectory must pass through would also be defined in the Events file.

3.2.1.4 Cost Constraints File. The Cost Constraint file is where the user defines the cost function which will be used for the problem. This simple file breaks the Bolza cost function from Equation 2.11 into the sum of the single point Mayer cost function and the integral Lagrange cost, thus allowing the user to define an event cost as well as a running cost.

3.2.1.5 Path Constraints File. Similar in structure to the Events file, the Path Constraints file contains the path constraint equations from Equation 2.14.

This file is an optional addition to the problem since it is not always necessary to restrict the path of the states or controls.

3.2.2 Method Verification. In order to verify both that the DIDO software worked as advertised and that it was implemented correctly, several problems with known solutions were simulated for comparison purposes. The most representative of these comparisons was a sample problem posed and solved by Bryson [6]. The problem (Problem 4.5.24 [6]), is to find the Minimum Time to Climb for a 727 aircraft climbing 2000 ft from sea level and returning to its initial velocity and flight path angle. The equations of motion for the aircraft, in normalized units, are simplified to the following four equations:

$$\dot{V} = T\cos(\alpha + \epsilon) - C_D V^2 - \sin(\gamma), \tag{3.1}$$

$$V\dot{\gamma} = T\sin(\alpha + \epsilon) - C_L V^2 - \cos(\gamma), \tag{3.2}$$

$$\dot{h} = V\sin(\gamma), \tag{3.3}$$

$$\dot{x} = V\cos(\gamma), \tag{3.4}$$

where V, γ, and h are the state variables and α is the only control variable in this free final time problem.

The results, as presented by Bryson, are shown in Figure 3.2(a) and (b) where the solid blue lines are the actual response and the dashed red lines are the steady-state optimal solution. These results, which match those provided in the book, were found by using the sample MATLAB script files provided by Bryson and the internal MATLAB function *fmincon*. On the other hand, solving the same problem through the use of DIDO provides the results found in Figure 3.2(c) and (d).

Comparing the results from the baseline Bryson solutions and the DIDO output reveals a few interesting discrepancies. First, though the results are very similar, the optimum time values provided by the two methods do not match. As seen in Table 3.6,

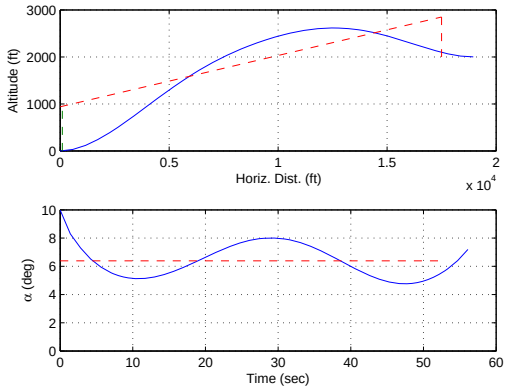

(a) Bryson State and Control Trajectory

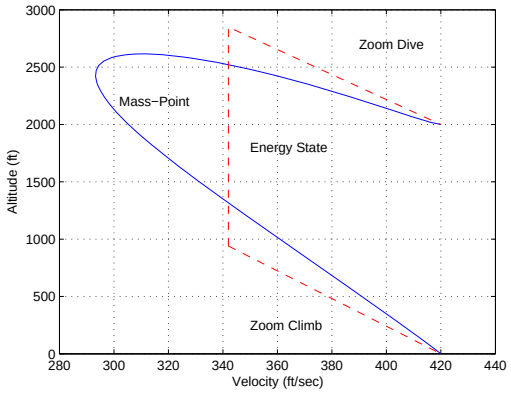

(b) Bryson Aircraft Energy Response

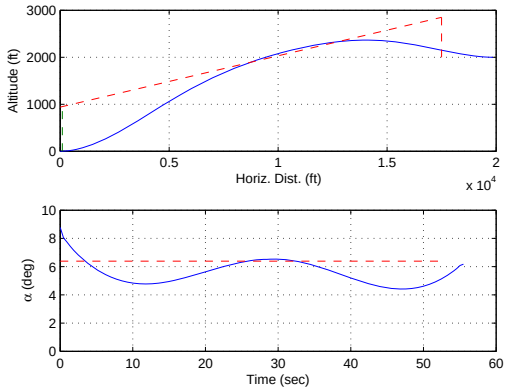

(c) DIDO State and Control Trajectory

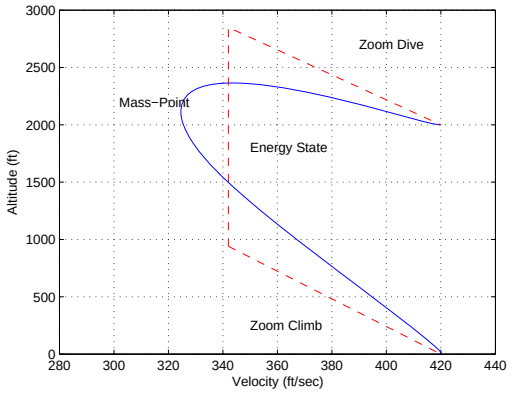

(d) DIDO Aircraft Energy Response

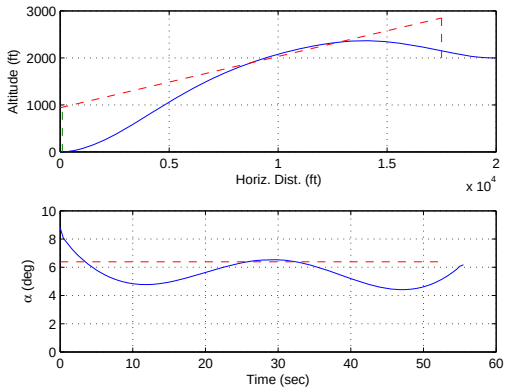

(e) Propagated State and Control Trajectory

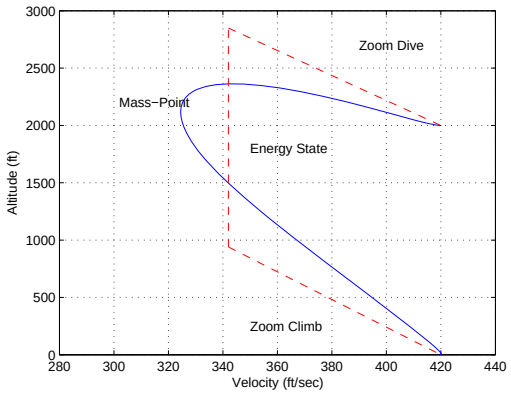

(f) Propagated Aircraft Energy Response

Figure 3.2: Results for the Bryson 727 sample optimization problem.

the DIDO solution results in a final time over a full second less than that predicted by Bryson through the use of *fmincon*.

Parameter	***fmincon***	**DIDO**	
t_f	56.114	55.003	*sec*

Table 3.6: Bryson 727 problem solution comparison.

Since, as previously discussed, the results from DIDO are an approximation of the actual solution, it is possible that the results are a poor approximation of the actual aircraft trajectory. The simple way to check that the approximation is valid is to propagate the aircraft states over time using a numerical integration scheme. The results of propagating the states forward using MATLAB's *ode45* function are found in Figure 3.2(e) and (f). The propagated results match the approximate trajectories almost exactly, which means that the aircraft is actually capable of reaching the target state by following the trajectory predicted by DIDO.

The next obvious question is: why are the DIDO results better than the *fmincon* results? The differences between the results are caused by a conglomeration of several different factors. First, as noted by Bryson in the comments in his sample code [6], this problem has very poor global convergence properties and converges very slowly when not near what it deems to be the optimal solution. Second, the guess for the DIDO problem setup and the *fmincon* setup are different. The guess given in the *fmincon* is actually the optimal control history and the final solution is limited to be within 10% of the guess. This is not a good way to determine an optimal solution, but this was the way the code was provided by Bryson, most likely as the result of numerous iterations, and deviations from this method result in the algorithm converging to a different local minimum. The guess of the control history provided to DIDO is a constant $\alpha = 0$, which is neither realistic nor representative of the actual solution. This was done to demonstrate the robustness inherent within DIDO since giving a similar guess in the *fmincon* method results not only in it failing to find the optimal solution, but in it actually failing to converge to any solution. Additionally, the solution found from using DIDO is also replicated if the initial guess is reverted back to the guess provided by Bryson. This shows that the pseudospectral method is not as susceptible to falling into non-optimal local minimums as the *fmincon* method.

3.3 Simulation Setup

3.3.1 Scaling and Balancing. As previously mentioned, the choice of scaling and balancing factors can significantly affect the results of an optimization routine. To that end, each state and control parameter was converted to a unitless system with typical values ranging from $-1 \leq x \leq 1$ through the use of Equation 2.19. The scaling and balancing factors chosen to accomplish this are listed in Table 3.7. These terms were chosen based on the range of values which each parameter is expected to see for a typical maneuver. Note that the boundaries of the typical values are not necessarily the same as the box constraints, which will be addressed later.

Table 3.7: Scaling and balancing factors used in the optimization scheme.

Parameter	**Typical Values**			**Scaling Factor**	**Balancing Factor**
	Lower	Upper			(Unitless)
V	0	1000	ft/s	500	-1
α	$-10°$	$25°$	deg	$17.5°$	-0.4286
β	$-15°$	$15°$	deg	$15°$	0
ϕ	$-180°$	$180°$	deg	$180°$	0
θ	$-87°$	$87°$	deg	$87°$	0
ψ	$-180°$	$180°$	deg	$180°$	0
P	$-180°$	$180°$	deg/s	$180°$	0
Q	$-45°$	$45°$	deg/s	$45°$	0
R	$-45°$	$45°$	deg/s	$45°$	0
P_N	-25000	25000	ft	25000	0
P_E	-25000	25000	ft	25000	0
h	10000	30000	ft	10000	-2
pow	0	100		50	-1
δ_T	0	1		0.5	-1
δ_e	$-24°$	$24°$	deg	$24°$	0
δ_a	$-21.5°$	$21.5°$	deg	$21.5°$	0
δ_r	$-30°$	$30°$	deg	$30°$	0
t	0	100	s	50	-1

3.3.2 Box Constraints. One of the most critical steps in solving the trajectory optimization problem for a fairly complicated 6-DOF mathematical model, was the development of the box constraints. As previously discussed, the box constraints

must include the limitations of the model, the physical limits, and reasonably large bounds on otherwise unbounded parameters. Table 3.8 lists the box constraints utilized in the Problem Setup File in both the original and scaled and balanced unit systems.

Table 3.8: Box constraints used in the optimization scheme.

Parameter	**Standard Units**			**Designer Units**	
	Lower	Upper		Lower	Upper
V	0.1	1000	ft/s	-0.9998	1
α	$-10°$	$25°$	deg	-1	1
β	$-30°$	$30°$	deg	-2	2
ϕ	$-540°$	$540°$	deg	-3	3
θ	$-87°$	$87°$	deg	-1	1
ψ	$-540°$	$540°$	deg	-3	3
P	$-270°$	$270°$	deg/s	-1.5	1.5
Q	$-180°$	$180°$	deg/s	-4	4
R	$-180°$	$180°$	deg/s	-4	4
P_N	$-100,000$	$100,000$	ft	-4	4
P_E	$-100,000$	$100,000$	ft	-4	4
h	0	$50,000$	ft	-2	3
pow	0	100		-1	1
δ_T	0	1		-1	1
δ_e	$-24°$	$24°$	deg	-1	1
δ_a	$-21.5°$	$21.5°$	deg	-1	1
δ_r	$-30°$	$30°$	deg	-1	1
t	0.001	250	s	-0.99998	4

There are several important pieces of information which fed into the development of these constraints. First, and foremost, were the model limitations imposed by the table lookup data in the aerodynamic and engine models. These limits defined the box constraints for V, α, β, h, pow, δ_T, δ_e, δ_a and δ_r. The lower limits of V and t are chosen as small numbers which were relatively close to zero without creating the singularity which an actual value of zero would cause. Similarly, the constraints on θ were chosen to avoid the inherent singularity at $\pm 90°$. The remaining limits on ϕ, ψ, P, Q, R, P_N, P_E, and the upper limit for t were chosen, after experimentation with the model, as reasonably large values which are used in place of $\pm\infty$ in order

to place reasonable limits on the solution space and subsequently reduce the required run time for the optimization scheme without impacting the final solution.

3.3.3 Maneuvers. In order to evaluate the effectiveness and utility of the trajectory optimization approach in determining aircraft agility characteristics, a wide range of maneuvers were simulated. The simulated maneuvers have been divided into three main categories: Demonstration Maneuvers, Agility Maneuvers, and Compound Maneuvers. Each of the maneuvers starts from an initial state with the aircraft trimmed for steady, wings level flight with the spatial setup defined in Table 3.9. The actual trimmed values of the remaining states and controls are found through the use of a trimmer routine modified from Stevens and Lewis [26] and vary slightly with each aircraft due to their thrust and surface area differences.

Table 3.9: Initial spatial setup for each maneuver.

Parameter	Initial Condition	
V	500	ft/s
P_N	0	ft
P_E	0	ft
h	$20,000$	ft

From this initial state, each of the three aircraft models is tasked to perform each maneuver in a time optimal fashion for later comparison and analysis.

3.3.3.1 Demonstration Maneuvers. The maneuvers in the Demonstration Maneuvers category are used as an initial demonstration of the utility of trajectory optimization. Through the three maneuvers in this category, the basic validity of the approach is demonstrated and verified before moving on to the more rigorous maneuvers in the Agility Maneuvers category.

Northing Position Change

The first maneuver in the Demonstration category is the Northing Position Change. In this maneuver, each aircraft is tasked to move downrange by 10,000 ft as

fast as possible. The basic setup is intended to resemble the classic *Brachistochrone* problem since this is a very common initial example in optimization literature. The brachistochrone problem, as posed by John Bernoulli in 1696 [7], is to find the shape of a frictionless wire which would allow a bead sliding along it to move from one point to another while only being acted upon by gravity. The solution is a shape known as a cycloid, which is defined as a path which is generated by a point on a circle that is rolling in a horizontal direction without slipping [7].

Though the Northing Position Change Maneuver differs from the classic brachistochrone maneuver through the inclusion of the aircraft dynamics as well as an initial velocity, the maneuver is intentionally designed to produce a similar trajectory. The maneuver is numerically defined by two events: the initial state, and the target state. Starting from the initial state discussed previously, the aircraft is tasked to transition to the state described in Table 3.10. Note that the variables with a target value of "–" are considered to be free variables and are allowed to take on any value within the solution space at that point. For this maneuver, the only restriction on the final state is that the aircraft must be 10,000 ft North of its original position.

Table 3.10: Numerical definition of the Northing Position Change maneuver.

State Variable	**Initial State**	**Target State**	
V	500	–	ft/s
α	α_{trim}	–	deg
β	0	–	deg
ϕ	0	–	deg
θ	θ_{trim}	–	deg
ψ	0	–	deg
P	0	–	deg/s
Q	0	–	deg/s
R	0	–	deg/s
P_N	0	$10,000$	ft
P_E	0	–	ft
h	$20,000$	–	ft
pow	pow_{trim}	–	

Unconstrained 3-D Position Change

The Unconstrained 3-D position Change maneuver, as defined in Table 3.11, is intended to demonstrate an out-of-plane maneuver. For this maneuver, each aircraft is tasked to transition to a point 10,000 ft North and East of its original position and return to the original altitude. The remaining states are left as free variables.

Table 3.11: Numerical definition of the Unconstrained 3-D Position Change maneuver.

State Variable	Initial State	Target State	
V	500	–	ft/s
α	α_{trim}	–	deg
β	0	–	deg
ϕ	0	–	deg
θ	θ_{trim}	–	deg
ψ	0	–	deg
P	0	–	deg/s
Q	0	–	deg/s
R	0	–	deg/s
P_N	0	$10,000$	ft
P_E	0	$10,000$	ft
h	$20,000$	$20,000$	ft
pow	pow_{trim}	–	

Constrained 3-D Position Change

Building on the previous maneuver, the Constrained 3-D Position Change maneuver tasks the aircraft with performing the same basic maneuver, but further constrains the target state. As defined in Table 3.12, this maneuver requires that the aircraft move to a point 10,000 ft North and East of its initial position and, aside from the position, return to its original wings level, trimmed state.

3.3.3.2 Agility maneuvers. After demonstrating the utility and robustness of the trajectory optimization scheme, the maneuvers in the Agility Maneuvers category are intended to be more rigorous tests of the limits of each aircraft's capabilities.

Table 3.12: Numerical definition of the Constrained 3-D Position Change maneuver.

State Variable	Initial State	Target State	
V	500	V_0	ft/s
α	α_{trim}	α_0	deg
β	0	β_0	deg
ϕ	0	ϕ_0	deg
θ	θ_{trim}	θ_0	deg
ψ	0	ψ_0	deg
P	0	P_0	deg/s
Q	0	Q_0	deg/s
R	0	R_0	deg/s
P_N	0	$10,000$	ft
P_E	0	$10,000$	ft
h	$20,000$	h_0	ft
pow	pow_{trim}	pow_0	

Bank Angle Capture

The first agility maneuver, the Bank Angle Capture maneuver, is one which is widely suggested as a possible agility metric. This maneuver, as defined in Table 3.13, requires that the aircraft achieve and hold a 90° bank angle. To make the maneuver more rigorous, the aircraft is also required to return to its initial heading, velocity, and cross-range position.

Unconstrained Heading Capture

Similar to the Bank Angle Capture maneuver, the Unconstrained Heading Capture maneuver is intended to test the nose pointing capabilities of an aircraft. For this maneuver the aircraft is required to reorient its nose to a direction defined by $\theta = 0°$ and $\psi = 45°$. Though the aircraft must capture this attitude, there are not any requirements for the aircraft to actually be moving in that specific direction. In that context, this maneuver is intended to simulate a situation where a pilot would like to rapidly reorient the nose of the aircraft to a point where a weapon may be employed as quickly as possible. The numerical definition of this maneuver is found in Table 3.14.

Table 3.13: Numerical definition of the Bank Angle Capture maneuver.

State Variable	Initial State	Target State	
V	500	V_0	ft/s
α	α_{trim}	–	deg
β	0	–	deg
ϕ	0	90°	deg
θ	θ_{trim}	–	deg
ψ	0	ψ_0	deg
P	0	P_0	deg/s
Q	0	Q_0	deg/s
R	0	R_0	deg/s
P_N	0	–	ft
P_E	0	P_{E_0}	ft
h	$20,000$	–	ft
pow	pow_{trim}	–	

Table 3.14: Numerical definition of the Unconstrained Heading Capture maneuver.

State Variable	Initial State	Target State	
V	500	–	ft/s
α	α_{trim}	–	deg
β	0	–	deg
ϕ	0	–	deg
θ	θ_{trim}	0	deg
ψ	0	45°	deg
P	0	P_0	deg/s
Q	0	Q_0	deg/s
R	0	R_0	deg/s
P_N	0	–	ft
P_E	0	–	ft
h	$20,000$	–	ft
pow	pow_{trim}	–	

Constrained Heading Capture

Taking the Unconstrained Heading Capture a step further, the Constrained Heading Capture maneuver requires that the aircraft change its course to a heading of $\psi = 90°$ and return to its original steady level flight conditions. The numerical definition for the Constrained Heading Capture maneuver is found in Table 3.15.

Table 3.15: Numerical definition of the Constrained Heading Capture maneuver.

State Variable	Initial State	Target State	
V	500	V_0	ft/s
α	α_{trim}	α_0	deg
β	0	β_0	deg
ϕ	0	ϕ_0	deg
θ	θ_{trim}	θ_0	deg
ψ	0	90°	deg
P	0	P_0	deg/s
Q	0	Q_0	deg/s
R	0	R_0	deg/s
P_N	0	–	ft
P_E	0	–	ft
h	$20,000$	h_0	ft
pow	pow_{trim}	pow_0	

Position-Free Heading Reversal

The Position-Free Heading Reversal is the first of three heading reversal maneuvers designed to fully tax the capabilities of each aircraft. Similar to the Bank Angle Capture maneuver, the generic heading reversal maneuver is often suggested as a aircraft agility metric. Additionally, previous investigation of this specific maneuver by Bocvarov [4] provides a good means of comparing the full 6-DOF results with results found through the use of a point-mass simplifying assumption.

In this maneuver, as defined in Table 3.16, the aircraft is tasked to reverse its heading and recapture the initial steady level flight conditions in minimum time. To that end, the only free variables in this maneuver are the three position variables P_N, P_E and h.

Position-Fixed Heading Reversal

The Position-Fixed Heading Reversal further constrains the target state of the Position-Free Heading Reversal maneuver. In this maneuver, the aircraft is required to fully recapture its initial state with the only variation being the new heading angle

Table 3.16: Numerical definition of the Position-Free Heading Reversal maneuver.

State Variable	Initial State	Target State	
V	500	V_0	ft/s
α	α_{trim}	α_0	deg
β	0	β_0	deg
ϕ	0	ϕ_0	deg
θ	θ_{trim}	θ_0	deg
ψ	0	$180°$	deg
P	0	P_0	deg/s
Q	0	Q_0	deg/s
R	0	R_0	deg/s
P_N	0	–	ft
P_E	0	–	ft
h	$20,000$	–	ft
pow	pow_{trim}	pow_0	

of $\psi = 180°$. For comparison purposes, this maneuver was also previously investigated by Bocvarov [4].

Table 3.17: Numerical definition of the Position-Fixed Heading Reversal maneuver.

State Variable	Initial State	Target State	
V	500	V_0	ft/s
α	α_{trim}	α_0	deg
β	0	β_0	deg
ϕ	0	ϕ_0	deg
θ	θ_{trim}	θ_0	deg
ψ	0	$180°$	deg
P	0	P_0	deg/s
Q	0	Q_0	deg/s
R	0	R_0	deg/s
P_N	0	P_{N_0}	ft
P_E	0	P_{E_0}	ft
h	$20,000$	h_0	ft
pow	pow_{trim}	pow_0	

Position-Free Heading Reversal with Altitude Floor

A third twist on the Heading Reversal maneuvers is the inclusion of a restrictive minimum altitude. As will be shown later, the inclusion of an altitude floor will only

have a large impact on the Position-Free Heading reversal maneuver, so this is the only one which is fully investigated. The numerical definition for this maneuver is exactly the same as that found in Table 3.16 for the Position-Free Heading Reversal. The difference between the two maneuvers is that the Box Constraints for this maneuver have been altered such that the minimum altitude is raised to 20,000 ft, which means that the aircraft is not allowed to loose any altitude during this maneuver.

Initial State Capture

Unlike the Position-Fixed Heading Reversal, the Initial State Capture maneuver requires the aircraft to fully recapture its initial state without any further variations. This means that the aircraft must return to trimmed, steady-level flight at its initial position, attitude, and velocity. The numerical definition of this maneuver is found in Table 3.18.

Table 3.18: Numerical definition of the Initial State Capture maneuver.

State Variable	Initial State	Target State	
V	500	V_0	ft/s
α	α_{trim}	α_0	deg
β	0	β_0	deg
ϕ	0	ϕ_0	deg
θ	θ_{trim}	θ_0	deg
ψ	0	ψ_0	deg
P	0	P_0	deg/s
Q	0	Q_0	deg/s
R	0	R_0	deg/s
P_N	0	P_{N_0}	ft
P_E	0	P_{E_0}	ft
h	$20,000$	h_0	ft
pow	pow_{trim}	pow_0	

Initial State Capture with Altitude Floor

As will be shown later, the Initial State Capture maneuver will result in a trajectory which utilizes an altitude loss to gain energy early in the maneuver. The

final agility maneuver, the Initial State Capture with Altitude Floor, is designed to remove the altitude loss option from the Initial State Capture maneuver. The numerical definition for this maneuver is exactly the same as that found in Table 3.18 for the Initial State Capture. The only difference between the two maneuvers is that the Box Constraints for this maneuver have been altered such that the minimum altitude is raised to 20,000 ft, which means that the aircraft is not allowed to loose any altitude during this maneuver.

3.3.3.3 Compound Maneuvers. Each of the maneuvers in the Demonstration and Agility categories have one major characteristic in common; they only look at the transition from an initial state to a final state. The next step in developing more complicated maneuvers for both agility evaluation and aircraft control in general is to specify a series of states which the aircraft must transition through on its way to a target state. With this observation, a discussion is warranted on the difference between a trajectory which is built by minimizing the time to each point and a trajectory which is built by minimizing the time through each point.

As noted by Miles [18], the minimum time trajectory through a series of points is almost always not the collection of minimum time trajectories between the points in question. The illustration in Figure 3.3 depicts this phenomenon by showing two notional minimum time trajectories through four points. In the first case, the orange line represents the path an aircraft might follow if it were tasked to reach each successive point in minimum time. Traversing from the initial point to Point A in minimum time would produce a straight line acceleration. Moving from Point A to Point B in minimum time would ideally be a straight line between the two, but the initial trajectory has set the aircraft up with a large velocity in the direction of Point A which causes the aircraft to execute a turn to reacquire a path to Point B. This same phenomenon is then repeated for the leg from Point B to Point C.

On the other hand, if the aircraft were tasked to reach Point C in minimum time while passing through Points A and B, the trajectory might look something like the

maroon line. In this case, the aircraft reaches Point A after the first aircraft, but by executing a heading change the aircraft has set itself up for a straight line acceleration through Points A and B on its way to Point C.

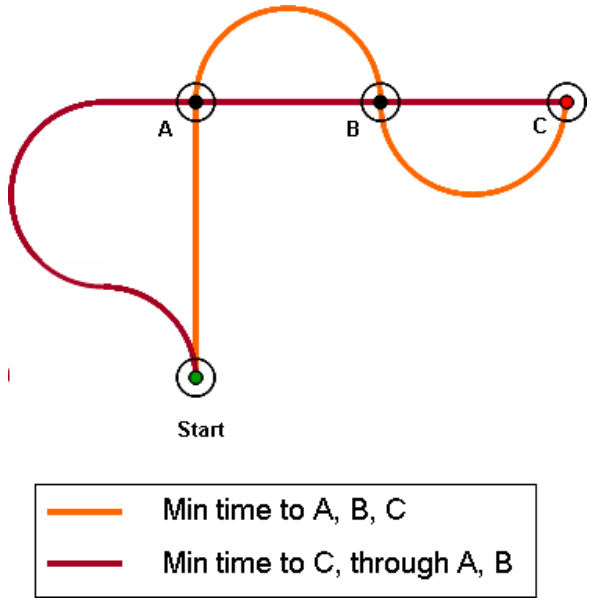

Figure 3.3: Notional Minimum Time Trajectory

4-Point Position Change

To demonstrate the multi-point capabilities inherent in DIDO through the use of the knotting method, the notional maneuver described in Figure 3.3 was illustrated through the use of the 4-Point Position Change maneuver. As defined in Table 3.19, the aircraft is tasked to reach a final state in minimum time while passing through two separate states along the way. The setup is actually identical to the course in Figure 3.3 in that the final three points all lie along the same line with only the starting point being offset from that line.

3.3.4 Result Verification. The final step in determining the optimal trajectories is to verify that they are actually feasible trajectories. Since the results returned from DIDO are only approximations of the state and control trajectories, it is entirely possible the results will be poor representations of the actual trajectory

Table 3.19: Numerical definition of the 4-Point Position Change maneuver.

State Variable	**Initial State**	**Target States**			
		A	B	Final	
V	500	–	–	–	ft/s
α	α_{trim}	–	–	–	deg
β	0	–	–	–	deg
ϕ	0	–	–	–	deg
θ	θ_{trim}	–	–	–	deg
ψ	0	–	–	–	deg
P	0	–	–	–	deg/s
Q	0	–	–	–	deg/s
R	0	–	–	–	deg/s
P_N	0	$5,000$	$5,000$	$5,000$	ft
P_E	0	0	$5,000$	$10,000$	ft
h	$20,000$	$20,000$	$20,000$	$20,000$	ft
pow	pow_{trim}	–	–	–	

of the aircraft. In order to verify that the trajectories are achievable, the control trajectories developed by DIDO are subsequently used as the input to a numerical integration scheme, namely *ode45* in MATLAB, which then propagates the reactions of the aircraft states to the control inputs. The resulting state trajectories should closely match those predicted by DIDO, if not, then the results are not valid.

IV. Simulations & Results

4.1 Stability Adjustments

Initial results from attempting the optimization of several of the basic maneuvers revealed some interesting phenomena. Initial attempts to optimize various maneuvers not only took an exceedingly long amount of time to complete, but it was also often the case that the optimization results would not match the propagated results at all. Further investigation into this issue revealed two instabilities in the system: one in the aircraft model and another in the optimization scheme itself.

4.1.1 Aircraft Model Stability. The mathematical model of the F-16 used in this research places the aircraft's center of gravity at the aircraft's aerodynamic center which in turn creates a neutrally stable aircraft. Although this is an accurate representation of the actual F-16, a real-life F-16 utilizes a stability augmentation system to keep the aircraft from going unstable. Since the basic mathematical model does not include a stability augmentation system, even fairly small control deflections are enough to cause the aircraft to go unstable and depart controlled flight.

In general, when attempting a trajectory optimization problem, the issue of an inherently unstable aircraft can be dealt with by increasing the number of nodes until they occur faster than the frequency of the instability. Practically, this is not desirable due to the fact that increasing the number of nodes in this fashion also exponentially increases the time required for convergence. The results of a trade study revealed that moving the aircraft's center of gravity from its original location of $0.35c$ to a new location at $0.25c$ would artificially stabilize the aircraft model without greatly affecting the aircraft's maneuverability.

4.1.2 Optimization Routine Stability. The second instability was not nearly as easy to diagnose. The basic symptom of this problem was the fact that the state trajectories resulting from the propagation of the aircraft controls did not match the estimated trajectories. By simply looking at the final results of an optimization run, it was not evident what was causing the problem; but it was glaringly evident that the

optimization solution was incorrect. This basic problem is illustrated in Figure 4.1 where the blue line is the optimal solution provided by DIDO and the red line is the result of propagating the states in time with *ode45*.

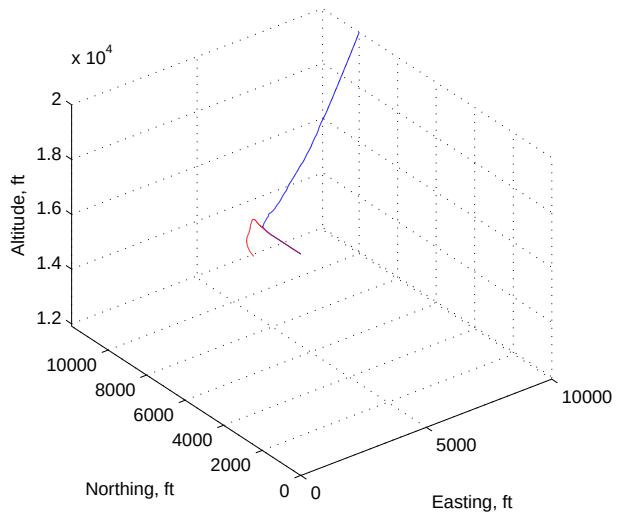

Figure 4.1: Departure of propagated trajectory from the optimal solution.

4.1.2.1 Unstable Responses. Further investigation revealed an interesting phenomenon in which the optimization routine actually causes the unstable behavior. This phenomenon is visible in the plots in Figure 4.2. This figure contains a control history and a 3-D trajectory plot for each of three points in the optimization routine. Though defined by the number of iterations which have occurred prior to these results, the specific number of iterations at each point is not important as this phenomenon occurs at different points in the iterative process for different maneuvers.

Figure 4.2(a) and (b) show the control history and 3-D trajectory for the Unconstrained 3-D Position Change maneuver at a point where the optimization routine has converged to a fairly good solution. In the trajectory plot, the blue line represents the approximate trajectory which DIDO thinks it is following and the red line represents the "truth" solution obtained by propagating the controls history with MATLAB's *ode45* numerical integration function. In this particular case, the red and blue lines

lie on top of each other, which means that the approximation is fairly good at this point.

After converging to a decent solution at 30,000 iterations, the optimization routine goes to work on whittling down the cost function, which, in this case, is the final time. By 100,000 iterations the routine has reduced the final time from a value of 22.838 s at 30,000 iterations to a new value of 21.885 s. At this point the optimization routine starts looking for ways to shave increasingly small amounts of time off of the final time.

Figure 4.2(c) depicts the result of the routine's searching for ways to shave off extra time. What is occurring here is that the system has noticed small oscillations in the roll, pitch, and yaw response of the aircraft which are the result of the light damping inherent in the F-16 model. Though not depicted here for space saving purposes, there are many examples of this phenomenon in the various figures in Appendix A. Basically, the system begins trying to nullify those small oscillations in an attempt to smooth the trajectory response. In doing so, the system begins a cycle, similar to a Pilot Induced Oscillation, where it begins to actually drive the oscillations and then begins to increase the amplitude of the controls to compensate for the new response.

In some cases the system is able to recover from this death spiral, but most cases result in a situation similar to Figure 4.2(e) and (f) where the system has driven the routine unstable and caused the aircraft to depart from the desired trajectory. The main problem here is that the optimization system does not know that the "optimal" trajectory is no longer feasible and will continue along this path, often actually producing results which it thinks are optimal solutions.

4.1.2.2 Artificial Stabilization Methods. Several methods of artificially stabilizing the optimization routine were attempted with varying success. By modifying the problem's cost function, it is possible to effectively penalize the routine for control histories such as those in Figure 4.2. When this phenomenon was first discovered, the penalty term found in Equation 4.1 was included in the running Lagrange

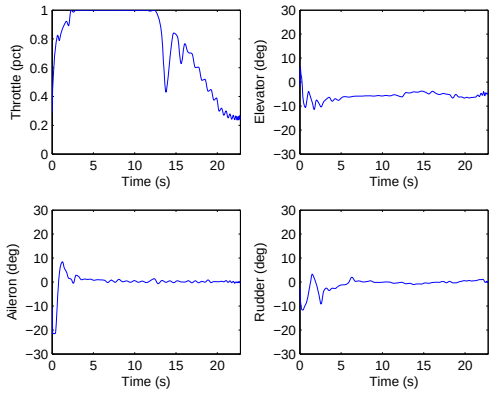

(a) Controls at 30k Iterations

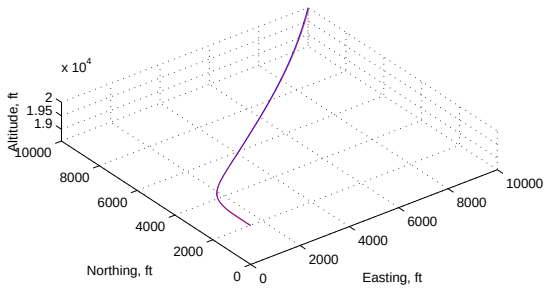

(b) Trajectory at 30k Iterations

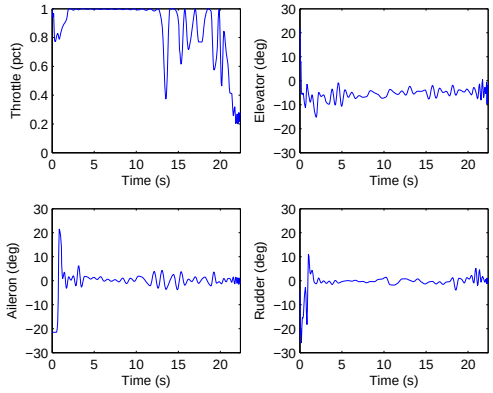

(c) Controls at 100k Iterations

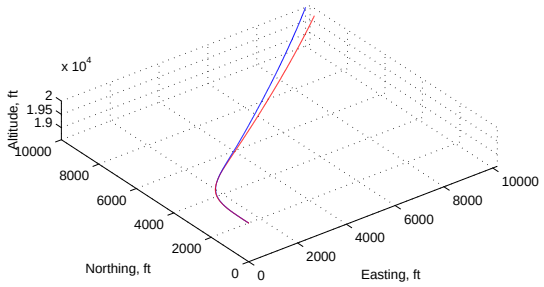

(d) Trajectory at 100k Iterations

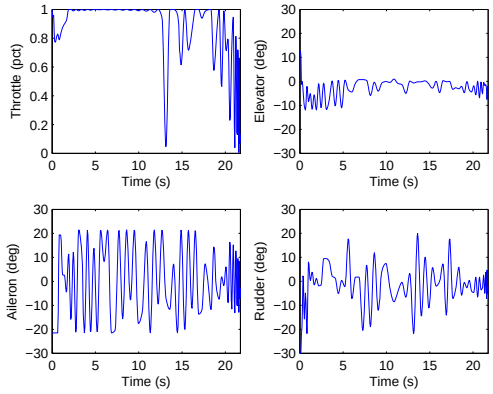

(e) Controls at 200k Iterations

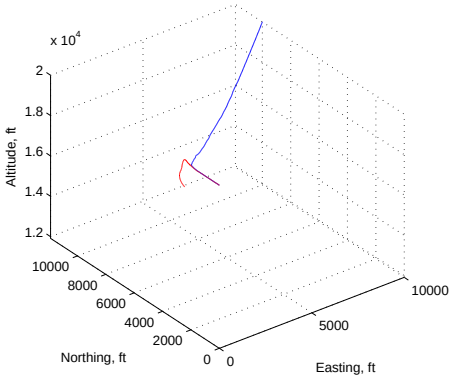

(f) Trajectory at 200k Iterations

Figure 4.2: Optimization induced oscillation development over time.

cost term (see Equation 2.11) of the performance index.

$$P_1 = \frac{1}{3\hat{t}_f}(B_1|\hat{\delta}_e| + B_2|\hat{\delta}_a| + B_3|\hat{\delta}_r|), \tag{4.1}$$

The basic goal of this term is to penalize the system for the large magnitude controls which are inherent in the unstable responses. In this equation, the hat over the terms, such as $\hat{\delta}_e$, is used to denote that these are values in the scaled and balanced unit system. By averaging these terms and dividing by the final time, $\hat{t}_f$, this term is reduced to a scalar value where $0 \geq P_1 \geq 1$. This scaling makes it easier to subsequently scale this term in relation to the Mayer Cost term from Equation 2.11 to adjust the relative importance of the final time and the penalty term through the use of the scaling terms B_N.

By itself, the inclusion of Equation 4.1 into the cost function resulted in faster convergence for a majority of the maneuvers simulated, but still couldn't handle certain maneuvers and is definitely working against the intent of pushing the limits of the aircraft's capabilities. To that end, a second Lagrange parameter, found in Equation 4.2, was developed to address the issue of rapid oscillations in the controls instead of their use in general.

$$P_2 = \frac{1}{4\hat{t}_f}(B_1\triangle\hat{\delta}_T + B_2\triangle\hat{\delta}_e + B_3\triangle\hat{\delta}_a + B_4\triangle\hat{\delta}_r), \tag{4.2}$$

The overall intent of this cost function is to force the system to smooth the control histories, therefore penalizing the cost function for large, rapid changes in the control history. Once again, this parameter works well for some maneuvers and not as well for others.

The next iteration of the penalty term borrows a page from the Digital Signals Processing world and adapts steady state statistical methods to the current problem. In essence, the new cost function attempts to minimize the variance (σ^2) of the control signals, which again is an attempt to smooth the control histories. The problem is

that normal methods of calculating the variance of a signal are based on a constant, or stationary, reference signal with noise [25]. Since the control histories are anything but stationary, a slightly different approach is required. By breaking the signal into small pieces and analyzing the variance of that section, a better estimation of the variance of the entire signal can be obtained [25]. As shown in Equation 4.3, the new cost function includes the average of the variance of N specific sections of the control histories.

$$P_3 = A\hat{t}_f + \frac{1}{N}\sum_{0}^{N}(B_1\sigma_N^2(\hat{\delta}_T) + B_2\sigma_N^2(\hat{\delta}_e) + B_3\sigma_N^2(\hat{\delta}_a) + B_4\sigma_N^2(\hat{\delta}_r)), \tag{4.3}$$

Though the inclusion of this cost function into the performance index stabilized the system for every maneuver under investigation it also had one major side effect. In order to increase the accuracy of the approximation of the signal's variance it is necessary to increase the number of sections into which the signal is divided. The most effective means of accomplishing this was to create a "window" of interest which would be propagated along the control signal and the variance of the signal within that "window" would be calculated at each step. This step drastically increased the computational time required to complete each iteration and subsequently each optimization run.

The final iteration on the penalty term takes the basic premise of Equation 4.3 one step further and provides the basis for the final performance index used throughout the remainder of this research. First, a noise corrupted stationary signal is created by taking the difference between a control signal and a moving average MA of that signal. The variance of this stationary signal is used as the variance of the actual control history and is summed with the variance of the other three control inputs. These calculations result in the penalty term found in Equation 4.4.

$$P_4 = \sum_{i=1}^{4} B_i\sigma^2(\mathrm{MA}_{\hat{\delta}_i} - \hat{\delta}_i), \tag{4.4}$$

The inclusion of this penalty term not only solved the instability issues, but also drastically reduced the computational time required from that of the previous cost function. The cost function used throughout the remaining portion of this research is seen in Equation 4.5. The relative weighting between the final time and the penalty terms depict the relative importance of each term to the final solution.

$$J = 100\hat{t}_f + 10\sum_{i=1}^{4}\sigma^2(\mathrm{MA}_{\hat{\delta}_i} - \hat{\delta}_i), \tag{4.5}$$

Unfortunately, this equation also depicts the fact that the trajectory optimization problem which uses this performance index is no longer solving for a time-optimal trajectory. This means that there will almost always exist a solution which would result in a slightly better final time. Fortunately, for the maneuvers investigated in this research, those difference are negligible.

The cost function in Equation 4.5 was used to create the control and trajectory development figures in Figure 4.3, which show the progression of the controls and trajectories of the same aircraft and maneuver as previously demonstrated. Note that this system also starts to exhibit some of the same unstable phenomenon at the 100,000 iteration mark. The difference now is that this type of control use is now penalized and the system converges to the solution in Figure 4.3 (e) and (f).

4.2 Results Format

The results presented in Sections 4.3 - 4.5 have been formatted for easier readability in several fashions which need to be mentioned. The first visual change is that the aircraft and its associated wing-tip paths are scaled anywhere from 1 to 20 times the size of an actual F-16. This was done to enable the reader to visualize the attitude of the aircraft along the associated trajectory and does not affect the actual position or attitude data from which the plots were created.

Additionally, each of the optimal trajectories are presented through the use of three 2-D plots and one 3-D plot. Through this combination it is possible for the

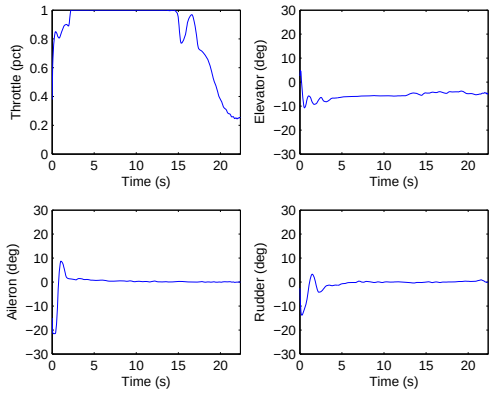

(a) Controls at 30k Iterations

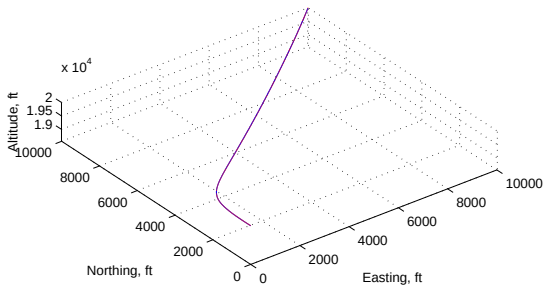

(b) Trajectory at 30k Iterations

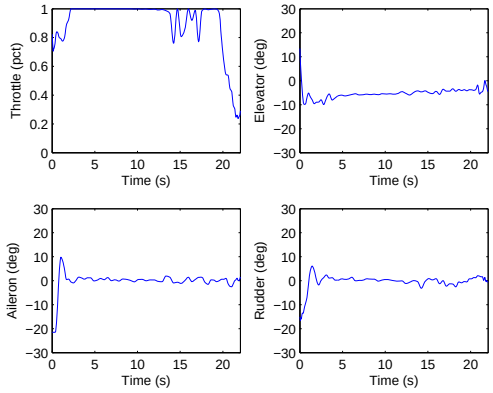

(c) Controls at 100k Iterations

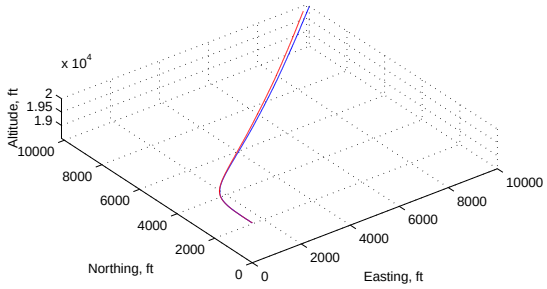

(d) Trajectory at 100k Iterations

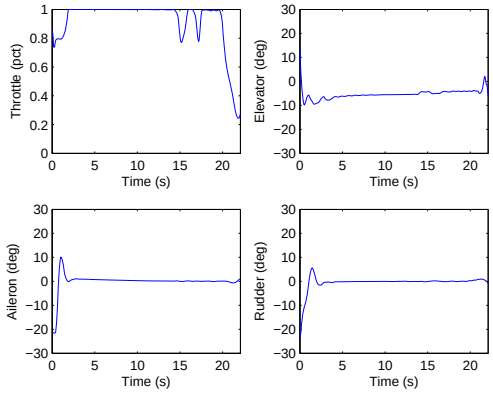

(e) Controls at 146k Iterations

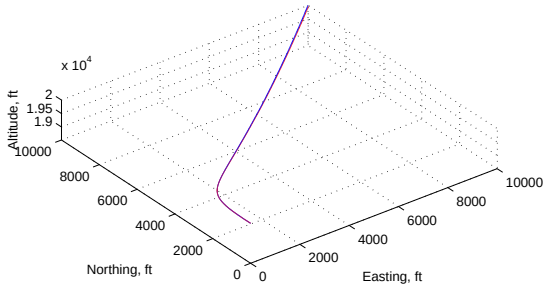

(f) Trajectory at 146k Iterations

Figure 4.3: Stable optimization trajectory development over time.

reader to glean a good understanding of each of the aircraft state variables with the exception of the engine lag state, *pow*. The full state and control time histories associated with each of the trajectories are located in Appendix A for more detailed investigations of what is occurring along the trajectory.

Finally, at this point the three aircraft models, as revisited again in Table 4.1, performed each maneuver in a very similar fashion. Though there were slight differences in each model's respective trajectory, the differences between them were not enough to warrant separate presentations of the results. To that end, unless otherwise noted, each of the trajectories presented in this paper depict the optimal trajectory for the baseline F-16 aircraft otherwise known as Model # 1.

Table 4.1: Summary of Aircraft Models Deviation from Baseline Model

Parameter	**Model # 1**	**Model # 2**	**Model # 3**	
Weight (W)	20,500	20,500	20,500	lbs
Max Thrust (T)	20,000	25,000	20,000	lbs
Wing Area (S)	300	300	375	ft^2
Wing Loading (W/S)	68.33	68.33	54.67	lbs/ft^2
Thrust-to-Weight Ratio (T/W)	0.9756	1.2195	0.9756	–

4.3 Demonstration Maneuvers

4.3.1 Northing Position Change. The results for the Northing Position Change maneuver, as described in Table 3.10 and seen in Figure 4.4, definitely represent the solution to the classic brachistochrone problem. For this maneuver, the aircraft first pitches nose down and trades altitude for increased velocity before pulling out level to finish with a dash to the target state. Aside from the initial portion of the maneuver, the resulting trajectory follows a path very similar to the cycloid solution of the classic brachistochrone maneuver.

Even though the trajectories of the three aircraft were very similar in basic shape, the resulting minimum times did differ slightly. The time required to accomplish the maneuver for each aircraft is found in Table 4.2. Along with the basic time

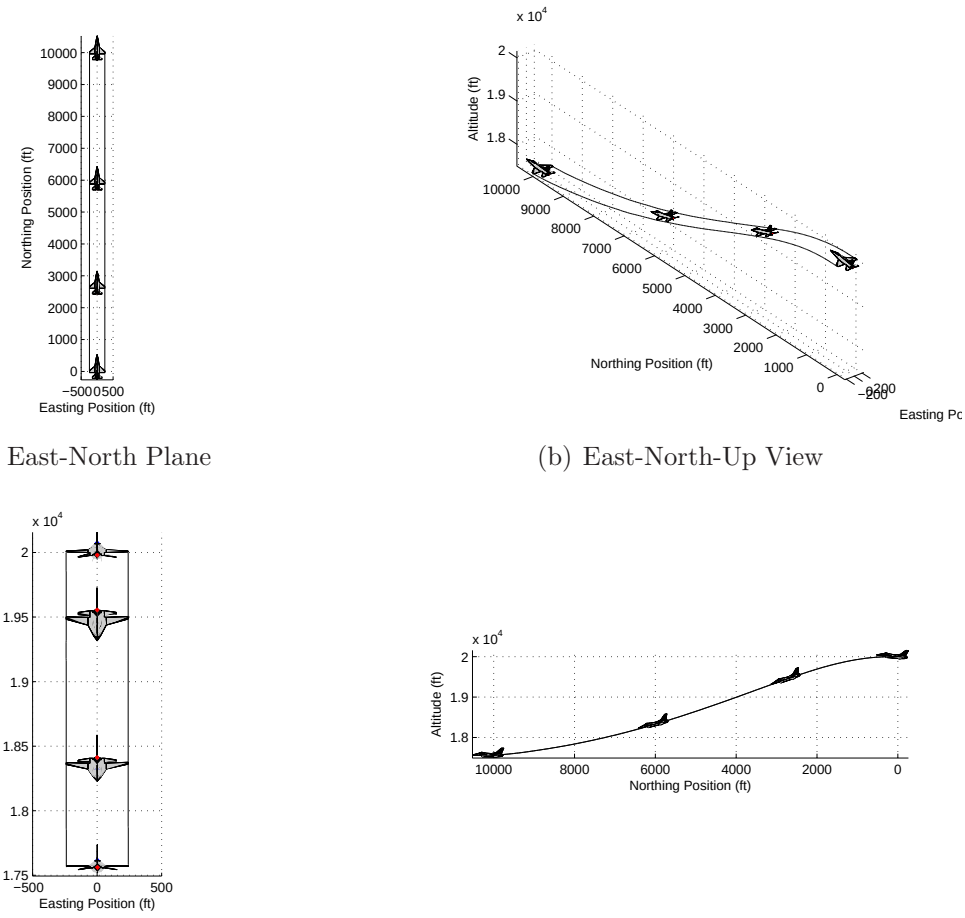

(a) East-North Plane

(b) East-North-Up View

(c) East-Up Plane

(d) North-Up Plane

Figure 4.4: Northing position change results. (Model # 1)

measurement, the final time is also normalized against the final time of the Model # 1 aircraft for comparison purposes. These results show, as expected, that the increased thrust of Model # 2 allows it to cover the distance faster and the increased drag caused by the wing area increase of Model # 3 make it the slowest of the three models for this maneuver.

Table 4.2: Northing position change maneuver times.

Aircraft	**Final Time**	**Normalized Time**
Model # 1	15.276 s	1.000
Model # 2	14.747 s	0.965
Model # 3	15.534 s	1.017

4.3.2 Unconstrained 3-D Position Change. The trajectory resulting from the unconstrained 3-D position change maneuver, as described in Table 3.11 and seen in Figure 4.5, resembles a classic Low Yo-Yo maneuver. The Low Yo-Yo, as perfected by Chinese fighter pilot Yo-Yo Noritake, is an out-of-plane lead-pursuit maneuver where a pilot pulls the nose of the aircraft down and inside of the turn in an attempt to both tighten the turn and increase speed at the same time [24]. In this specific case, the aircraft rolls past 100° of bank while also dropping the nose as much as 15° below the horizon. Subsequently, the aircraft slowly returns to wings level as it pulls out of the dive on a course towards the final target position.

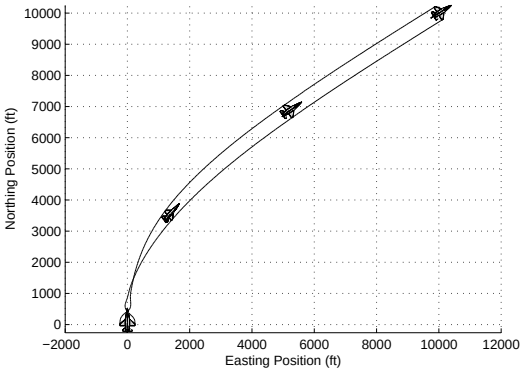

(a) East-North Plane

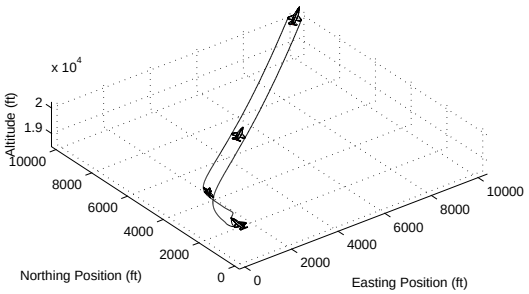

(b) East-North-Up View

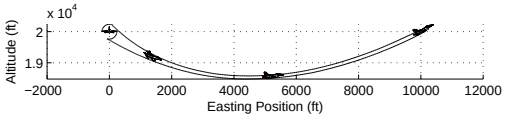

(c) East-Up Plane

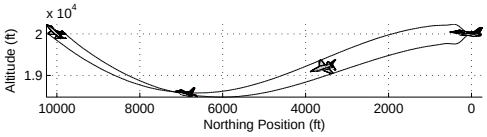

(d) North-Up Plane

Figure 4.5: Unconstrained 3-D position change Results. (Model # 1)

Once again, though the differences in final times between the three aircraft are very small, the higher thrust of Model # 2 allows it to complete the maneuver slightly faster than the other two, as depicted in Table 4.3.

Table 4.3: Unconstrained 3-D position change times.

Aircraft	**Final Time**	**Normalized Time**
Model # 1	21.994 s	1.000
Model # 2	20.721 s	0.942
Model # 3	21.619 s	0.983

4.3.3 Constrained 3-D Position Change. Building on the previous maneuver, each of the aircraft accomplish the 3-D position change maneuver by similarly rolling and dropping the nose of the aircraft to perform a tighter turn and trading altitude for speed. The main difference in this maneuver, as described in Table 3.12 and seen in Figure 4.6, is the rapid bank angle and heading change at the end of the maneuver to allow the aircraft to return to its initial state minus the position values.

As with the previous two maneuvers, the increased thrust available to Model # 2 enables it to beat the other two aircraft to the final position in this maneuver, as found in Table 4.4. Unlike the previous maneuvers, the detrimental effect of the increased drag of Model # 3 is offset by the increased maneuverability which allow it to best the baseline model as well.

Table 4.4: Constrained 3-D position change times.

Aircraft	**Final Time**	**Normalized Time**
Model # 1	23.891 s	1.000
Model # 2	22.962 s	0.961
Model # 3	23.396 s	0.979

4.4 Agility Maneuvers

4.4.1 Bank Angle Capture. Kicking off the agility maneuver category, the bank angle capture maneuver is not simply a 90° roll as may be deduced from the

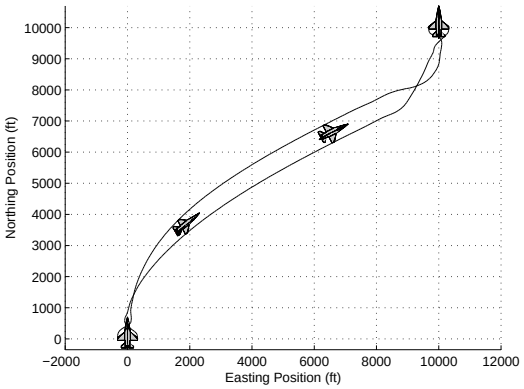

(a) East-North Plane

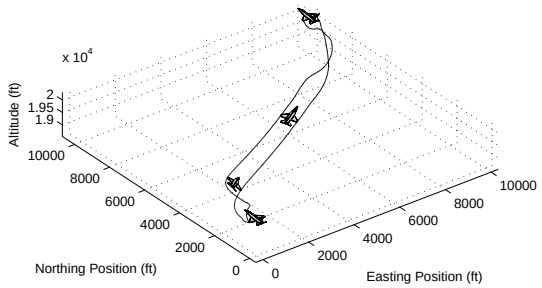

(b) East-North-Up View

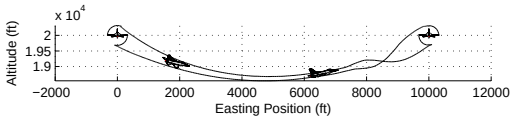

(c) East-Up Plane

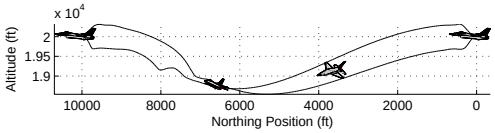

(d) North-Up Plane

Figure 4.6: Constrained 3-D position change results. (Model # 1)

trajectories in Figure 4.7, but a much more complicated maneuver due to the other target state requirements depicted in Table 3.13.

As expected, the increased wing area and the associated effective control surface area increase allows Model # 3 to accomplish this maneuver much faster than the other two aircraft, as seen in Table 4.5. The Model # 2 aircraft pulls out the second best time by achieving a slightly higher velocity, even in the short maneuver times, which creates a higher dynamic pressure and therefore better control performance.

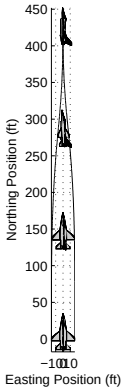

(a) East-North Plane

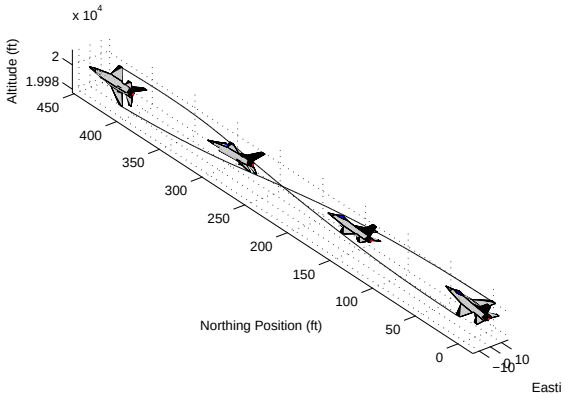

(b) East-North-Up View

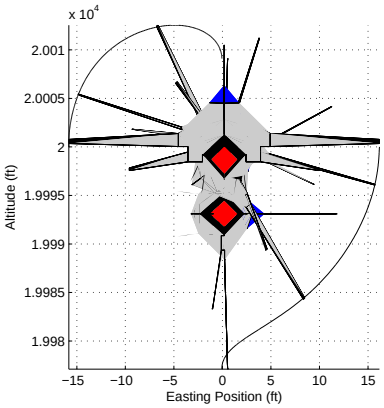

(c) East-Up Plane

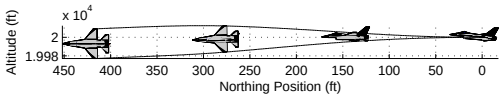

(d) North-Up Plane

Figure 4.7: Constrained bank angle capture results. (Model # 1)

Table 4.5: Constrained bank angle capture times.

Aircraft	**Final Time**	**Normalized Time**
Model # 1	0.835 s	1.000
Model # 2	0.835 s	0.999
Model # 3	0.754 s	0.903

4.4.2 Unconstrained Heading Capture. The results for this maneuver similarly favored Model # 3 with its increased control authority, which is caused by the wing area being a scaling factor for the control effect coefficients. The resulting trajectory can be described as a rapid roll and pull with the aircraft achieving the final heading angle while maintaining a high angle of attack, and still traveling along a

path which deviates only slightly from its original heading. Figure 4.8 depicts the time-optimal trajectory and Table 4.6 lists the corresponding final times associated with this maneuver as numerically defined in Table 3.14.

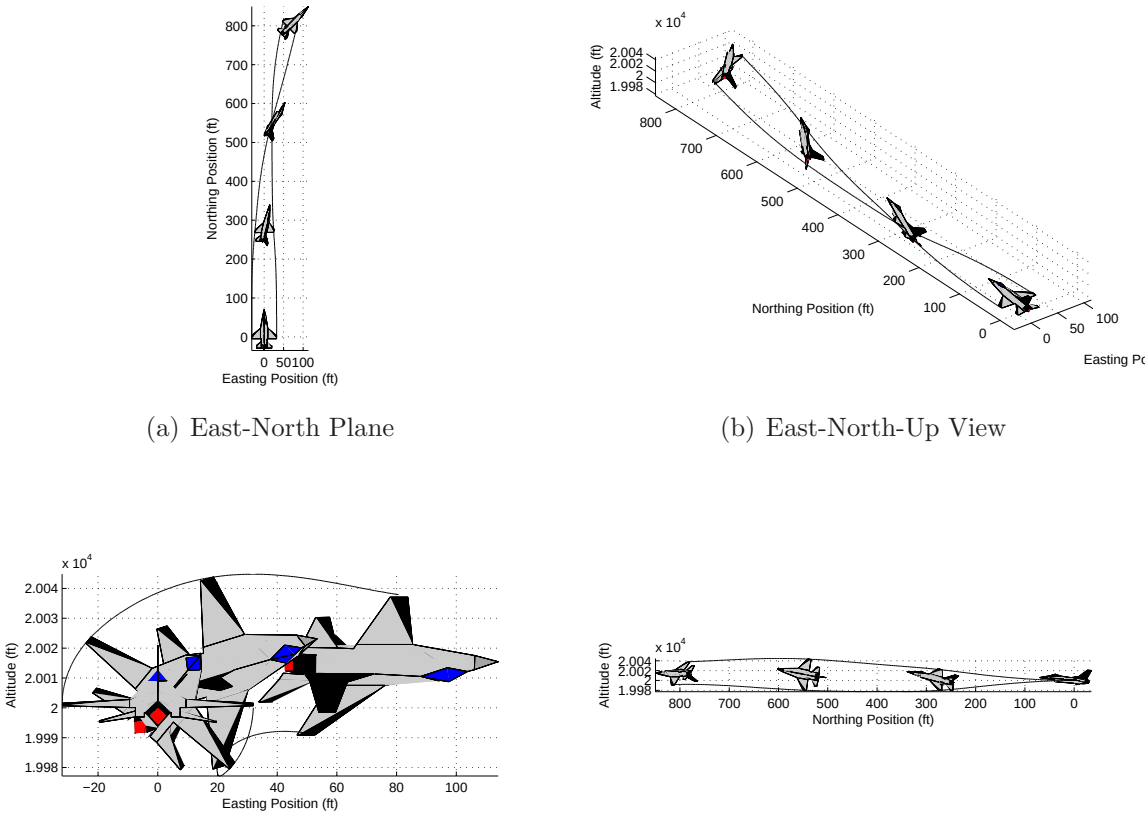

(a) East-North Plane

(b) East-North-Up View

(c) East-Up Plane

(d) North-Up Plane

Figure 4.8: Unconstrained Heading Capture Results. (Model # 1)

Table 4.6: Unconstrained heading capture times.

Aircraft	**Final Time**	**Normalized Time**
Model # 1	1.657 s	1.000
Model # 2	1.595 s	0.963
Model # 3	1.453 s	0.877

In an attempt to demonstrate other potential uses for this type of trajectory optimization system, two addition variations of the Unconstrained Heading Capture

were investigated. The first variation was created by varying the target heading angle where $-180° \leq \psi \leq 180°$. The results of this investigation are found in Figure 4.9 (a) where the radial distance from the center depicts the time required to complete an Unconstrained Heading Capture of that specific heading angle. As expected, these results show that larger changes in the heading angle result in increased final times.

One interesting side note from these results is the asymmetry in the result data. Upon further investigation, it was found that this asymmetry is the direct result of asymmetries in the aerodynamic model data. Two examples of this phenomenon are found in Figure 4.10. Figure 4.10 (a) depicts the yawing moment coefficient, C_N as a function of the angle-of-attack, α, and the sideslip angle, β, and Figure 4.10 (b) depicts the rolling moment cause by an aileron input, δ_l/δ_α, also as a function of α and β. Note that the data is definitely not symmetric about $\beta = 0$ as would be expected for a symmetric aircraft.

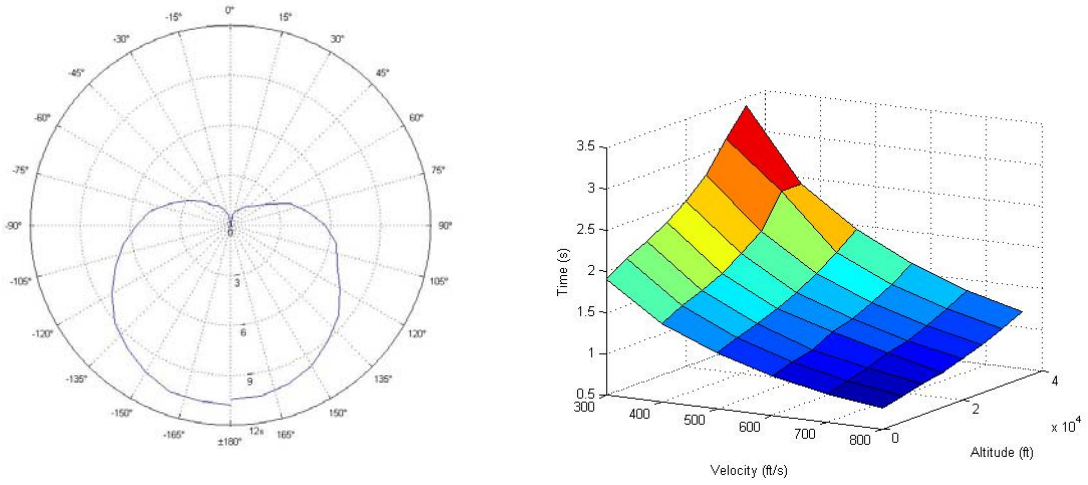

(a) Target Heading Variation

(b) Initial State Variation

Figure 4.9: Variation of the Unconstrained Heading Capture Maneuver.

The second variation on the 45° heading change was to vary the maneuver's initial conditions. Figure 4.9 depicts the results of varying the initial velocity from 300 ft/s to 800 ft/s and the initial altitude from Sea Level to 35,000 ft. With the vertical axis representing the resulting final time, the results show that, as expected, this maneuver can be accomplished faster at higher initial velocities and lower initial

altitudes. The slowest trajectory was found at the point where the aircraft started at 300 ft/s and 35,000 ft initial altitude, at which the aircraft is actually very close to the stall conditions.

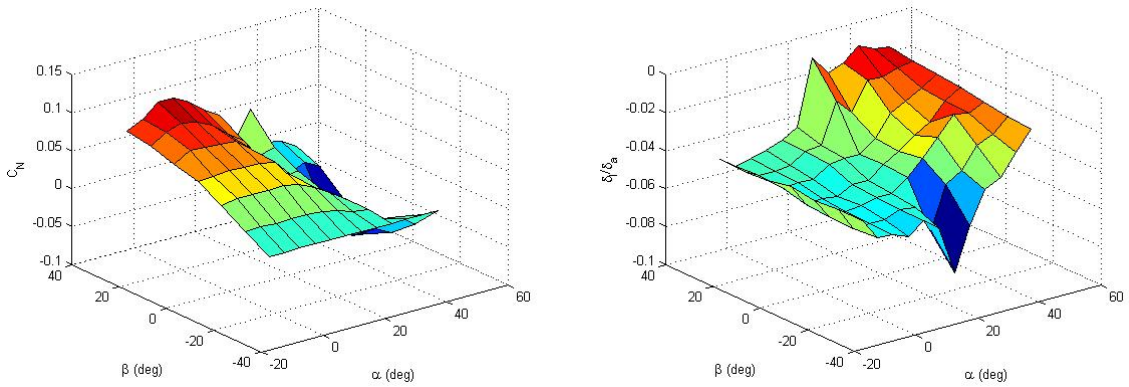

(a) C_N Asymmetry (b) δ_l/δ_α Asymmetry

Figure 4.10: Aerodynamic Model Asymmetries.

4.4.3 Constrained Heading Capture. The constrained heading capture maneuver required the aircraft to both achieve a desired heading angle and return to steady level flight. In that capacity, the resulting trajectory resembles a tight sustained turn, as described in Table 3.15 and seen in Figure 4.11. As would be expected for a sustained maneuver such as this, the increased thrust of Model # 2 allows that aircraft to maintain its energy level throughout the turn and complete the maneuver before either of the other two aircraft, as depicted in Table 4.7. One final note in this table is that there is not a final time listed for Model # 2. This is due to the fact that this run did not complete successfully during this data collection series. This is one of the model and maneuver combinations which have necessitated the revised cost function.

4.4.4 Position Free Heading Reversal. The general results from the position free heading reversal maneuver ended up matching the results and predictions made by Bocvarov [4] almost exactly. The basic trajectory, defined in Table 3.16 and seen in Figure 4.12, is a classic Split-S maneuver in which the aircraft rolls inverted and pulls

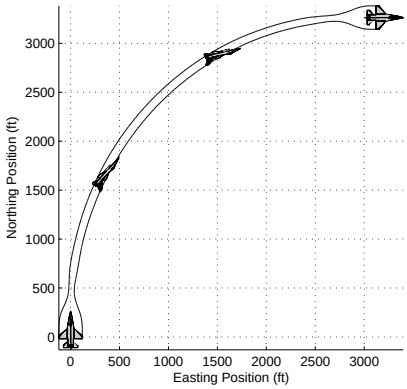

(a) East-North Plane

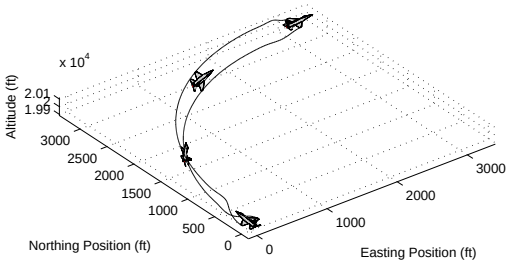

(b) East-North-Up View

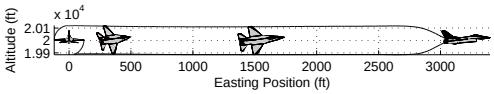

(c) East-Up Plane

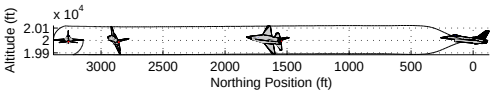

(d) North-Up Plane

Figure 4.11: Constrained heading capture results. (Model # 1)

Table 4.7: Constrained heading capture times.

Aircraft	**Final Time**	**Normalized Time**
Model # 1	10.121 s	1.000
Model # 2	9.759 s	0.964
Model # 3	9.189 s	0.908

through in a downward semicircle until achieving the target state [24]. This maneuver matches the solution found by Bocvarov's optimization of an F/A-18 aircraft model.

Additionally, in his analysis, Bocvarov discussed the findings that the most important factor in performing a rapid reorientation of this nature was the lift force acting on the aircraft [4]. Though not directly addressed by Bocvarov, a simple

extension of this analysis would lead to the observation that an aircraft with a lower wing loading should be capable of achieving large scale reorientation maneuvers faster than an aircraft with a higher wing loading. This is exactly what is seen in the results for this maneuver found in Table 4.8. The lower wing loading of Model # 3 allows it to complete this maneuver almost 13% faster than the baseline F-16 model and over 9% faster than Model # 2 with its higher thrust to weight ratio.

One item of note with this maneuver is its lateral deviation from the vertical plane as seen in Figure 4.12(a) and (c). This phenomenon is entirely based on the external limits imposed in the optimization scheme's box constraints. In this setup, the aircraft's pitch angle, θ, is limited to $\theta = \pm 86^\circ$ to avoid the singularity at $\theta = \pm 90^\circ$. The lateral deviation from the vertical plane, seen in Figure 4.12 as a 600 ft progression in the Easting Position, is caused by the optimization program's inability to push the aircraft to higher pitch angles without violating the box constraints.

Table 4.8: Position free heading reversal times.

Aircraft	**Final Time**	**Normalized Time**
Model # 1	13.623 s	1.000
Model # 2	13.080 s	0.960
Model # 3	11.854 s	0.870

4.4.5 Position Fixed Heading Reversal. Again corroborating the predictions made by Bocvarov, the results for the position fixed heading reversal are drastically different from the position free maneuver. In this maneuver, defined in Table 3.17 and found in Figure 4.13, the aircraft performs a maneuver which can be likened to a classic Hi Yo-Yo maneuver [24]. The maneuver commences with the aircraft performing a small negative heading change before pulling vertical to trade kinetic energy for potential energy as it attempts to stop its forward velocity. Inverted and approaching stall near the top of the arc, the aircraft has successfully reversed its velocity vector and continues to regain speed and energy as it approaches the bottom of the loop and the terminal state.

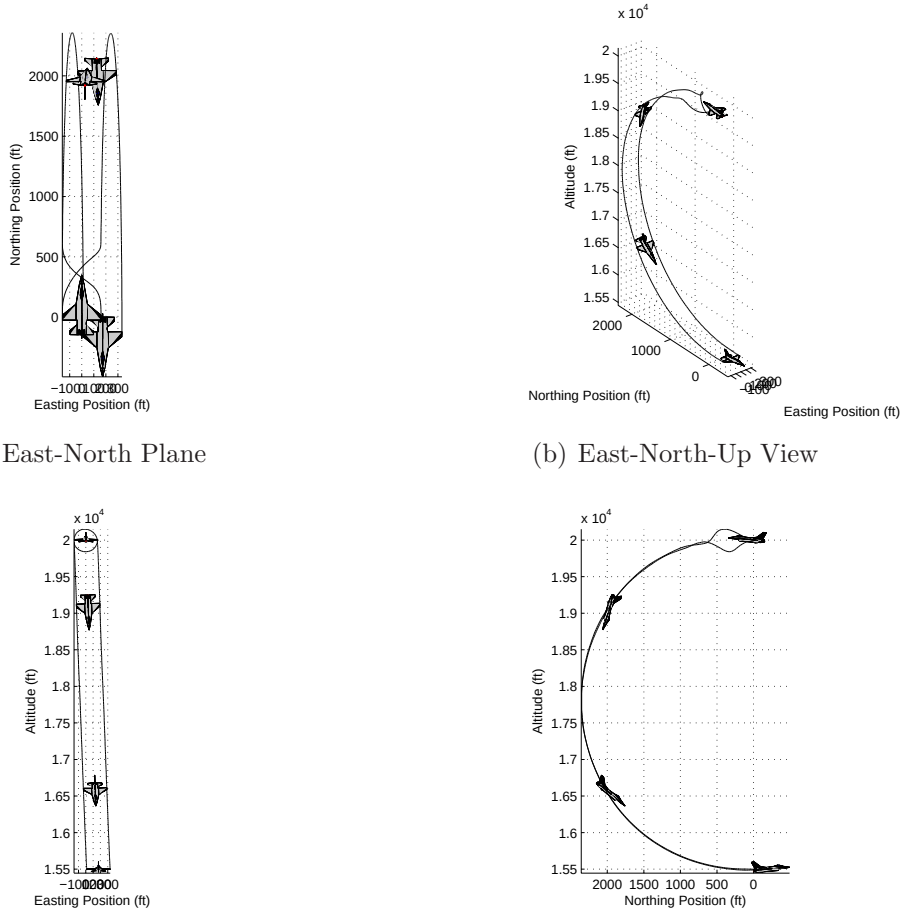

(a) East-North Plane

(b) East-North-Up View

(c) East-Up Plane

(d) North-Up Plane

Figure 4.12: Position Free Heading Reversal Results. (Model # 1)

One interesting observation, also predicted by Bocvarov, is that the optimal trajectory calls for maximum throttle for the majority of the maneuver. Though this leads to the fact that Model # 2 can perform the maneuver faster than the baseline F-16, the superior lift characteristics of Model # 3 again allow it to perform this maneuver nearly 6% faster than Model # 2, as seen in Table 4.9.

Table 4.9: Position fixed heading reversal times.

Aircraft	**Final Time**	**Normalized Time**
Model # 1	37.352 s	1.000
Model # 2	35.049 s	0.938
Model # 3	32.580 s	0.872

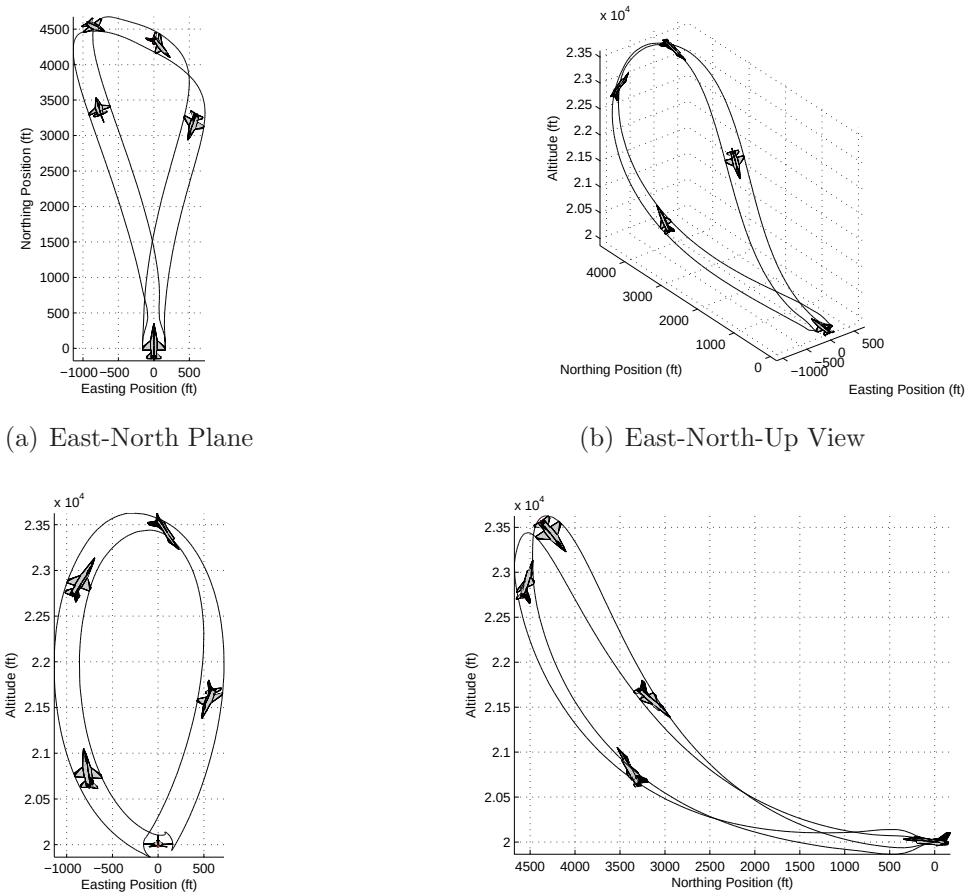

(a) East-North Plane

(b) East-North-Up View

(c) East-Up Plane

(d) North-Up Plane

Figure 4.13: Position Fixed Heading Reversal Results. (Model # 1)

4.4.6 Position Free Heading Reversal with Altitude Floor. The addition of a altitude floor restriction changes the position free heading reversal from an out-of-plane Split-S maneuver to an in-plane sustained turn, as seen in Figure 4.14. With the floor restrictions, the advantage in this maneuver shifts back to Model # 2 with its increased thrust and ability to sustain its energy through tighter turns, as found in Table 4.10.

4.4.7 Initial State Capture. The results for the Initial State Capture maneuver, as defined in Table 3.18, are found in Figure 4.15. In this maneuver, the aircraft rolls inverted and pulls through a full negative loop while trading altitude to gain velocity before pulling vertical again and completing the loop as it returns to

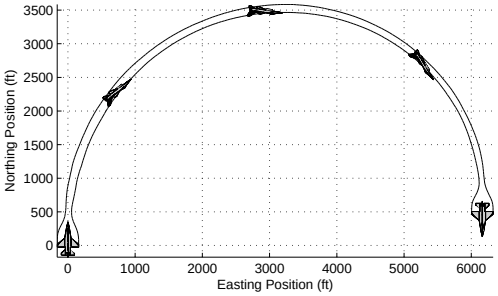

(a) East-North Plane

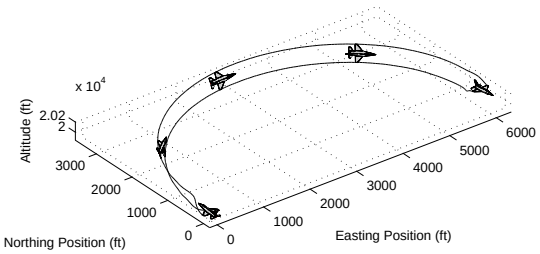

(b) East-North-Up View

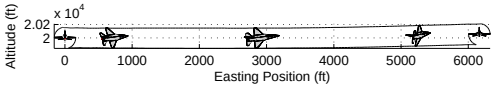

(c) East-Up Plane

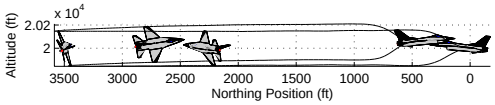

(d) North-Up Plane

Figure 4.14: Position free heading reversal with altitude floor results. (Model # 1)

Table 4.10: Position free heading reversal with altitude floor times.

Aircraft	**Final Time**	**Normalized Time**
Model # 1	19.599 s	1.000
Model # 2	18.547 s	0.946
Model # 3	17.007 s	0.868

its initial state. The resulting times from the three different aircraft models, found in Table 4.11, depict the interesting twist that this maneuver throws into the agility characterization problem. Unlike the case of the heading reversal maneuvers where the resulting trajectories relied heavily on the attitude reorientation capabilities of the aircraft, the results from this maneuver actually favor Model # 2 with its increased

ability in vertical maneuvers. Though the increased lift available to Model # 3 allows it to reach the $\psi = -180°$ point faster, the increased thrust of model # 2 gives it the edge in regaining the lost altitude.

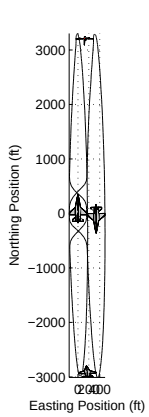

(a) East-North Plane

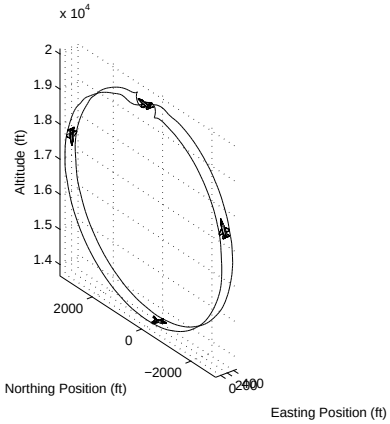

(b) East-North-Up View

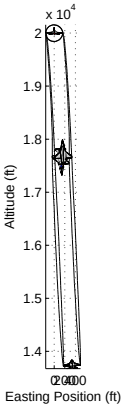

(c) East-Up Plane

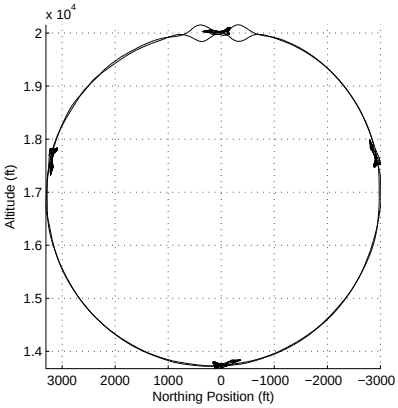

(d) North-Up Plane

Figure 4.15: Initial state capture results. (Model # 1)

Table 4.11: Initial state capture times.

Aircraft	**Final Time**	**Normalized Time**
Model # 1	30.856 s	1.000
Model # 2	27.900 s	0.904
Model # 3	28.387 s	0.920

4.4.8 Initial State Capture with Altitude Floor. As in the case of the position free heading reversal, the addition of a altitude floor restriction changes the initial state capture maneuver from an out-of-plane vertical maneuver to an in-plane sustained turn, as seen in Figure 4.16. With the floor restrictions, the advantage in this maneuver shifts back to Model # 3, as found in Table 4.12.

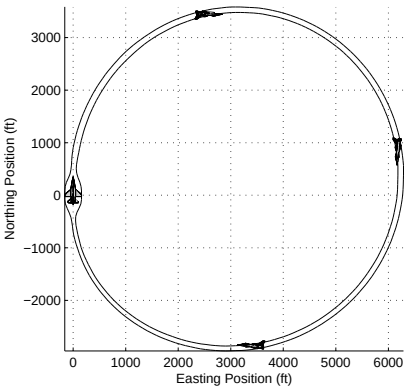

(a) East-North Plane

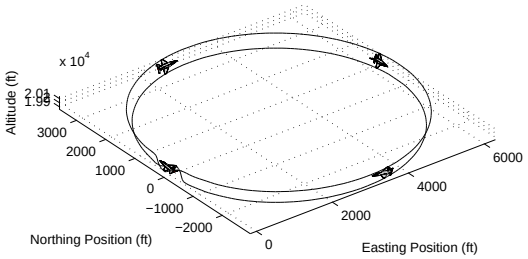

(b) East-North-Up View

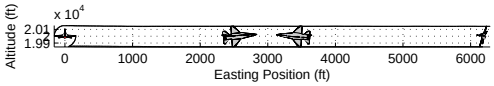

(c) East-Up Plane

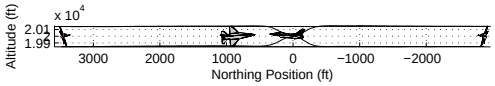

(d) North-Up Plane

Figure 4.16: Initial state capture with altitude floor results. (Model # 1)

Table 4.12: Initial state capture with altitude floor times.

Aircraft	**Final Time**	**Normalized Time**
Model # 1	36.999 s	1.000
Model # 2	33.667 s	0.910
Model # 3	32.227 s	0.871

4.5 Compound Maneuvers

4.5.1 4-Point Position Change. The results from the 4-Point Position Change maneuver, as defined in Table 3.19, are found in Figure 4.17. As expected, the resulting trajectory commences with the aircraft deviating from a straight line acceleration with a slight negative heading change. With bank angles approaching 90°, the aircraft pulls through the first waypoint in a tight turn changing its heading rapidly and setting itself up to increase its velocity through the final intermediate point on its way to the final state. Performing the maneuver in this manner allows the aircraft to perform only minor heading changes and therefore maintain a higher velocity on its approaches to the final two points. The final time results for the various models can be found in Table 4.13.

Table 4.13: 4-Point position change times.

Aircraft	**Final Time**	**Normalized Time**
Model # 1	30.877 s	1.000
Model # 2	26.348 s	0.853
Model # 3	26.836 s	0.869

4.6 Potential as Control Method and Agility Prediction Tool

Once the final new cost function, Equation 4.5, was implemented, the approximate solutions provided by the DIDO optimization software almost always matched the "truth" results found from propagating the state and controls histories as shown in Section 4.1.2.2. To that end, the use of trajectory optimization as a tool for developing control histories to drive a simulation, though feasible, is not necessary. The same results can now be achieved by simply using the state and control trajectories from the optimization results for analysis and visualization purposes.

If the desire is truly to drive a separate simulation system, then the optimization software will be required to interface with that system and run the optimization routine on the full scale system. Any simplification of the simulator model could

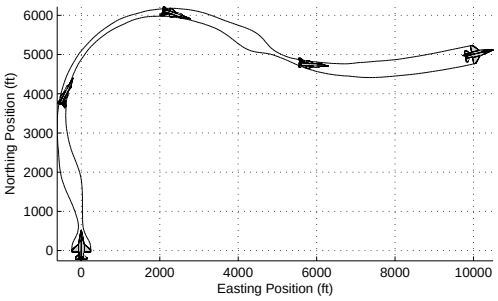

(a) East-North Plane

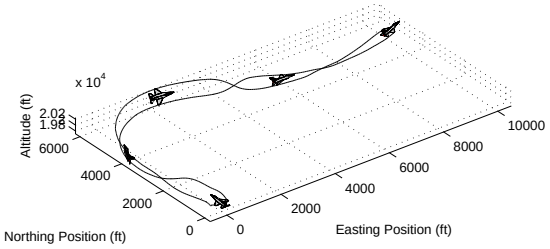

(b) East-North-Up View

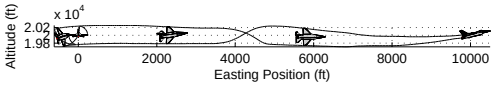

(c) East-Up Plane

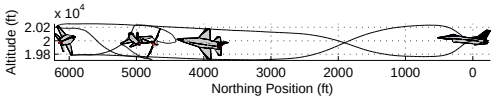

(d) North-Up Plane

Figure 4.17: 4-Point position change results. (Model # 1)

results in very poor results when propagating the optimum control paths in a different simulation. This issue is illustrated in Figure 4.18 where the control histories found for Model # 3 to perform the Fixed-Position Heading Reversal maneuver are used to propagate the solution for both Model # 1 (a) and Model # 3 (b) side by side, with poor results for the Model # 1 case.

Another key benefit of optimizing the trajectory of a full 6-DOF mathematical model is that it now enables the calculations of almost every proposed agility metric [17]. Since the solution to a trajectory optimization problem provides time history data for each of the state and control parameters, using a 6-DOF model now pro-

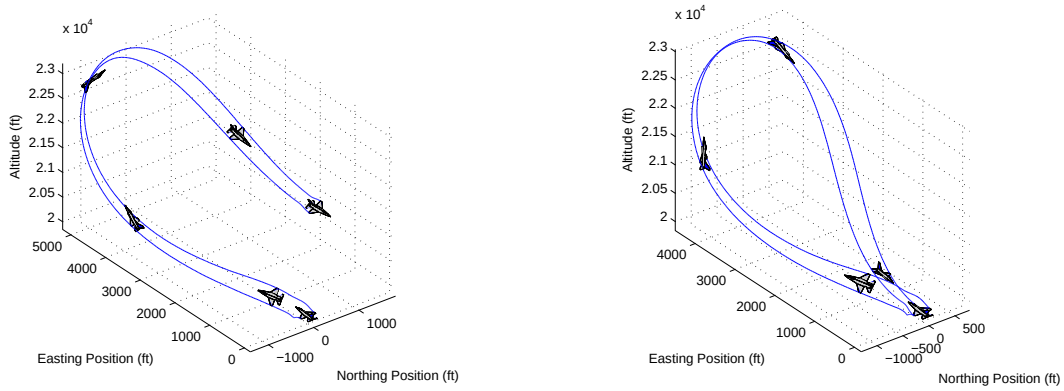

(a) Model # 1 (b) Model # 3

Figure 4.18: Control interchangeability example.

vides the necessary data for calculating every metric except those based on combat effectiveness.

4.7 Overall Analysis

As expected, the various maneuvers have shown that, though each aircraft has definite advantages in certain conditions, none of these aircraft is superior throughout all flight regimes. Figure 4.19 shows a summary of the normalized optimum maneuver times for each aircraft and each maneuver. With lower values being better, it was found that the aircraft with increased thrust, Model # 2, performed better than the other aircraft in maneuvers such as the Northing Position Change or Constrained Heading Capture where straight line acceleration or sustained maneuvers were required. On the other hand, the aircraft with an increased wing area, Model # 3, performs best with instantaneous reorientation maneuvers such as the bank angle capture and large scale reorientations like the heading reversal maneuvers.

Since the various aircraft used in this research are completely fictional, the actual final times depicted in Figure 4.19 are of little value. The real implication of the information in Figure 4.19 is that the use of a trajectory optimization system such as DIDO is a valid and potentially very useful tool for predicting the differences

in aircraft agility characteristics for various aircraft. Additionally, this tool is robust enough to handle all but the most abstract of the proposed agility metrics.

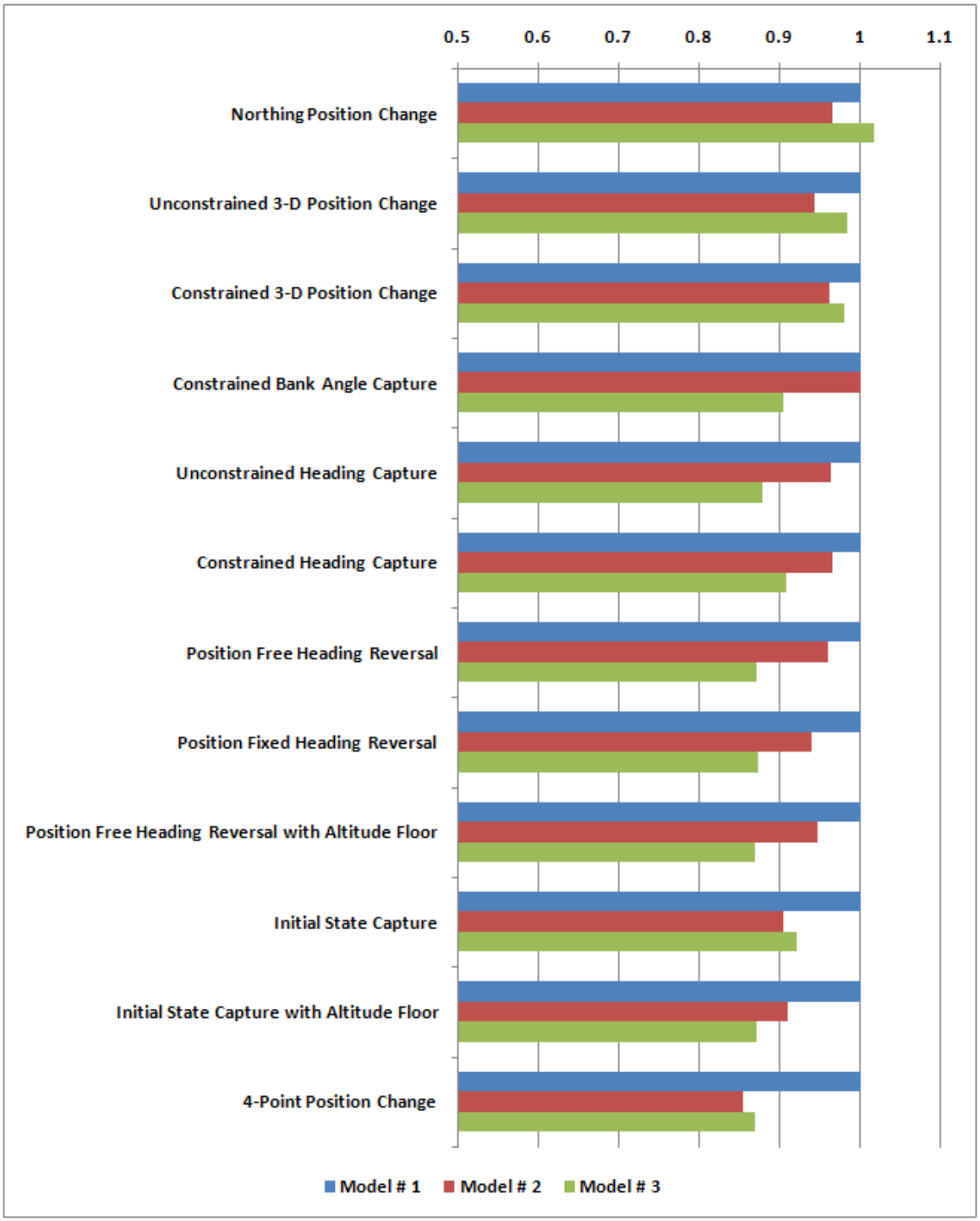

Figure 4.19: Maneuver final times for the various aircraft.

V. Conclusions and Recommendations

5.1 Conclusions

The objective of this research was to develop a trajectory optimization system which will alow a user to investigate and compare the agility characteristics of various aircraft by simulating a wide range of maneuvers. As demonstrated in Chapter 4, a system was developed which allows a user to simulate a wide variety of maneuvers with enough accuracy to render further investigations unnecessary. In that light, this research was fundamentally successful.

Initial results gleaned from using the baseline minimum time cost function, though promising, illustrated an instability in the interface between the optimization scheme and the mathematical model. This instability was characterized by increasing magnitude and frequency in the control histories as a result of the system attempting to shave insignificantly small times off of the final time. Since the tolerances for defining an optimal solution in DIDO are not accessible to the external user, it was necessary to construct a penalizing term for the cost function. Initial version of the penalizing term focused on penalizing the actual use of the controls. Though these modifications provided solutions in almost every case, the time required for convergence increased drastically as a result of the increased number of methods of affecting the systems final cost. Results from the use of various penalizing terms, which instead focused on smoothing the control histories, depict faster convergence times and better results than were previously achieved. The final cost function used in this research utilized a penalty term which was based on the statistical variance of the difference between the actual control history and a smoothed version of the same signal. Through the use of this cost function, the optimization system was stabilized and a wide variety of maneuvers were successfully simulated.

In the area of agility prediction in general, this research has shown that it is now possible to optimize the trajectory of a full 6-Degree-of-Freedom mathematical aircraft model. It is no longer necessary to make point-mass approximations or any other major simplifying assumptions which would cause the results to be useless

outside of academic circles. With few exceptions, it is now possible to predict the full gamut of metrics which have been proposed to describe the agility characteristics of an aircraft. Additionally, if the mathematical model is a close enough representation to the aircraft itself, the results from a trajectory optimization run can now be used as actual flight control inputs.

5.2 Recommendations

The results from this research, and the subsequent discussions and conclusions, lead to several basic improvements and modifications which should be made to the actual trajectory optimization system. The inherent instabilities in the optimization scheme are the first, and most obvious, area in need of future work. Further work is needed to characterize and mitigate these instabilities by determining if the instabilities are a result of the mathematical aircraft model, the optimization software, or some combination of the two. Once the optimization routine instabilities have been addressed, one could take another look at the ability of the system to handle unstable mathematical models.

Initially, it was envisioned that this research would result in the development of a Graphical User Interface through which a user would have easy access to all of the parameters required for the numerical maneuver definition and the associated constraints. This would allow this tool to be easily used for classroom projects and demonstrations. Due to time constraints, this portion of the work was only addressed at a very basic level. A tool of this nature could be useful and would be a good area for future work which should not entail much additional effort.

The trajectory optimization system produced in this research would be an ideal foundation for a wide variety of trajectory optimization problems. Relying heavily on the basic DIDO problem architecture, the basic interface resulting from this research creates a highly intuitive means of setting up an aircraft trajectory optimization problem. With only slight modifications, this basic structure can be used to simulate any mathematical model which can be transformed into a self-contained

set of MATLAB script files. By doing so, many of the aircraft path and trajectory optimization projects currently underway could benefit from this intuitive format. For example, though the problem definitions in this research did not make use of the path constraint capabilities, this system could easily be used for subjects such as UAV path planning in urban environments or path planning against RADAR threats.

On a slightly different note, by using the path constraint capabilities in this system to define the observed flight path of an actual aircraft, the control and state history required to get the aircraft to follow that flight path could be backed out of the trajectory optimization solution. This capability would be beneficial for both accident investigation and reverse engineering applications where a certain subset of the required information is not readily available.

Appendix A. Expanded Simulation Results

A.1 Northing Position Change

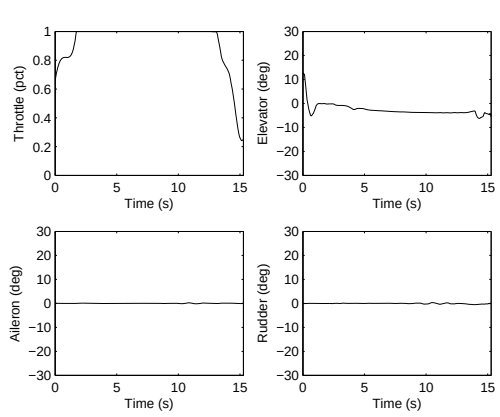

(a) Controls

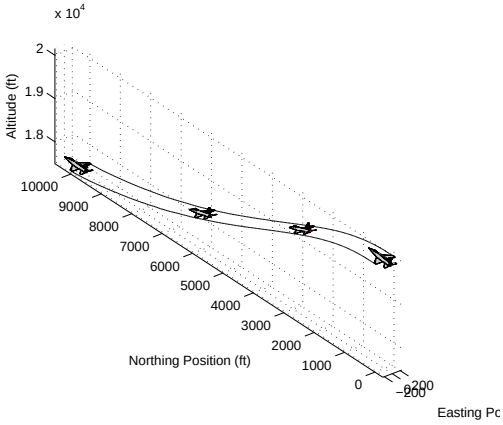

(b) Trajectory

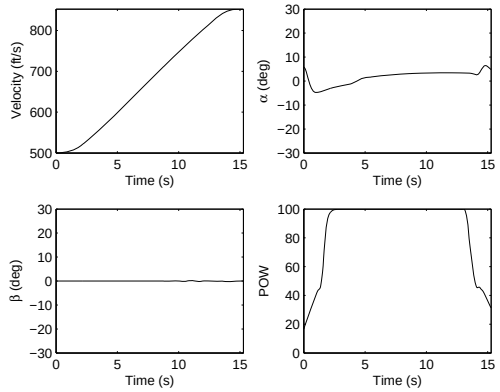

(c) Aerodynamic States

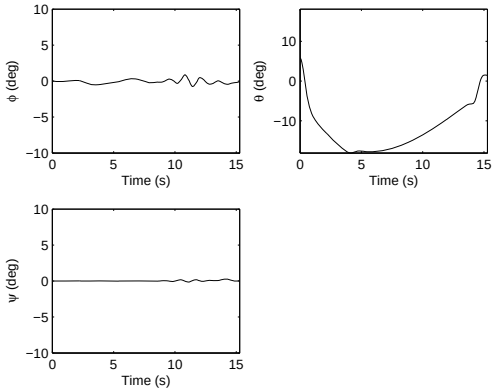

(d) Euler Angles

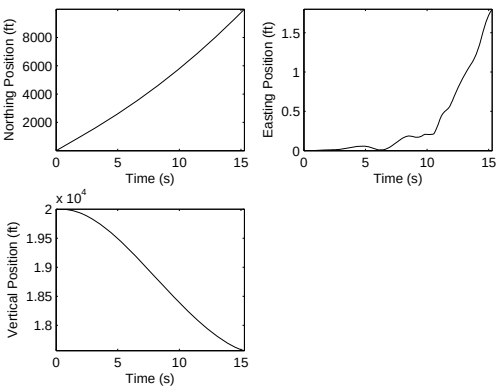

(e) Position

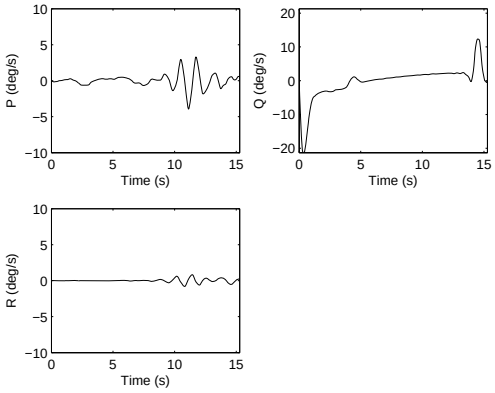

(f) Angular Rates

Figure A.1: Northing position change state and control histories. (Model # 1)

A.2 Unconstrained 3-D Position Change

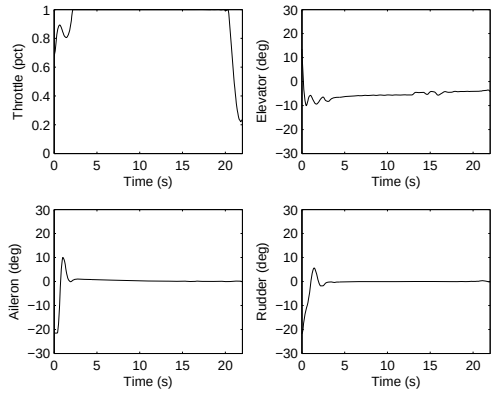

(a) Controls

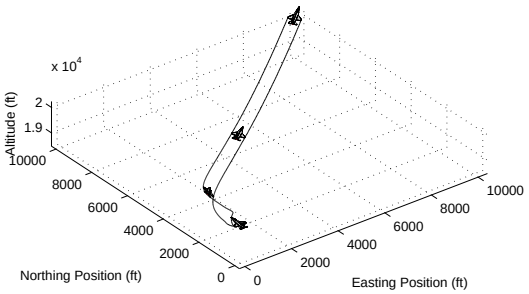

(b) Trajectory

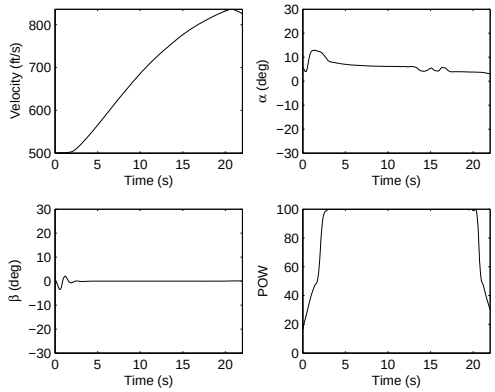

(c) Aerodynamic States

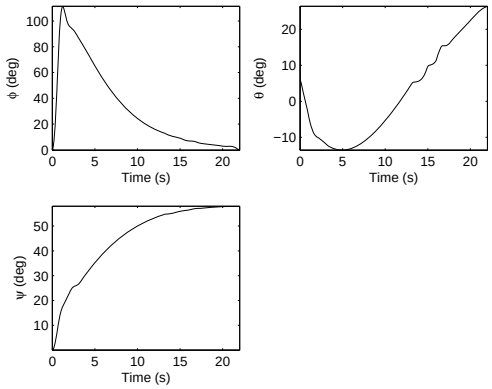

(d) Euler Angles

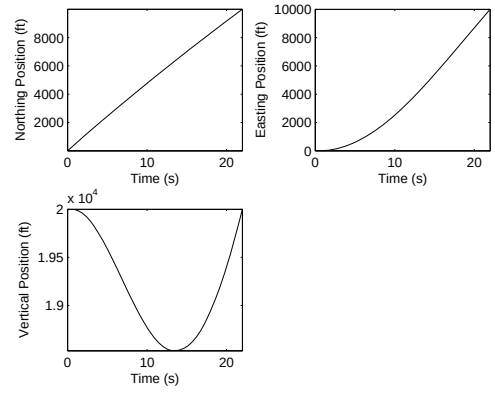

(e) Position

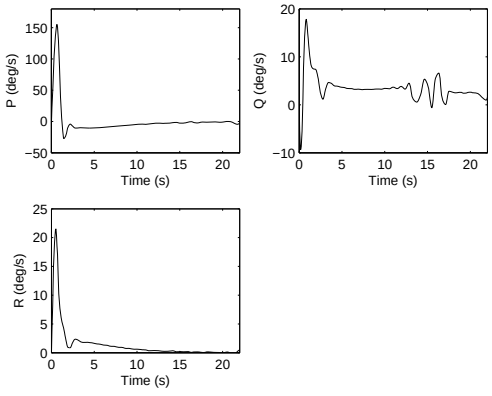

(f) Angular Rates

Figure A.2: Unconstrained 3-D position change state and control histories. (Model # 1)

A.3 Constrained 3-D Position Change

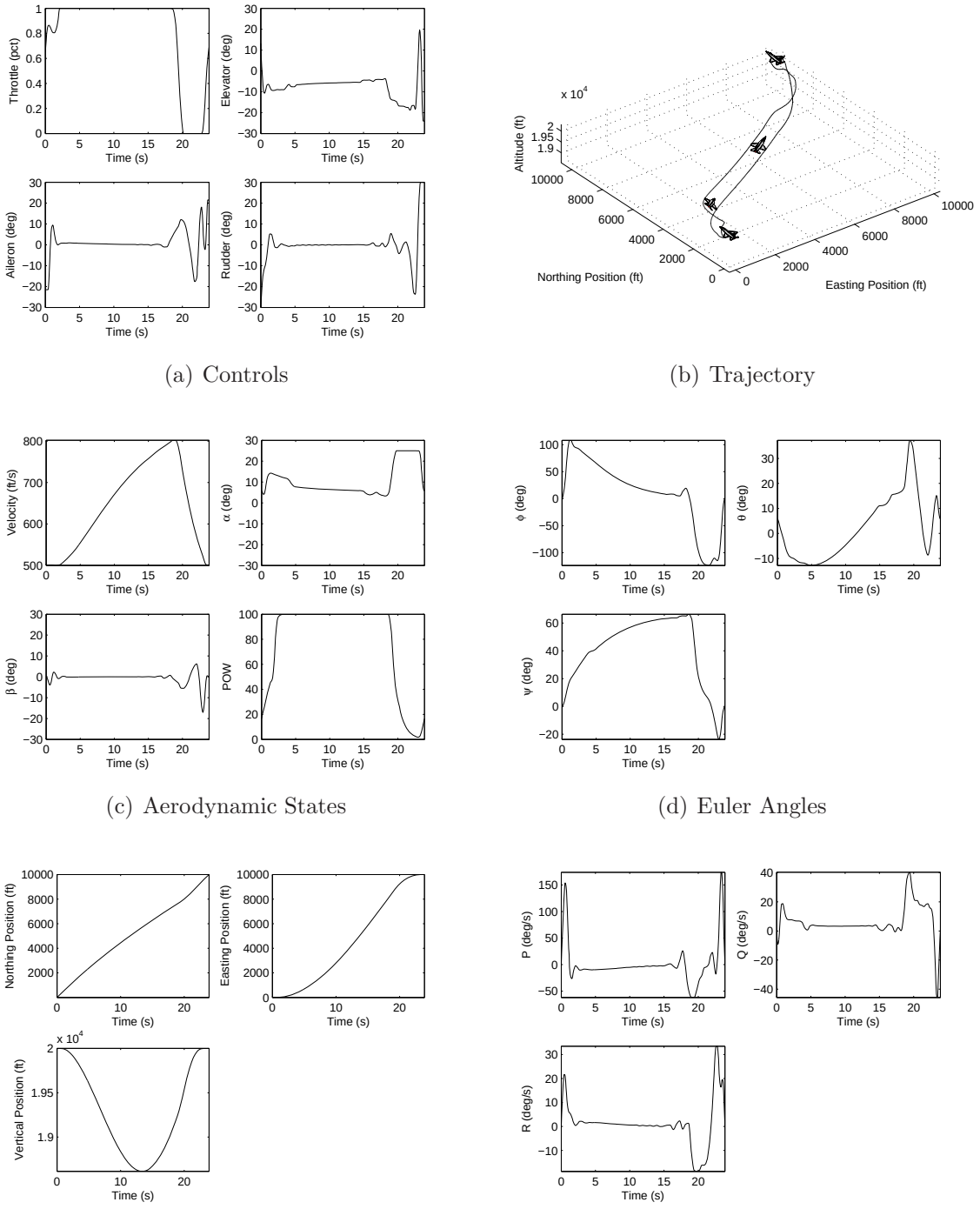

(a) Controls

(b) Trajectory

(c) Aerodynamic States

(d) Euler Angles

(e) Position

(f) Angular Rates

Figure A.3: Constrained 3-D position change state and control histories. (Model # 1)

A.4 Bank Angle Capture

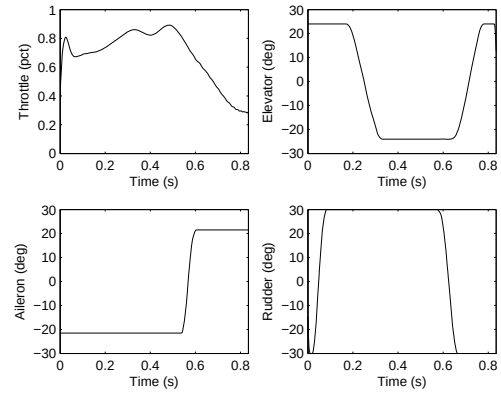

(a) Controls

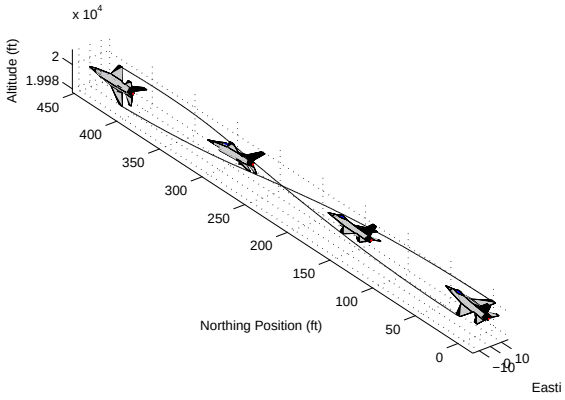

(b) Trajectory

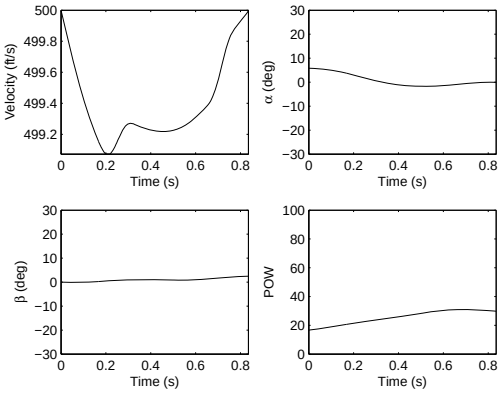

(c) Aerodynamic States

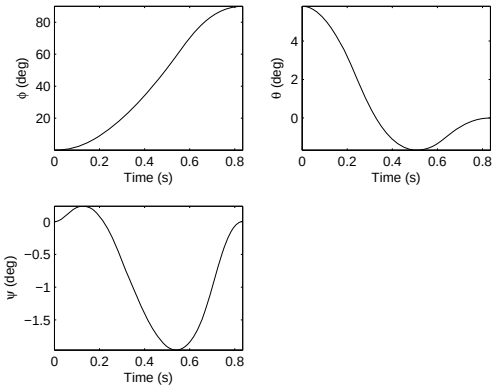

(d) Euler Angles

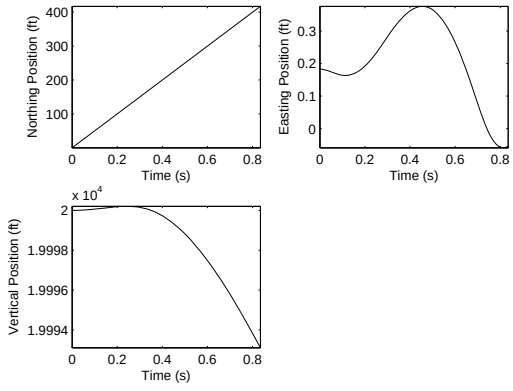

(e) Position

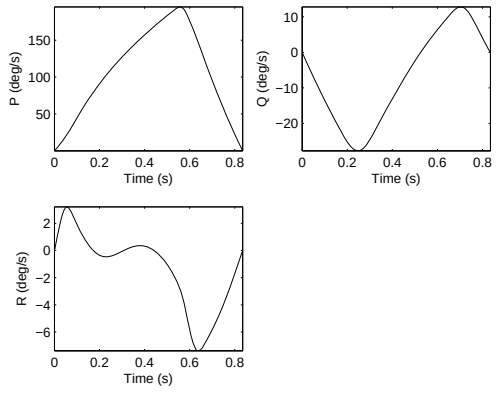

(f) Angular Rates

Figure A.4: Constrained bank angle capture state and control histories. (Model # 1)

A.5 Unconstrained Heading Capture

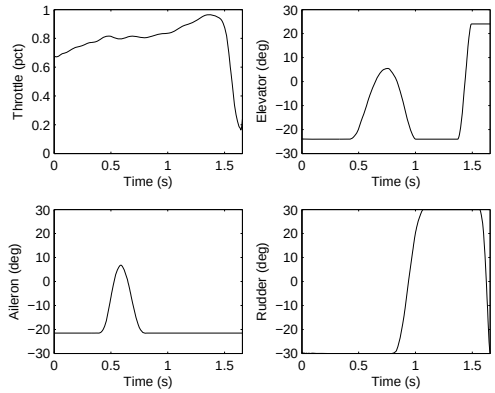

(a) Controls

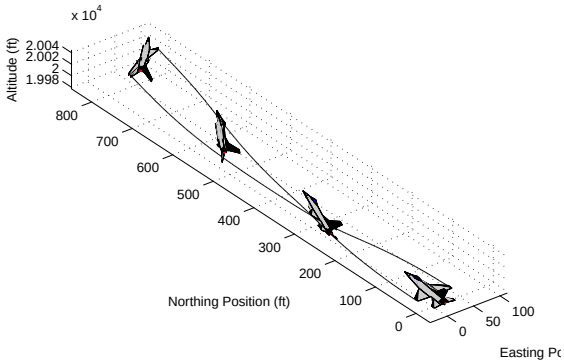

(b) Trajectory

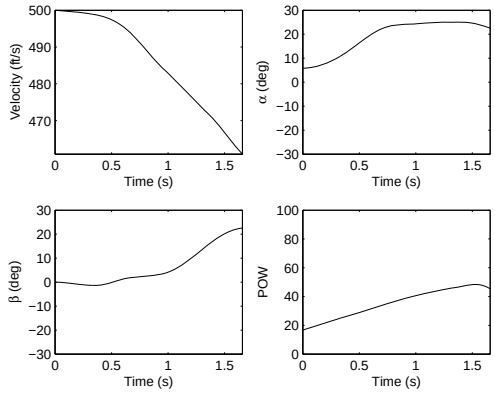

(c) Aerodynamic States

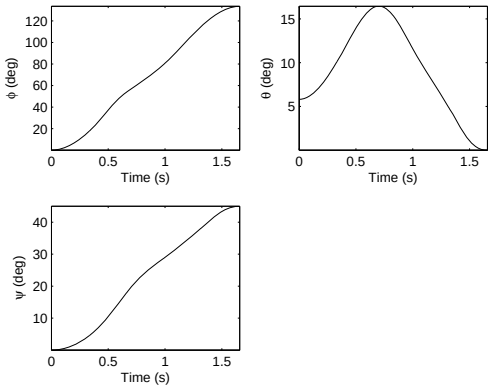

(d) Euler Angles

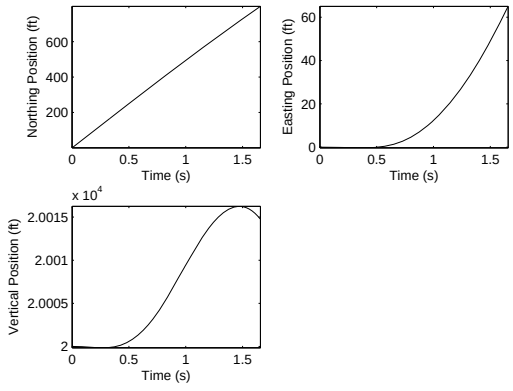

(e) Position

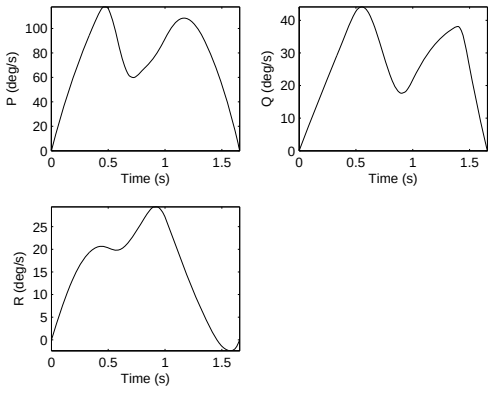

(f) Angular Rates

Figure A.5: Unconstrained heading capture state and control histories. (Model # 1)

A.6 Constrained Heading Capture

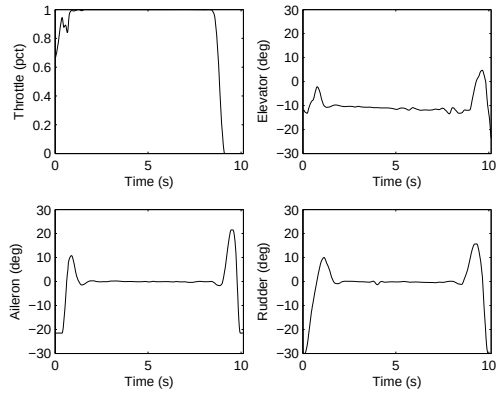

(a) Controls

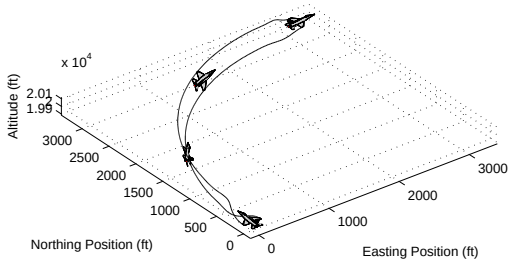

(b) Trajectory

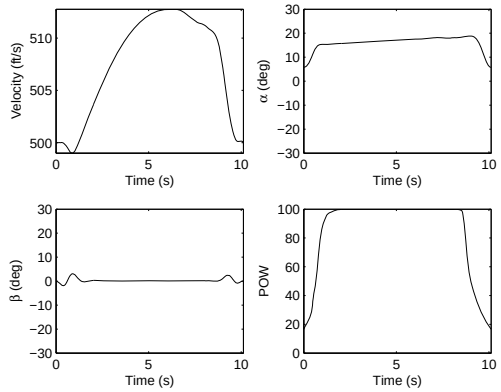

(c) Aerodynamic States

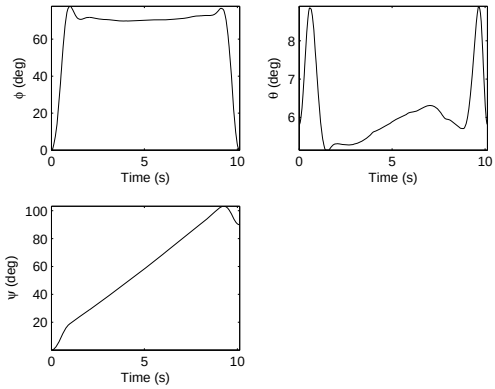

(d) Euler Angles

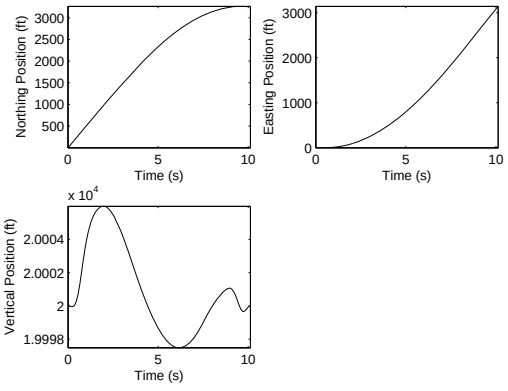

(e) Position

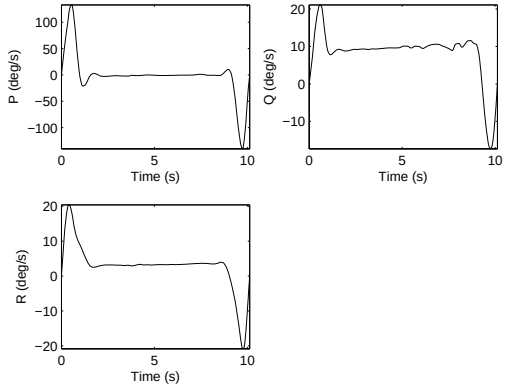

(f) Angular Rates

Figure A.6: Constrained heading capture state and control histories. (Model # 1)

A.7 Position Free Heading Reversal

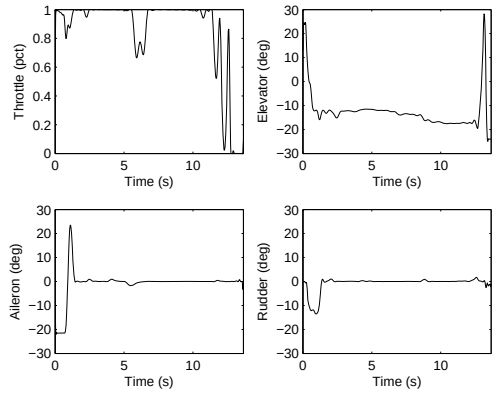

(a) Controls

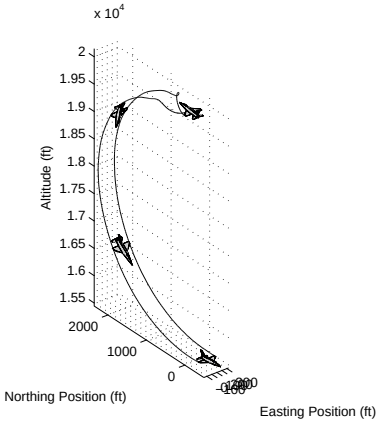

(b) Trajectory

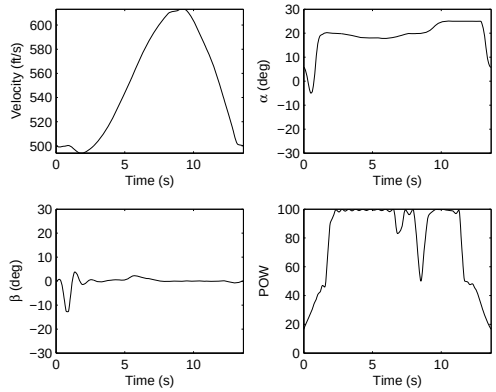

(c) Aerodynamic States

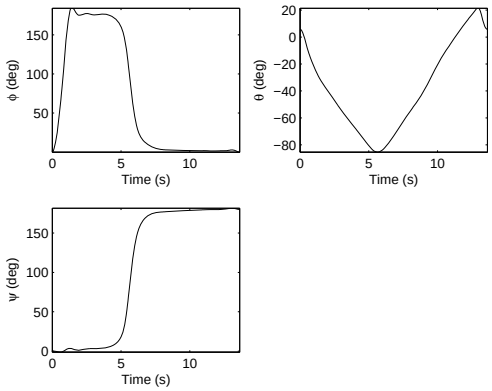

(d) Euler Angles

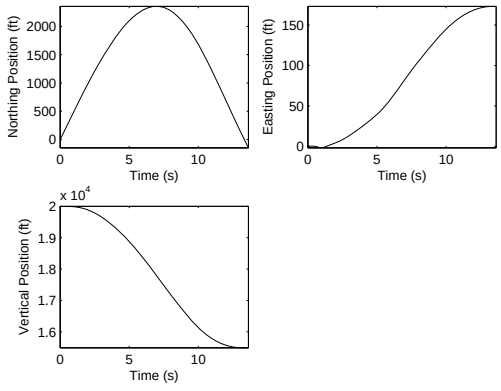

(e) Position

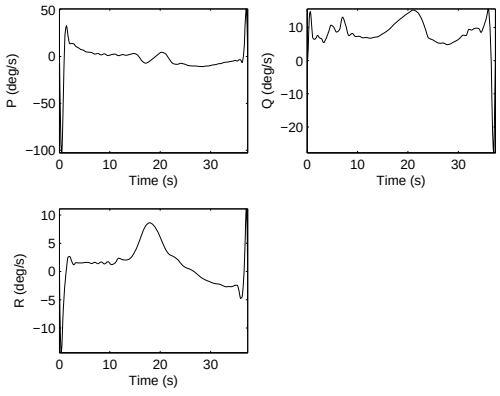

(f) Angular Rates

Figure A.7: Position free heading reversal state and control histories. (Model # 1)

A.8 Position Fixed Heading Reversal

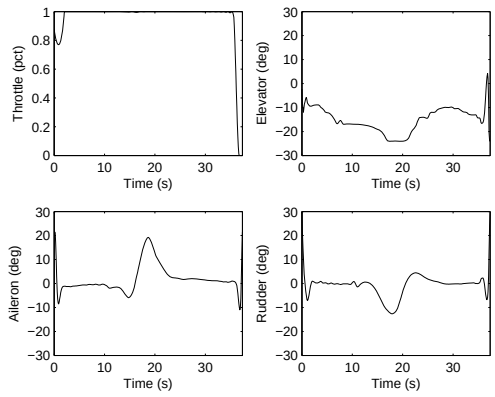

(a) Controls

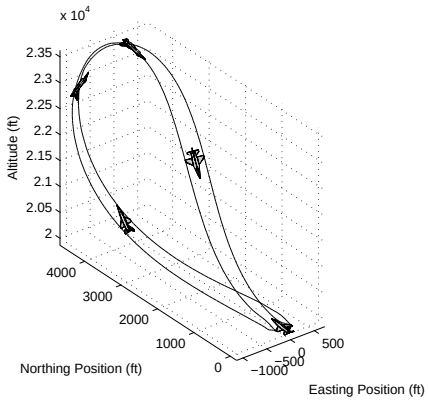

(b) Trajectory

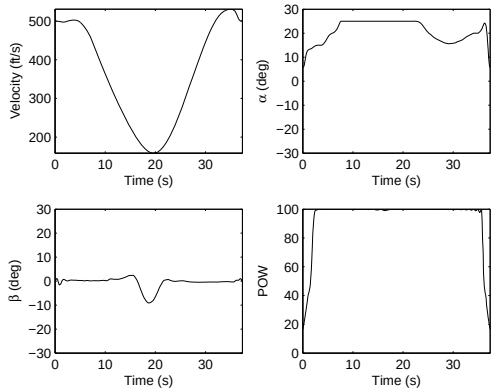

(c) Aerodynamic States

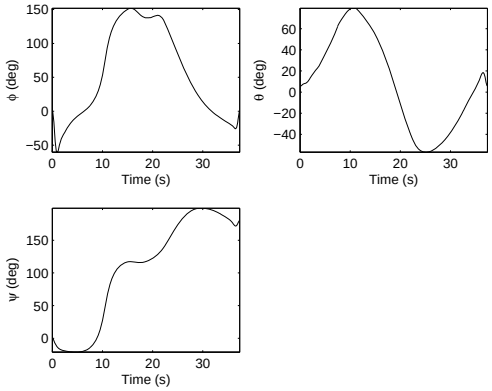

(d) Euler Angles

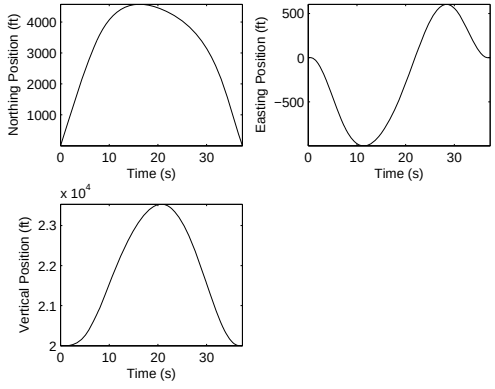

(e) Position

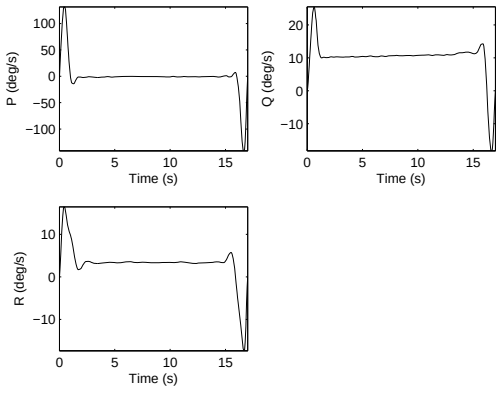

(f) Angular Rates

Figure A.8: Position free heading reversal state and control histories. (Model # 1)

A.9 Position Fixed Heading Reversal with altitude floor

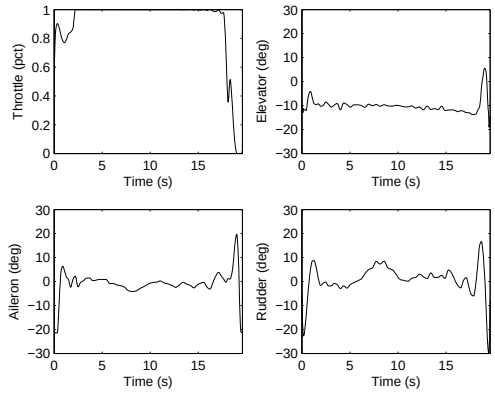

(a) Controls

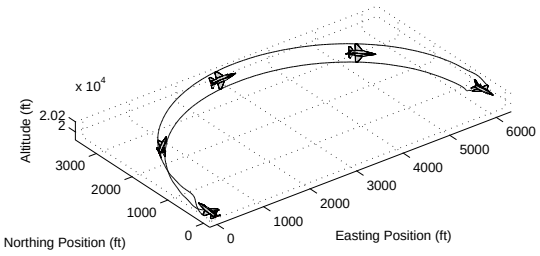

(b) Trajectory

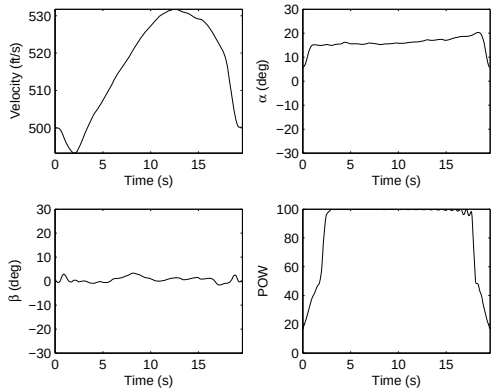

(c) Aerodynamic States

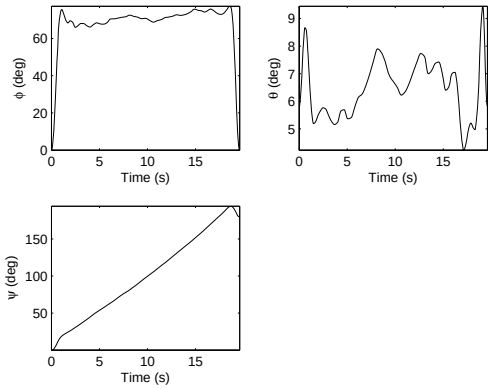

(d) Euler Angles

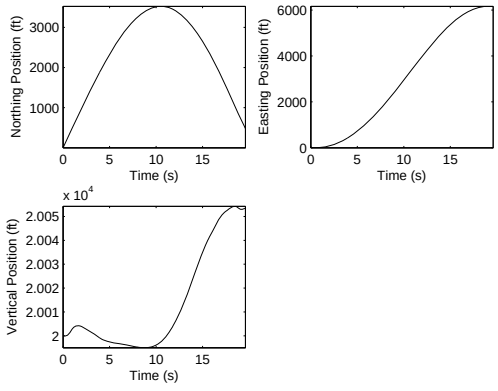

(e) Position

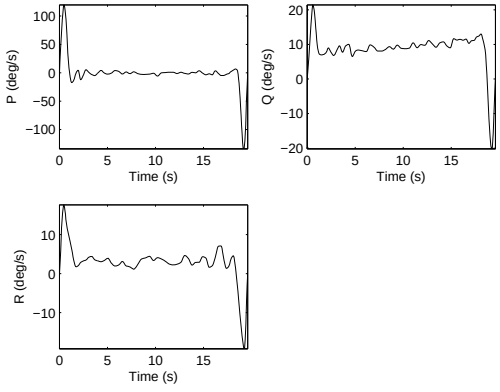

(f) Angular Rates

Figure A.9: Position free heading reversal with altitude floor state and control histories. (Model # 1)

A.10 Initial State Capture

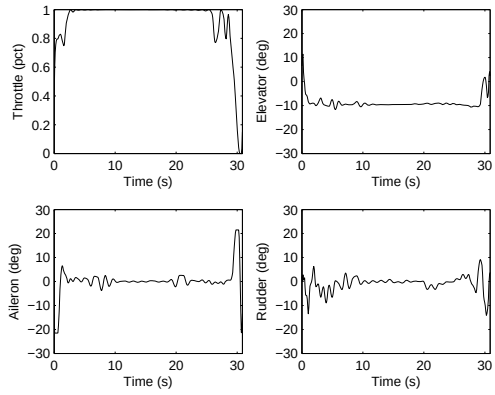

(a) Controls

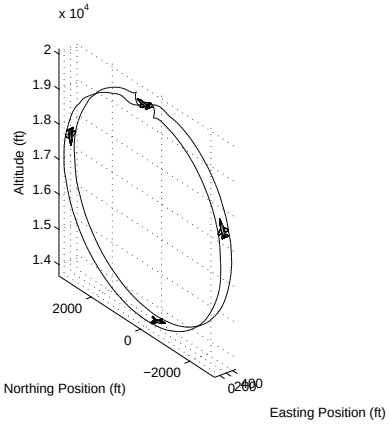

(b) Trajectory

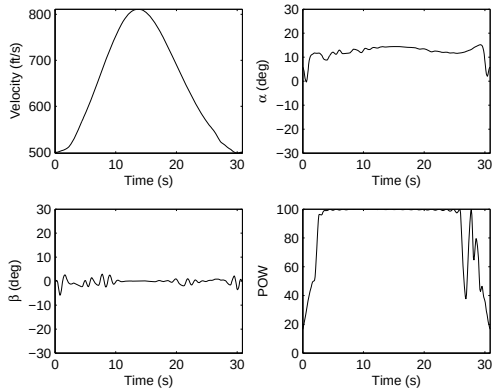

(c) Aerodynamic States

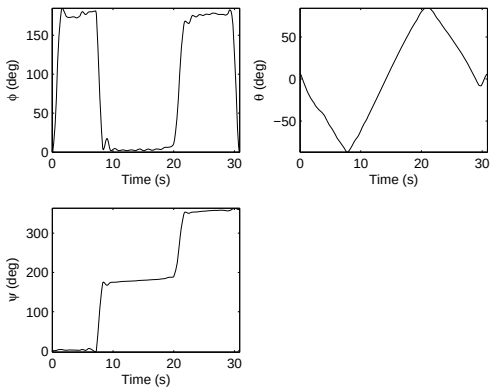

(d) Euler Angles

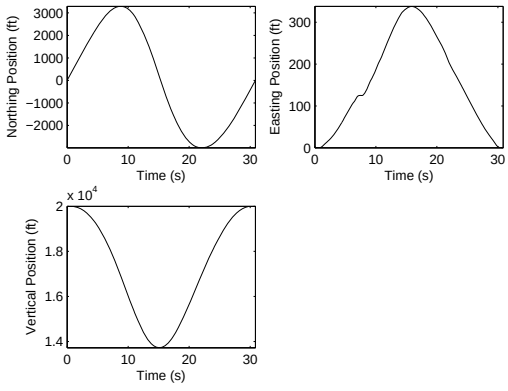

(e) Position

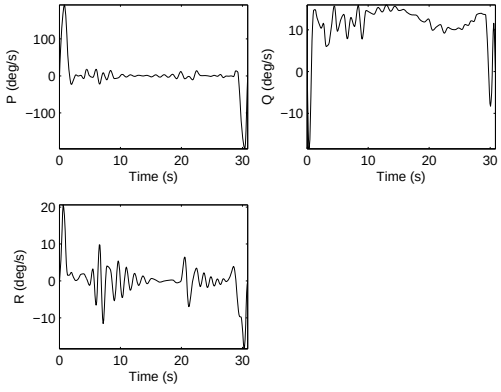

(f) Angular Rates

Figure A.10: Initial state capture state and control histories. (Model # 1)

A.11 Initial State Capture with altitude floor

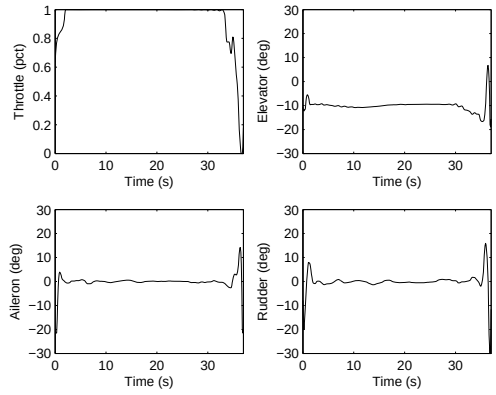

(a) Controls

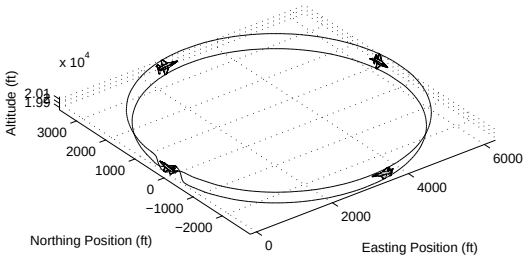

(b) Trajectory

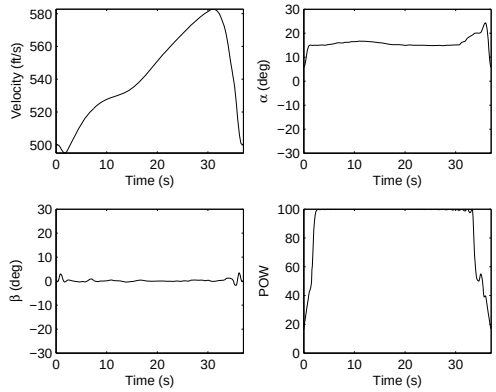

(c) Aerodynamic States

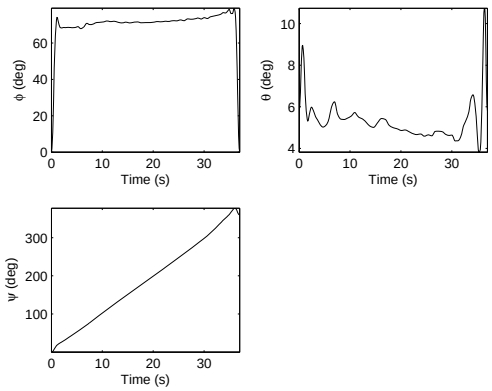

(d) Euler Angles

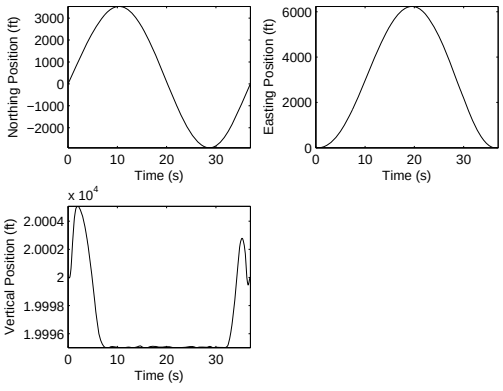

(e) Position

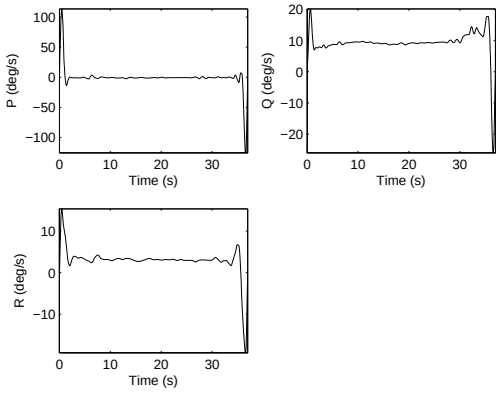

(f) Angular Rates

Figure A.11: Initial state capture with altitude floor state and control histories. (Model # 1)

A.12 4-Point Position Change

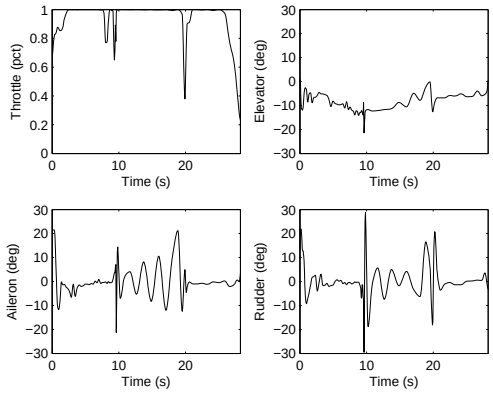

(a) Controls

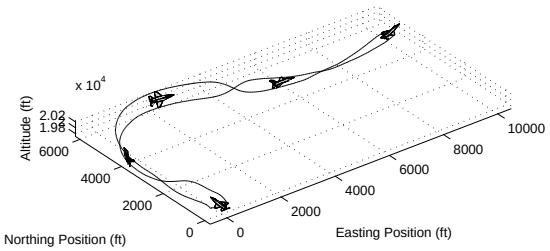

(b) Trajectory

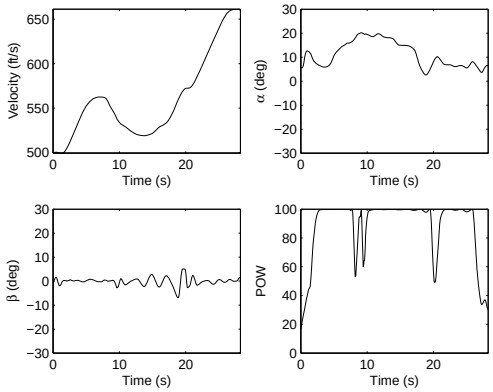

(c) Aerodynamic States

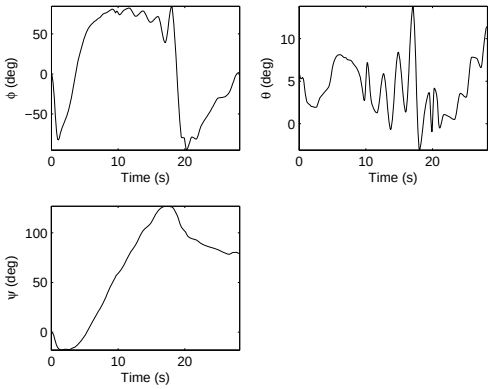

(d) Euler Angles

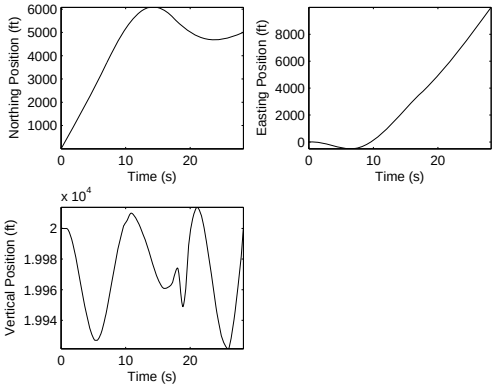

(e) Position

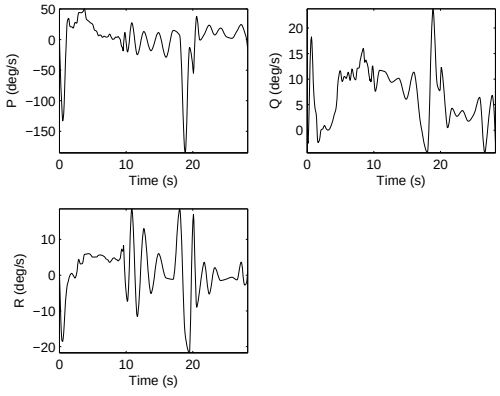

(f) Angular Rates

Figure A.12: 4-Point Position Change state and control histories. (Model # 1)

Bibliography

1. "Air Force Link - Art", January 2008. URL `http://www.af.mil/art`. United States Air Force.

2. Betts, John T. "Survey of Numerical methods for Trajectory Optimization". *Journal of Guidance, Control, and Dynamics*, 21(2):193–206, March-April 1998.

3. Betts, John T. *Practical Methods for Optimal Control Using Nonlinear Programming*. Society for Industrial and Applied Mathematics (SIAM), 2001.

4. Bocvarov, Spiro, Eugene M. Cliff, and Frederick H. Lutze. "Aircraft Time-Optimal Heading Reversal Maneuver". *AIAA Guidance, Navigation and Control Conference*. Scottsdale, AZ, August 1994. AIAA Paper 94-3556.

5. Bocvarov, Spiro, Frederick H. Lutze, Eugene M. Cliff, and Klaus H. Well. "Time-Optimal Reorientation Maneuvers for an Aircraft With Thrust-Vector Control". *AIAA Guidance, Navigation and Control Conference*. New Orleans, LA, August 1991. AIAA Paper 91-2709.

6. Bryson, Arthur E. Jr. *Dynamic Optimization*. Addison-Wesley, 1999.

7. Bryson, Arthur E. Jr. and Yu-Chin Ho. *Applied Optimal Control*. Ginn and Company, 1969.

8. Cliff, Eugene M., Frederick H. Lutze, Klaus H. Well, and Brian G. Thompson. "Toward a Theory of Aircraft Agility". *AIAA Atmospheric Flight Mechanics Conference*. Portland, OR, August 1990. AIAA Paper 90-2808.

9. Cliff, Eugene M. and Brian G. Thompson. "Aircraft Agility Maneuvers". *AIAA Atmospheric Flight Mechanics Conference*. Hilton Head Island, SC, August 1992. AIAA Paper 92-4489.

10. Dorn, M. "Aircraft Agility: The Science and the Opportunities". *AIAA/AHS/ASEE Aircraft Design, Systems and Operations Conference*. Seattle, WA, August 1989. AIAA Paper 89-2015.

11. Gill, Philip E., Walter Murray, and Margaret H. Wright. *Practical Optimization*. Academic Press, 1981.

12. Hull, David G. *Optimal Control Theory for Applications*. Mechanical Engineering Series. Springer, 2000.

13. Huntington, Geoffrey, David Benson, and Anil Rao. "A Comparison of Accuracy and Computational Efficiency of Three Pseudospectral Methods". *AIAA Guidance, Navigation, and Control Conference and Exhibit*. Hilton Head, SC, August 2007. AIAA Paper 2007-6405.

14. Jardin, Matt R. and Arthur E. Jr. Bryson. "Neighboring Optimal Aircraft Guidance in Winds". *AIAA Guidance, Navigation, and Control Conference and Exhibit*. Denver, CO, August 2000. AIAA Paper 2000-4264.

15. Kabamba, Pierre T., Semyon M. Meerkov, and Frederick H. III Zeitz. "Optimal Path Planning for Unmanned Combat Aerial Vechiles to Defeat Radar Tracking". *Journal of Guidance, Control, and Dynamics*, 29(2):279–288, March-April 2006.

16. Larson, Reid A., Meir Pachter, and Mark J. Mears. "Path Planning by Unmanned Air Vehicles for Engaging an Integrated Radar Network". *AIAA Guidance, Navigation and Control Conference and Exhibit*. San Francisco, CA, August 2005. AIAA Paper 2005-6191.

17. Liefer, Randall K., John Valasek, David P. Eggold, and David R. Downing. "Assessment of Proposed Fighter Agility Metrics". *AIAA Atmospheric Flight Mechanics Conference*. Portland, OR, August 1990. AIAA Paper 90-2807.

18. Miles, David W. and Stephen M. Rock. "Real-Time Dynamic Trajectory Optimization". *AIAA Guidance, Navigation and Control Conference*. San Diego, CA, July 1996. AIAA Paper 1996-3741.

19. Raymer, Daniel P. *Aircraft Design: A Conceptual Approach*. American Institute of Aeronautics and Astronautics, Inc., 3rd edition, 1999.

20. Ross, I. Michael. *User's Manual for DIDO*. Elissar, LLC, Monterey, CA, 2006. Version PR.1.

21. Ross, I. Michael. *A Beginner's Guide to DIDO*. Elissar, LLC, Monterey, CA, 2007. Version 7.3.

22. Ross, I. Michael and Fariba Fahroo. "A Perspective on Methods for Trajectory Optimization". *AIAA/ASS Astrodynamics Specialist Conference and Exhibit*. Monterey,CA, August 2002. AIAA Paper 2002-4727.

23. Ross, I. Michael and Fariba Fahroo. "Pseudospectral Knotting Methods for Solving Optimal Control Problems". *Journal of Guidance, Control, and Dynamics*, 27(3):397–405, May-June 2004.

24. Shaw, Robert L. *Fighter Combat: Tactics and Maneuvering*. Naval Institute Press, Annapolis, MD, 1985.

25. Smith, Steven W. *The Scientist and Engineer's Guide to Digital Signal Processing*. Electronic Edition, 1998. URL `www.DSPguide.com`.

26. Stevens, Brian L. and Frank L. Lewis. *Aircraft Control and Simulation*. Wiley, 2nd edition, 2003.

27. Tamrat, B.F. "Fighter Aircraft Agility Assessment Concepts and Their Implications on Future Agile Fighter Design". *AIAA/AHS/ASEE Aircraft Design, Systems and Operations Meeting*. Atlanta, GA, September 1988. AIAA Paper 88-4400.

28. Zollars, Michael, Paul Blue, and Brian Burns. "Wind Corrected Flight Path Planning for Autonomous Micro Air Vehicles Utilizing Optimization Techniques". *AIAA Atmospheric Flight Mechanics Conference and Exhibit*. Hilton Head, SC, August 2007. AIAA Paper 2007-6497.

Vita

Capt David Hall was born in Beeville, TX. He graduated from Annapolis Senior High School in Annapolis, MD in May 2003. He then enrolled at Virginia Tech in Blacksburg, VA, from which he graduated with honors in May 2003 with a Bachelor's of Science in Aerospace Engineering. He then reported to the Air Force Officer Training School at Maxwell AFB in Montgomery, AL and received a commission in September 2003.

His first assignment was at Kirtland AFB in Albuquerque, NM where he was a Program Manager and Flight Test Manager for the Optics Division of the Air Force Research Lab's Directed Energy Directorate. While there he conducted developmental tests of numerous ground and airborne laser systems. In August 2006, he entered the Graduate School of Engineering and Management, at the Air Force Institute of Technology. Upon graduation, he will be assigned to the National Air and Space Intelligence Center at Wright-Patterson AFB in Dayton, OH.

REPORT DOCUMENTATION PAGE

Form Approved
OMB No. 0704–0188

1. REPORT DATE (DD–MM–YYYY)	2. REPORT TYPE	3. DATES COVERED *(From — To)*
12–03–2008	Master's Thesis	Sept 2007 — Mar 2008

4. TITLE AND SUBTITLE

Demonstrative Maneuvers for Aircraft Agility Predictions

5a. CONTRACT NUMBER

5b. GRANT NUMBER

5c. PROGRAM ELEMENT NUMBER

6. AUTHOR(S)

David M. Hall, Capt, USAF

5d. PROJECT NUMBER

5e. TASK NUMBER

5f. WORK UNIT NUMBER

7. PERFORMING ORGANIZATION NAME(S) AND ADDRESS(ES)

Air Force Institute of Technology
Graduate School of Engineering and Management (AFIT/EN)
2950 Hobson Way
WPAFB OH 45433-7765

8. PERFORMING ORGANIZATION REPORT NUMBER

AFIT/GAE/ENY/08-M13

9. SPONSORING / MONITORING AGENCY NAME(S) AND ADDRESS(ES)

N/A

10. SPONSOR/MONITOR'S ACRONYM(S)

11. SPONSOR/MONITOR'S REPORT NUMBER(S)

12. DISTRIBUTION / AVAILABILITY STATEMENT

APPROVED FOR PUBLIC RELEASE; DISTRIBUTION UNLIMITED

13. SUPPLEMENTARY NOTES

14. ABSTRACT

This study was motivated by a need to develop a reliable method of predicting the agility characteristics of various aircraft. To fully investigate the agility of an aircraft, maneuvers which push the limits of an aircraft's maneuvering capabilities must be simulated. In these cases, classic trajectory optimization techniques either require too many assumptions for a realistic solution or require a good guess of the final solution before the problem is even attempted. This study investigated both the utility of pseudospectral optimization methods for robust trajectory optimization as well as the potential for demonstrating differences in aircraft agility characteristics of several specific maneuvers. Three variations of a basic F-16 mathematical model were simulated for various maneuvers specifically designed to demonstrate aircraft maneuvering limits.

15. SUBJECT TERMS

aircraft agility, trajectory optimization, pseudospectral methods, aircraft maneuvers, agility maneuvers, agility metrics, aircraft control

16. SECURITY CLASSIFICATION OF:			17. LIMITATION OF ABSTRACT	18. NUMBER OF PAGES	19a. NAME OF RESPONSIBLE PERSON
a. REPORT	b. ABSTRACT	c. THIS PAGE			Lt Col Christopher M. Shearer, PhD (ENY)
U	U	U	UU	112	19b. TELEPHONE NUMBER (Include Area Code) (937) 255-3636, ext 4643; e-mail: christopher.shearer@afit.edu